Feldspar replacement reactions by interface-coupled dissolution-precipitation: a case study from the Larvik Plutonic Complex, SE-Norway

MSc Thesis

Karin Los
Supervisors:
Ass. prof. Oliver Plümper
Prof. dr. Martyn R. Drury

Faculty of Geosciences
University of Utrecht
Monday June 16^{th} 2014

Abstract

Hydrothermal fluids can migrate through large amounts of impermeable crustal rock and are often associated with element fluxes and heat. This can change structural rock properties and locally result in ore deposits. To interpret fluid-rock interaction correctly, understanding their driving mechanisms is of vital importance. A stepwise insight in replacement processes is provided by the hydrothermal alteration of feldspar rocks in the Larvik Plutonic Complex in SE-Norway, which acts as a perfect natural laboratory.

Fluid-rock interactions are visible as a colour change: the blue larvikite rock is (partly) replaced by red tønsbergite. It started as a red discolouration around grains but at pervasive alteration, mineral replacement occurred and porous crystals surround the larvikite feldspar relics. The degree of alteration varies throughout the area of interest. Textural and chemical analysis was done using scanning electron microscopy, X-ray tomography, an electron microprobe and XRF; trace elements were measured using an ICP-MS. These techniques show that alteration is zoned, from non-porous larvikite feldspar at the core to porous albite and orthoclase at the rim. Isocon diagrams are used to quantify element mobilisation. Surprisingly, major and minor element analysis show no large elements flux related to fluid flow. Instead, only element redistribution has taken place when water entered the rock. Albite and orthoclase patches replaced the larvikite, co-precipitating due to a changing fluid activity for Na^+ and K^+ in a feldspar-saturated system. Mineral textures changed because of energy reduction facilitated by the fluid. Trace elements have remained constant throughout the reaction. Feldspar re-equilibration with immobility of REE limits fluid temperatures to 250–300 °C at neutral pH, and minor phases such as hematite and pumpellyite place fluid conditions at 1–3 kb in a slightly oxidizing environment. The absence of element mobility rules out the process of albitisation and makes a link to the nearby Kodal ore deposits very unlikely.

Fluid flow is controlled by an interaction between grain boundary diffusion and reaction front migration through an interface-coupled dissolution-reprecipitation process. It involves atomic scale bond-breaking and dissolution of the primary mineral followed by pseudomorphic precipitation of the new, porous phase. The reaction proceeds by this porosity generation, enabling fluid to remain in contact with the old phase at the reaction interface.

Contents

1 Introduction

Hydrothermal alteration is a common feature in the Earth's crust, and has many implications yet unknown to us. Fluid systems can severely affect deep and shallow rocks, changing their chemistry and texture. Alteration stays visible in the texture and chemical signature of the rock, enabling us to derive tectonic history and PT-conditions from them. Fluid movement is often associated with element transport, with useful applications ranging from storage of CO_2 or chemical waste to ore deposition and surface weathering (rock stability). But which mechanisms of mineral replacement and equilibration are active and how fluids continue to infiltrate rock often remains a question. Diffusion allows slow homogenization of a system, while dissolution and precipitation can cause rapid element transport over longer distances. Especially for ore deposits, the type of fluid that infiltrates and the transporting mechanisms are of vital importance. Main questions in this study therefore are: How can fluids move through rock and cause pervasive alteration, and on what scale do mechanisms act?

At fluid infiltration, a body can react by diffusion, net volume reactions or dissolution-precipitation with the formation of porosity and possible formation of minor phases [Putnis *et al.*, 2007]. For these processes, temperature dependence of the reaction rate is given by the Arrhenius equation $k = A'e^{-E/RT}$ in which k is reaction rate, R is the gas constant and E stands for activation energy; for dissolution this lies around 5 kcal/mole and diffusion has a value around 20 kcal/mole [Brantley *et al.*, 2008]. Because of the lower energy barrier to start a process, reactions in the presence of a fluid are more likely and more rapid. This fluid infiltration or metasomatism does not have to be related to a certain tectonic event or a change in PT-conditions, although it is usually the case. At low temperatures it is harder to transport mass (especially by diffusion) because of the low energy present in the system; it especially has a transport inhibition effect in low permeability rocks [Oliver, 1996]. The dissolution-precipitation mechanism creates a pathway for fluid infiltration, altering rock properties such as permeability and porosity during the reaction. This affects the ease of mass movement, a process called reactive transport. It enables the fluid to move even through grains, as long as the fluid stays in contact with fresh rock and the pores are connected [Hövelmann *et al.*, 2010].

Previous studies have shown that careful rock analysis can reveal several stages of fluid-infiltration, as captured in SE-Sweden [Plümper and Putnis,

2009]. Dissolution-precipitation mechanisms are said to have acted here, dissolving the old mineral and precipitating a new phase, in equilibrium with the entering fluid and added components from primary mineral dissolution. The first research on feldspar dissolution was done by Helgeson and co-workers, who treated the system in a thermodynamic way. Dissolution is considered to drive the reaction, and the relationship to pH and temperature [Chou and Wollast, 1984, 1985; Helgeson *et al.*, 1984; Holdren and Speyer, 1985b, 1987] are investigated. This approach assumes equilibrium in a multi-component system forming new phases out of old ones. Later studies [Lasaga *et al.*, 1994; Zhu *et al.*, 2004a; Ganor *et al.*, 2007] have already shown that this principle does not always hold, which results in large deviations from the expected mineral assemblage. Therefore, another approach focuses on a kinetic background, studying surface processes such as ligands [Chou and Wollast, 1985; Muir and Nesbitt, 1991; Nesbitt *et al.*, 1991] or etch pits [Knauss and Wolery, 1986], dislocation density [Holdren and Speyer, 1987] and surface chemistry, including leached layers depleted in easily removed cations [Petrović*et al.*, 1986; Chou and Wollast, 1984; Blum and Lasaga, 1988, 1991; Casey *et al.*, 1988, 1989a,b; Muir *et al.*, 1989, 1990; Hellmann *et al.*, 1990]. Many of these studies were experimental, using solutions that are highly undersaturated with respect to feldspar [Holdren and Berner, 1979; Burch *et al.*, 1993; Hellmann, 1994; Oelkers *et al.*, 1994; Brantley and Stillings, 1996]. This is not the case in many natural systems [Paces, 1972; Saigal *et al.*, 1988] where feldspars precipitate in low temperature surface waters under normal burial conditions. Because of large variations in possible fluid regimes, lithology and PT-conditions, out-of-equilibrium reactions may not be severely feldspar undersaturated. Batch reactor experiments done by Fu *et al.* (2009) have shed more light on the mechanisms behind dissolution of silicates. They showed that at low pH, despite high temperatures, no full equilibrium was reached. Albite dissolved and K-feldspar precipitated throughout the experiment, according to the following reaction.

$$\text{Albite } (NaAlSi_3O_8) + K^+ = \text{K-feldspar } (KAlSi_3O_8) + Na^+$$

However, cation exchange is more complex than shown in the formula above, also involving tetrahedral bond breaking as is visible in the oxygen isotope change between old and new minerals [O'Neil and Taylor, 1967] and a thin discontinuity between the old and new mineral at the interface [Labotka *et al.*, 2004]. Precipitation on the surface limits albite dissolution rates.

The current study focuses on hydrothermal fluids percolating into a monzonitic feldspar rock in SE-Norway. The samples originate from the Larvik Plutonic Complex, which formed in stages during rifting in the Permian. Because of the different timing of intrusions, overprinting by fluids can have occurred in several episodes. To see if a record of fluid-mineral reactions is captured, feldspar analysis is done, comparing the old larvikite rock with the new reddish tønsbergite alteration. By analyzing the resulting change in texture, mineralogy and element distribution, the main questions to be answered are:

- What was the composition of the infiltrating fluid(s) and are they related to ore deposition?
- Which process(es) caused alteration, and under what pressure-temperature conditions?
- Why did alteration occur?

Together, this can help to establish a hydrothermal history for the area. Red and orange discolourations of the originally blue rock show the extent of fluid infiltration and interactions with the minerals, enabling precise chemical analysis of altered and unaltered rock. Two types of alteration are observed, one only affecting the grain boundaries, forming a fine grained reddish material, and the other one completely consuming the blue grains and forming orange porous minerals. The first is present in all rocks, the reddish band becoming thicker with increased alteration; the latter is only observed in the more affected samples to different extents, from orange discolouration at the grain edges till full replacement by orange minerals. These observed re-equilibration textures are studied in the light of large scale tectonics.

1.1 Albitisation

A common example of feldspar alteration is replacement by albite. This process is observed by Engvik *et al.* (2008) in the Bamble sector, where textures closely resemble alteration observed in the larvikites, including reddening in altered parts by hematite formation and the alteration anastamosing through the rock. Albitisation is often related to hydrothermal fluids [Lee and Parsons, 1997; Engvik *et al.*, 2008], since high temperature conditions that favour Na-partitioning in the fluid phase also induce REE-enrichment. The resulting fluid is enriched in these elements, which can be related to ore deposition

[Oliver *et al.*, 2004]. The origin of these fluids is still quite unknown [Kinnaird, 1985]. Albitisation is a form of autometasomatism, affecting and coming from the host rock [Harlov and Austrheim, 2013]. At cooling of an igneous body, alkali atoms become transported in the remaining magma. Increasing volatile content in a melt causes an increased Na-concentration which results in the formation of albite crystals. At the same time, K goes into the fluid phase and can be transported to the wall rock [Bowden, 1985]. At a decreasing volatile content or B and HCl addition to the system, Na partitions into the fluid and the wall rock becomes albitised [Pichavant and Manning, 1984]. Saigal *et al.* (1988) found that in a compaction environment, at depth albitisation filled existing pores while at shallow depths it created pores from alkali feldspar dissolution and coupled albite precipitation.

In feldspars, ion uptake responds to normal equilibrium laws, decreasing K uptake at decreased temperature and increased pressure [Orville, 1972]. Trace element uptake depends on their availability; they replace cations that are similar in size and charge [Iiyama, 1979]. If several locations in the lattice are available for a trace element, it will prefer one over the other, increasing the entropy of the crystal. This excess energy can cause distortion of the lattice. Trace elements can also concentrate in ore minerals which can be mined.

This study will not focus on the ore potential of the Larvik area but on the hydrothermal history, although special attention will be given to the common feldspar alteration process of albitisation. Before describing the current study, some background theory on the origin and geological setting of these rocks will be given. Afterwards, feldspar chemistry and the several mechanisms that can lead to the observed alteration textures will be introduced.

2 Background information on larvikites

2.1 Geological setting and history

The Larvik Plutonic Complex is situated in the south-east of Norway, close to the Oslo rift. During the Permian, intracontinental rifting created space for intrusions, which range in age from 295–245 Ma [Sundvoll, 1978a]. The complex was built up of separate magma chambers that differentiated in situ, resulting in several types of intrusive rocks of mafic to intermediate composition [Neumann, 1980]. Their rise to the surface depended on stresses in the crust; dense basalts could only rise during extensive tensile stresses while intermediate magmas were also able to reach the surface during mild extension. This process is called density filtering. Larvikite, a hypersolvus monzonitic rock, is one of the larger intruding plutons [Andersen *et al.*, 2010] which crystallised at 850–860 °C from a differentiating magma at constant pressure [Andersen and Sørensen, 2003]. Since larvikites contain a single ternary feldspar phase, they must have crystallised from an anhydrous alkali feldspar system [Philpotts and Ague, 2009]; a hydrous system would result in the crystallisation of two feldspar phases. Trace element and isotope signatures suggest an enriched lithospheric mantle origin without severe contamination by the wall rock [Sundvoll, 1978a; Neumann, 1980; Neumann *et al.*, 1992]. Next to feldspar, minor amounts of augite, apatite, olivine and Fe-Ti-oxides are present [Muir and Smith, 1956]. The complex relationship between the different intrusions in the Larvik area is described by Andersen and Sørensen (2003). The larvikite pluton is the biggest, which shows channels of the red tønsbergite variety. This pluton is crosscut by gabbros and nepheline syenites; both contain xenocrysts of larvikite. A porphyritic syenite cuts these intrusions. Apart from several intrusions, other indicators for extension in the area are possible pseudotachylytes [Verberne, 2013] and faults. Field images are displayed in the Results section.

The Permian rifting stage caused partial melting of the mantle by decompression. A mafic pluton intruded, which decreases in alkalinity and thickness towards the north [Brøgger, 1890]. When crustal tensile stress reduced with time, the mafic pluton remained at depth and started to fractionate, resulting in a rhomb-porphyry deposit emplacement in higher levels in the crust. Petersen (1978) was the first to recognize several ring intrusions in this monzonite complex (fig. 1), the oldest one being located in the east and being saturated in silica; Rasmussen *et al.* (1988) dated these rocks to be around

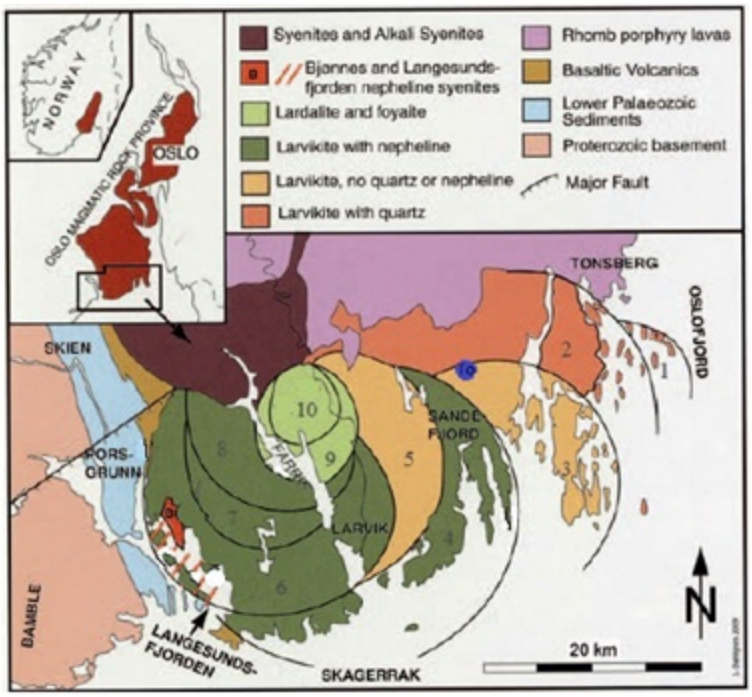

Figure 1: Intrusion structure with younging to the West. Rings vary in composition, the oldest ones being rich in quartz. From: Dahlgren, 2010.

270 Myrs old. Larvikite, mainly made up of feldspars, is present in the eastern rings and considered to be the plutonic equivalent of the shallower found rhomb-porphyry in the area [Brøgger, 1890] which has become exposed by erosion. From larvikite, two possible fractionation trends are possible, one under- and one over-saturated in silica depending on the additional mineral phase [Oftedahl, 1948], nepheline or quartz, respectively. These trends were used by Petersen (1978) to distinguish several generations of ring intrusions within the Plutonic Complex and compose Fig. 1. However, other mechanisms such as a partial melting or metasomatism of larvikite are proposed to form the surrounding rocks [Petersen, 1978; Raade, 1973]. The presence of different types of both the plutonic and volcanic rocks and the shift of the centre of igneous activity are all expected to be related to the Oslo rift system [Sundvoll, 1978a]. In the Permian rift zone, ore deposits such as the Kodal apatite-ilmenite-magnetite deposits [Bergstøl, 1972; Lindberg, 1985] or Nordli silver deposits (for more info, see Neumann, 1944) can be found.

2.2 Feldspar chemistry and crystallography

Feldspar is one of the main constituents of the Earth's crust, mainly found in magmatic rocks. It is built up of connected chains of SiO_4- and AlO_4-tetrahedra, forming a silicate network (fig. 2). Interstitial sites are taken up by cations of different valency state, related to the charge difference between Si and Al. Feldspar compositions are variable because of the variation in these interstitial cations. There are three pure endmembers of feldspar: anorthite ($CaAl_2Si_2O_8$), orthoclase ($KAlSi_3O_8$) and albite ($NaAlSi_3O_8$). Most feldspars are a mixture between these three, their components given in percentage of An, Or and Ab. The order of Al and Si in the network is very important and directly relates to the exchange of cations between lattice sites.

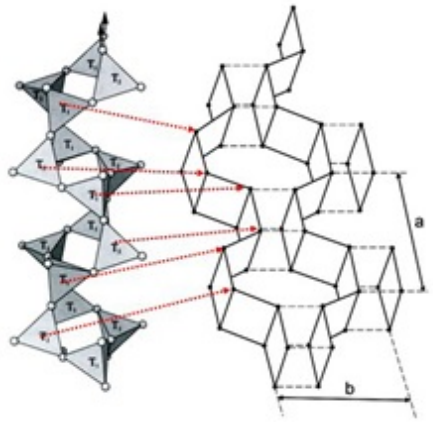

Figure 2: Feldspar structure showing chains of connected tetrahedra (displayed as dots in the right image), without interstitial cations. From: Putnis, 1992.

Igneous crystallisation of feldspar is often out of equilibrium; the assumption of a eutectic system in which pure endmembers crystallise is incorrect. Instead, a single feldspar crystal is precipitated as a solid solution (following the vertical line in fig. 3), which starts to shrink at cooling. Al- and Si-tetrahedral chains collapse around the smaller Na^+ and Ca^{2+} cations in the system; bond lengths can become stretched by distortion and the mineral starts to unmix [O'Neil and Taylor, 1967], forming lamellae of different compositions, called perthites. Larger cations (like K^+) support the structure; they result in a larger angle between tetrahedra because of charge repulsion

[Smith, 1974]. By this, ordering of Al and Si starts due to the charge of the bigger Al-tetrahedra, which repulse each other when they come closer during shrinking of the structure. Cations accompany this exchange in order to maintain the charge balance [Putnis, 1992]. For alkali feldspars, the Al:Si ratio is 1:3 which results in a quite ordered structure. Aluminium concentrates on the T1-site in the tetrahedral chain which has the closest bond with a cation. Rotation of small parts of the crystal by changing bond angles results in twins; periodic twinning is often observed as a result of unmixing of a well-mixed solid solution. Larger changes in orientation include angular rotations over a plane, which cause a change in crystal symmetry, from monoclinic to triclinic. For sanidine, the high temperature variant of orthoclase, the unmixing is known to have the following steps: (1) unmixing of Na and K (both monoclinic phases); (2) albite twinning of the Ab parts; (3) symmetry loss of the K-feldspar from monoclinic to triclinic; (4) formation of lozenge structures [Willaime and Gandais, 1972]. The more ordered plagioclase structure (Al:Si as 1:2) is less sensitive to twin formation.

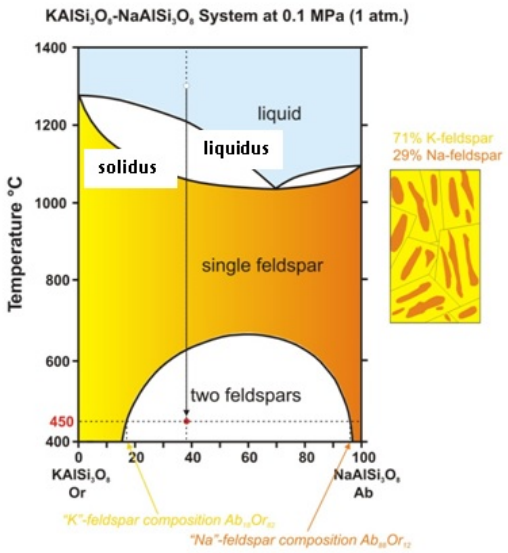

Figure 3: Crystallisation and unmixing of impure feldspar phases. At crystallisation from magma, a single feldspar or solid solution forms. When this becomes unstable (around 600 °C), 2 pure endmembers form as perthites shown in the inset on the right. After: Dexter Perkins, University of North Dakota.

Unmixing starts by spinodal decomposition, a compositional perturbation that grows in amplitude until the metastable state is reached [Yund and McCallister, 1970]. Ion exchange takes place over a small distance, making it a more favourable mechanism than volume or boundary diffusion. From the initial point, the formed perturbations grow outward, adjusting the lattice planes. Their regular spacing distance is determined by the thickness of the lamellae [Brown and Parsons, 1988; Willaime and Gandais, 1972] and by temperature [Yund, 1984]; low temperatures result in perthites with less spacing that are purer in composition. Strain is said to have some influence on the obliquity of twin planes [Parsons, 1965] but thermal history (i.e. cooling rate) and chemical composition of the rock are of main importance for the coarseness of these perthitic structures [Smith and Muir, 1958; Parsons, 1965; Willaime and Gandais, 1972].

Larvikite is a monzonitic rock of intermediate silica composition, which was formed by fractional crystallisation out of a basaltic magma [Neumann, 1980]. The rock consists mainly of a ternary feldspar, $Or_{19}Ab_{68}An_{13}$ [Brown and Parsons, 1984] approximately. Crypto- and micro-perthites are observed in the larvikite feldspar [Willaime *et al.*, 1973], indicating that the mixed primary composition has led to exsolution features upon cooling [Muir and Smith, 1956]. Smith and MacKenzie (1958) have been able to pinpoint the temperature of unmixing experimentally around 500 °C. Albite twins are present in the monoclinic alkali feldspar and intergrowths with nepheline are observed. The mineral started as disordered anorthoclase crystallised at high temperature [Muir and Smith, 1956], which formed cryptoperthites of albite and (still monoclinic) K-rich feldspar at cooling [Muir, 1962; Widenfalk, 1972]. Differences between core and rim are visible; such chemical zoning is related to rapid cooling. Ca-rich cores formed microperthites at unmixing while rims were richer in K and formed cryptoperthites [Smith and Muir, 1958]. Another common feature of the larvikites is cross-hatched twinning, a result of periodic albite twins and overgrown pericline twins deforming the albite twins [Deer *et al.*, 2001].

Normally, K-feldspar is red to yellow, while plagioclase is white to grey and glassy. However, larvikite rocks are blue and tønsbergite is red. Explanations for unusual colours can be found in element substitutions and irregular textures. Porosity in feldspars often makes them 'milky' to see, while thin lamellae cause interference of light waves, changing the colour [Peterson, 1972]; redox changes do the same by altering internal energies. Impurities also affect feldspar appearance; when Fe substitutes for K or Ca,

a yellow colour is produced (0.5 wt percent is already enough). It can also occupy the tetrahedral site in the crystal structure [Carmichael, 1967]. Blue feldspars like amazonite are found to have Pb or Rb in their crystal structure [Nunes, 1979]. However, inclusions are the most likely to form colours. Red discolouration is previously found to be related to small hematite needles [Putnis et al. 2007; Plümper and Putnis, 2009] while black may be due to Ti-oxides. This study will try to find a similar explanation for the observed discolouration in the larvikite alteration environment.

3 Alteration mechanisms: a theoretical background

3.1 Diffusion

3.1.1 Driving forces

Free energy reduction is the main driving force of all reactions and resulting mass transport. Diffusion in particular is driven by entropy; the random thermal motion of particles in the presence of a chemical gradient results in mass displacement in order to homogenize the system. Because this process is slow and random, the reaction front formed by diffusion will be gradual, not sharp. Fick's law describes mass transport by diffusion as

$$J = -D\frac{\partial C}{\partial x} \tag{1}$$

where D is the diffusion coefficient denoted in $m^2 s^{-1}$ and C the concentration an element in the rock. The minus sign indicates that flow occurs from high to low concentration. Over time, the gradient changes laterally as $\frac{\partial C}{\partial t} = \frac{\partial}{\partial x} D \frac{\partial C}{\partial x}$. Distance that matter travels by diffusion is related to the root of time: $x = \sqrt{Dt}$ [Zhang, 2010]. In general, the speed of diffusion depends on the diffusion coefficient $D = D_0 e^{-E_A/RT}$ in which D_0 is the value at infinite temperature, E_A is the activation energy of the reaction (which can depend on pressure), R is the gas constant and T is temperature in K. With increasing temperatures, diffusion speeds up which is observed in the good relationship between log D_0 and E_A for all minerals. Pressure dependence is more complicated [Brady and Cherniak, 2010]. Rules for diffusion rates (in silicate minerals) include [Zhang *et al.*, 2010]:

- Increased temperatures speed up diffusion (activation energy is more easily reached)
- Adding water speeds the process (it lowers the activation energy)
- Interstitial atoms diffuse the easiest
- Diffusion of atoms on this M-site in feldspar depends on charge (being most important in orthoclase) and size; the higher both factors are, the slower the process by stronger bonding

- Tetrahedral atoms diffuse the slowest. Their bonding energy is quite strong and they need vacancies in the crystal structure to jump to.

Crystal structure also affects diffusion; open spaces for ions, called ionic porosity, increases ion mobility and makes diffusion easier [Brady and Cherniak, 2010].

3.1.2 Diffusion in feldspars

Other factors described below are related to fluid-induced diffusion, and are of minor importance or vary in significance for specific cations in feldspar minerals [Zhang *et al.*, 2010]. **Fluid composition** has only a very small influence; **fluid pressure** is of greater importance, especially for O-diffusion. This has to do with water easing transport and providing hydrogen, which can substitute for cations and forms weaker bonds [Farver, 2010]. Mono- and divalent cations in feldspars are strongly dependent on the **composition of the feldspar mineral** through which they need to diffuse, as well as on oxidation state. They move anisotropically through the mineral, preferring certain crystal orientations over others. K-diffusion is especially sensitive to temperature because of its large size; iron strongly depends on **oxidation state** of the system, Fe^{3+} diffusing slower than Fe^{2+} [Cherniak, 2010].

Larger trivalent REEs often need vacancies to diffuse, which goes best in a rock with low anorthite content. Since albite has a more flexible **crystal structure**, diffusion is faster in it. In general, alkali ion mobility depends on the size of sites available in the crystal, smaller ions diffusing easier ($D_{Li} > D_{Na} > D_{Rb} > D_K$). The presence of F usually increases diffusion of all components because it creates dislocations or holes in the structure for the ions to jump to [Cherniak, 2010].

When it comes to tetrahedrally coordinated atoms, water presence is vital for diffusion rates. **pH** and oxidation state as well as water pressure influence bond strengths; an obstacle that is not inhibiting for other cations. Because water lowers the bond strengths, it is likely that another mechanism than diffusion (such as dissolution) takes over in the release of these atoms. Si bond rupture is often the rate limiting step.

In general, interdiffusion is slower than single atom diffusion because it is limited by the slowest step and needs two bond breaking events [Cherniak, 2010]. Interdiffusion of K and Na which occurs during perthite formation increases when the mineral compositions converge towards endmember compositions, moving against the concentration gradient. This shows that diffusion

depends on the chemical potential gradient which results in a concentration gradient, the latter (often observed as the driving force) being overruled in order to reduce the Gibbs free energy [Zhang, 2010]. This process is especially sensitive to temperature changes and not to the presence of water. However, pure Al-Si interdiffusion is facilitated by water in the structure which points to another mechanism taking over the exchange process; H^+ presence is very important for CaAl-NaSi and Al-Si interdiffusion [Cherniak, 2010]. The role of H^+ will be discussed in more detail in section *3.2.6* which deals with dissolution kinetics.

3.1.3 Grain boundary diffusion

Grain boundaries have a less strict crystallographic structure, making diffusion much easier and thus faster. Diffusion rates along grain boundaries are similar for all ions while lattice diffusion varies in orders of magnitude and is often anisotropic. This shows that at grain boundaries, diffusion is no longer limited by atomic properties such as size and charge or by bonding energy. Instead, enough space is present for all atoms to diffuse and kinetics of fluid transport take over; diffusion rates depend on width δ of the boundary through which fluids can flow [Dohmen and Milke, 2010]. Because of the open structure, boundaries may be richer in incompatible elements. H^+ is incompatible and concentrates along boundaries, making diffusion in feldspars even easier because of weakened bonds by protonation. At large time scales, diffusion can also go through grains, which is called volume diffusion; at smaller time scales however this is uncommon and such textures should be explained by dissolution.

3.2 Dissolution-precipitation

3.2.1 Basics and characteristics of the mechanism

Out-of-equilibrium systems will re-equilibrate in contact with a fluid, based on reduction of free energy. Not only entropy differences (driving diffusion) can cause mass transport, but also changes in chemical potential or surface energy which results in dissolution. Equilibrium constants can be determined, approximating the system and exploring what reactions should occur. However, kinetics should be favourable for this process in order to cause replacement. The mechanism of re-equilibration is driven by dissolution and precipitation, which can be closely coupled through surface kinetics. This results in epitaxial growth if crystal structures are similar [Xia *et al.*, 2009], for example in the KBr-KCl system [Putnis and Putnis, 2007]. An energy decrease can be realised by grain coarsening; the lower surface:volume ratio results in a smaller surface energy. This contributes to the total energy of the system and free energy reduction decreases solubility. Another way to reduce surface energy is by porosity generation. This feature is vital for reaction progress because it alters rock permeability and facilitates fluid infiltration. Porosity is created during the reaction by differences in solubility between parent and daughter or differences in volume (which are negligible in feldspar-feldspar replacement). The extent of porosity can be used as a textural indicator for fluid-rock interaction, marking the boundary between infiltrated and pristine domains. However, pores can be filled later on [Putnis *et al.*, 2005].

In mass balance calculations concerning feldspars, aluminium is considered immobile in metasomatic reactions. However, this would increase the volume, which does not coincide with pseudomorphic textures observed by Hövelmann *et al.* (2010), so no component may be considered truly immobile. Element input is necessary in replacement reactions, meaning that on a small scale the system is always open, even when at a large scale it may be closed. In the above situation, Al is said to form a complex with alkalis before they are released. The kinetics will be discussed in more detail in section *3.2.6*.

Early feldspar equilibration experiments with a chloride-bearing solution by Wyart and Sabatier (1958), Orville (1962, 1963) and O'Neil and Taylor (1967) found that oxygen isotope equilibration accompanied cation exchange, showing that the entire structure was broken down and rebuilt. These last

authors predicted a small gap at the interface between parent and daughter, which was confirmed only lately with modern techniques (Raman spectroscopy) by Niedermeier *et al.* (2009). Labotka *et al.* (2004) additionally observed a very sharp reaction front, replacement being induced by KCl fluid addition at 600 °C. A thin fluid layer at the boundary is found to actually host the reaction, its composition being the factor that controls the precipitating phase [Putnis and Mezger, 2004; Putnis *et al.*, 2005]. Engvik *et al.* (2009) examined the structure of the daughter albite, which appeared to be porous and contains numerous dislocations.

Characteristics of the dissolution-precipitation mechanism thus involve: (1) close coupling between the two processes, (2) a sharp reaction front, (3) porosity generation, with possibly (4) an epitactic relationship between daughter and parent or volume increase with reaction-induced fracturing. Microstructures show competition between thermodynamics of reducing energy and kinetics of the process. Small differences in free energy are enough to cause disequilibrium and can result in pervasive alteration in large parts of the crust [Putnis, 2009], the reaction proceeding by a continuous contact with the fresh rock. Albitisation is thought to proceed through this process. Because the dissolution-precipitation mechanism coincides with observed textures and allows fluid to move through rock, it will be discussed in more detail in this study.

3.2.2 Fluid pathways and reactive transport

Transport in porous rocks involves advection (active movement by a medium), (molecular) diffusion, mechanical dispersion (spreading a drop in a large pond) and fluid-solid reactions such as dissolution and precipitation. For all processes, the slowest step is rate limiting; transport-controlled reactions show a leached layer because of fast (when compared to diffusion) removal from the surface while surface-reaction-controlled reactions do not [Schott *et al.*, 2009]. In the presence of a fluid phase, mass transport can go through pores or fractures as well as along grain boundaries. Because these pathways are never straight, tortuosity must be introduced as a measure for the actual length of a path in the rock given by $\frac{L}{L_e}$, dividing distance L over the actual path length L_e. This factor is always smaller than 1, decreasing the actual transport rates in all mechanisms. Because of the generated porosity during dissolution-precipitation, the fluid creates its own pathway and the focus will

be on this way of infiltration.

Fluid flow is not possible in very narrow or unconnected pores, making the rock impermeable. Monolayers (0.5 nm) of adsorbed H_2O or CO_2 may be present but fluid cannot move normally. So for flow and fluid connectivity, pore geometry is a key factor. Fluid wettability (the ability to form a connected network) is related to surface energy of the fluid-solid and solid-solid interface between grains. This free energy regulates the dihedral angle between two wetting surfaces which determines whether fluid droplets will be connected or not. With a fluid presence of 1% of the rock volume, a dihedral angle $\theta < 60°$ will allow the fluid to penetrate further and wet the whole boundary; if not, the fluid occurs as isolated droplets [fig. 4, Watson *et al.*, 1990]. Fluid chemistry affects surface free energy, so ions in solution can cause the dihedral angle to decline, as well as reduced temperatures [Philpotts and Ague, 2009]. Mass transport through connected fluid channels is limited by grain boundary diffusion rates of material into the boundary [Thompson, 1983].

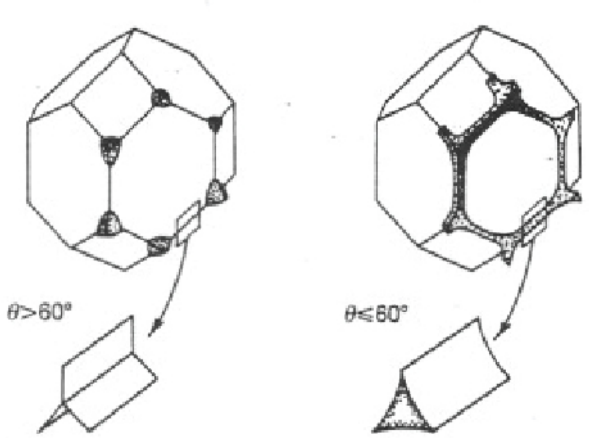

Figure 4: Fluid distribution along one single grain, showing the effect of wettability angle θ. At a large angle (left), fluid occurs in isolated pockets while at a smaller angle (right), these pockets become interconnected and form a network. Image from Watson et al., 1990.

But why would fluids move through rock in the first place? Fluid flow is caused by a gradient, which can be in parameters related to fluid and rock composition, or external parameters such as pressure and temperature. Flow due to a pressure gradient is described by Darcy's law:

$$J_z = -\frac{k}{\eta}[\frac{\partial P}{\partial z} + \rho_f g] \quad (2)$$

which includes permeability k, viscosity η, a pressure gradient, gravity and density of the fluid. The actual flow rate is larger than the flux J since fluid moves in a much smaller area (pores only). A pressure gradient may be caused by convection close to rift settings [Norton and Dutrow, 2001], or by lithostatic pressures at depth, favouring flow to the surface [Philpotts and Ague, 2009].

When flow results from a compositional gradient, Fick's first law for diffusion is often used (see Eq. 1). Particle concentrations in the fluid change over time and the flux of elements changes with distance: $\frac{\partial C}{\partial t} = \frac{\partial J}{\partial x}$. Strictly speaking, this formula only applies in a perfect dilute system with uncharged particles. Because this is never truly the case, electrochemical potential must be included in the gradient that causes the flux: $J_i^{migr} = -z_i u_i F C_i \frac{\partial \phi}{\partial x}$ with ϕ being electrochemical potential, F is the Farraday's constant and u is species mobility; z is charge of the particle. Even without an electric current, a potential gradient can still exist [Steefel and Maher, 2009]. For feldspars, electrochemical potential is important because of the great flux in H^+. If H^+ diffuses faster, it facilitates cation exchange which increases feldspar dissolution rates [Steefel *et al.*, 2007].

Often, reactions change over time because physical properties of the porous rock are affected by it. In this case, the reaction progress becomes coupled to transport and we speak of reactive transport. In modelling this, a very small area dx is considered, with a concentration gradient that forms during the reaction. Time is an important factor because when the reaction proceeds, parameters such as porosity and permeability will be affected. To see whether surface or transport processes are rate limiting for the ongoing reactions, transport times are divided over reaction times, $\frac{t_{tr}}{t_{react}}$ which is called the Damköhler number and includes factors such as porosity, solubility and reactive surface area. At high values, transport is rate controlling. This is often observed in the more distant parts of a system, far away from large pores or cracks, where connectivity is bad and transport is slow (see plagioclase example in Oelkers *et al.*, 1994). Next to large pores however, surface reactions can become rate limiting. These systems are hard to model correctly due to continuously changing parameters such as rock porosity, permeability

and fluid composition at the interface. Instead, reaction rates are obtained by looking at concentration profiles observed in minerals or solutions during an experiment [Steefel and Maher, 2009].

3.2.3 Driving force and initial concept of geochemical reactions

When a fluid is in contact with a rock, re-equilibration occurs. These reactions in geochemical systems are based on the second law of thermodynamics: obtaining the lowest energy state, defined as Gibbs free energy G. Changes in this energy can be caused by changes in the condition of the system:

$$dG = V\,dP - S\,dT\Sigma_{i=1}^{k}\mu_i\,dN_i \tag{3}$$

where V is the volume of rock, P is pressure of the system, S is entropy, μ is chemical potential of an ion in solution and N stands for the number of ions present. When external parameters such as pressure and temperature are fixed, reactions depend on the chemical components of the system only, represented by the last term in the equation. In calculations, a hypothetical standard state is used as a reference to the current state, for which the thermodynamic properties are well-defined. For mineral reactions, stoichiometry of the several components is taken into account. The number of components as well as variable pressure and temperature define the freedom of the system (Gibbs phase rule); equilibrium is defined by univariant lines in a diagram and can only change one parameter at the time.

However, aqueous solutions are less easy to analyse because the chemical components present are not always known. Additionally, extra parameters such as density and molal volume (dependent on ionic radius, ionization constant of the species and the dielectric constant) have to be taken into account [Oelkers *et al.*, 2009]. Solutions are assumed to be infinite-dilute so that they behave like a gas with a standard state molality of 1 mol/kg; in this case, component activity a will be very close to its concentration c. This activity is important to define a species reactivity in solution, which is quantified using the chemical potential μ [Langmuir, 1997] and activity coefficients γ as

$$\mu_i = \mu_i^0 + RTln(\gamma_i c_i) \tag{4}$$

The standard molality for a solution has a standard free energy $\Delta G_r^0 = \Sigma n_{i,r}\Delta G_{r,i}^0$ which represents the sum of all chemical components; they are all

separately influenced by entropy, heat capacity and PT-conditions [Helgeson *et al.*, 1978].

3.2.4 Feldspar equilibrium reactions: solid-solution in contact with aqueous solution

For the reaction of a solid with a liquid, elements A and B are exchanged as

$$AB_s \rightleftharpoons A_{aq}^{n+} + B_{aq}^{n-} \tag{5}$$

with an equilibrium constant $K = \dfrac{A_n B_n}{a_{AB}}$, the activity a_{AB} being 1 because it represents the solid phase activity in a fluid. Often, mineral systems are not that simple in their components. Minerals can have an alternating composition, allowing several types of cations to occupy one lattice site. Feldspar is the most common example of such a solid-solution. Exchange reactions between a solution and this solid will cause new growth of purer phases by a dissolution-recrystallisation mechanism, separating the different cations based on their activity in a solution. To represent this, a mixture of CA and BA mineral phases will be considered that is in contact with a solution carrying soluble C^{n+}, B^{n+} and some A^{n-}.

In this case, equilibrium conditions of two systems (for both components) must be considered, each with their own thermodynamic solubility product K_i. Activity of a single component is not 1 but all components of the solid solution together are 1. They are defined by $a_{AB} = \gamma_{AB}\dfrac{X_{AB}}{X_{AB}^0}$ as mole fraction of each component in the solid phase and the activity coefficient of it. The free energy of the system is also dependent on mole fractions as $G_M = X_{BA}G_{BA} + X_{CA}G_{CA}$. The total change in energy at unmixing of the system is given by

$$G_{solid-solution} - G_{mixture} = \Delta G = \Delta H - T\Delta S \tag{6}$$

In an ideal solid solution, collisions between all atom types are the same and $\Delta H = 0$ so there is no excess enthalpy, which implies perfect randomness. Then, chemical potential of components is directly linked to their concentration in the system. However, no solution is truly ideal and atomic distribution is never purely random. In that case, the chemical potential is related to activity, only linked to concentration through an activity coefficient (see Eq. 4) which is different for every species. Since solubility of components is linked to activity, the same problem arises. To determine the total activity and

total solubility products, the product of activity coefficients and equilibrium constants for each composition must be summed [Lippmann, 1980]:

$$\Sigma\Pi = ([B^{n+}][C^{n+}])[A^{n-}] \tag{7}$$

where Π is the solubility product and $[X^n]$ represents the activity of component X in the solution. This formula represents the solidus line (solid phase composition, see Fig. 3). At equilibrium, this product is defined by $\Sigma\Pi_{eq} = a_{BA}K_{BA} + a_{CA}K_{CA}$ with activity a_i defined by $X_i\gamma_i$ (eq. 4). The solutus line (or solution composition, represented by liquidus line in a magmatic system in Fig. 3) defines the total solubility product as a function not of concentration fraction X_{BA} but of activity fraction $X_{BA,aq}$ in the solution. At stoichiometric uptake, where the ion ratios are the same in liquid and solid, equilibrium is defined by $\Omega = \dfrac{Q}{[K_{BA}\gamma_{BA}X_{BA}][K_{CA}\gamma_{CA}X_{CA}]}$, the denominator being equal to $\Sigma\Pi$ at stoichiometric dissolution and the numerator being equal to the activity product Q. At $\Omega = 1$, there is equilibrium while at $\Omega < 1$, the crystal dissolves congruently, decreasing the free energy of the system [Prieto, 2009].

For ion partitioning between the solid and fluid phase, equilibrium is given by $K_D = \dfrac{a_{BA}[C^{n+}]}{a_{CA}[B^{n+}]}$. Big differences in uptake lead to a large gap between solidus and solutus [Prieto, 2009]. If no ideal solution exists and the enthalpy of the system decreases at B-C collision, a tendency towards ordering means that unmixing is favoured, the pure endmembers being the most stable state. Solid solutions with negative enthalpy are less easily dissolved because their unmixed state is energetically stable [Böttcher, 1997a].

3.2.5 Kinetics of dissolution

Sometimes the thermodynamic approach fails to predict mineral replacements and a more soluble component is kinetically favoured to precipitate [Pina and Putnis, 2002] because of its high abundance and the more likely collisions. The equilibrium approach is thus hypothetical; in practice, other processes (like interfacial tension to facilitate nucleation) may overrule them. Lasaga (1984) even found that despite supersaturation of a mineral in the solution, precipitation may not occur at all due to (surface) kinetics. The well-known 'partial equilibrium' assumption of Helgeson (1971), which states that kinetics are infinitely fast and reactions are only limited by saturation

and pH, is thus not always justified. Lu *et al.* (2013) found the same when a CO_2-rich fluid was supersaturated in some minerals but precipitation was inhibited; CO_2 may either have altered the surface reaction with cation complexes or pH changes may have inhibited reactions. So next to changes in free energy, kinetics are crucial for replacement reactions. Especially for near-equilibrium conditions, the reaction path linked to kinetics may play a vital role for activity-activity diagrams [Lasaga *et al.*, 1994]. This approach involves step-like breakdown, each step depending on energy.

Feldspar dissolution (and precipitation) rates can be given as $\frac{dn_{feldspar}}{dt} = -\frac{d\xi}{dt}$ with ξ is reaction progress [Lasaga *et al.*, 1994]. All mass is said to be transferred by this mechanism; solid state mineral reactions are orders of magnitude slower. If R_i relates to the net rate of dissolution or precipitation of a mineral, $\frac{dn_{new}}{d\xi} = \frac{R_{new}}{R_{old}}$; R_i close to equilibrium is defined by $k_i(\Delta G_i/RT)$ where k involves reactive surface of the mineral and ΔG is the net free energy change of a reaction; the other parameters are constants [Lasaga, 1984]. This relationship holds for both dissolution and precipitation (only if ΔG is not extremely large). The ratio $\frac{k_{diss}}{k_{prec}}$ determines the shape of the activity-activity diagram. When the ratio is large, mineral activity is fully determined by kinetics and mass transfer is similar to the equilibrium case (all feldspar dissolved in the beginning). When the ratio decreases, metastability becomes normal and minerals can occur outside their stability field and coexist with a new phase for a while. Only when another mineral starts to grow, it disappears; apparently, the mineral sequence becomes more sensitive to kinetics than to fluid composition and equilibrium.

Berner and Holdren (1977) showed that cation exchange roughened the interface, which increases the surface in contact with the fluid. Since surface area stands for the amount of loose bonds and directly relates to free energy, small grains would allow a larger deviation from equilibrium when kinetics are rate-limiting. Reaction rate is given by Lasaga *et al.* (1994) as

$$R = k_0 A_{min} e^{(-E_n/RT)} a_{H+}^{nH} \Pi a_i^{ni} f(\Delta G_r) \tag{8}$$

with A is reactive surface area (including surface roughness), E_n is the activation energy, a is ion activity and if $f(0)$=0, so without free energy change, the reaction is at equilibrium at a net rate of 0. The linear relation between surface and reaction rate shows that the process is surface-controlled.

Negative change results in dissolution (undersaturation), a positive one in precipitation (supersaturation). At very negative values of ΔG, dissolution rates go to a constant value for far-from-equilibrium conditions as can be seen in $f(\Delta G) = -[1 - e^{(\Delta G/RT)}]$ [Lasaga, 1981; Aagaard and Helgeson, 1982]. Near equilibrium though, the function is found to be linearly dependent on ΔG. When dislocations are located on the surface, a new mineral precipitates there and $f(\Delta G) = [e^{(\Delta G/RT)}]^2$ [Blum and Lasaga, 1987]; near equilibrium, the system will depend on $(\Delta G)^2$. Under these conditions, dislocation density effects are also the biggest [Blum *et al.*, 1990]. However, later surface studies revealed that the connection between rate and reactive surface is in fact not linear but more complex:

$$r = kS|1 - (\frac{Q}{K})^p|^q \tag{9}$$

where S is surface area, Q is activity quotient and K is equilibrium constant [Burch *et al.*, 1993; Alekseyev *et al.*, 1997]. Of course, the actual mechanism of re-equilibration relies on interplay between reduction of free energy and reaction kinetics.

3.2.6 Surface processes: the actual mechanisms of cation exchange

In the lab, no near-equilibrium experiments are executed, because they are slow and often stop. Instead, extrapolation of far-from-equilibrium conditions is used. One of these extrapolation techniques is the Transition State Theory [Lasaga, 1981] which focuses on the molecular configuration at the surface. Reaction rates depend on the presence of an activation complex [Eyring, 1935] at this surface: $r' = k_{AB'}$ with r' is the forward reaction rate, k is a rate constant and [AB'] is the concentration of the particular species at the surface needed for reaction. Because this provides a direct link between kinetics and thermodynamics, reaction rates can also be expressed in terms of free energy [Lasaga, 1981; Aagaard and Helgeson, 1982]:

$$r = r'[1 - e^{(\Delta G/\sigma RT)}] \tag{10}$$

The theory works quite well, but for every reaction, this stoichiometrically correct activation complex should be found, denoted as a σ factor in the exponential term which linearly relates to free energy difference between aqueous and solid phase and stability of the surface complex [Schott *et al.*, 2009].

Because of electrostatic potential, protons from the water adsorb to metal ions (in feldspars these are Si and Al) and form activation complexes [Stumm *et al.*, 1983]. Adsorption is a surface process by which a mineral component (sorbent) takes up a component from the solution (sorbate) and forms a connection. This can be an actual bond to one site or bond to a layer; in the latter it maintains its mobility. Either way, the particles are taken up into the crystal surface monolayer in which the site number density determines the amount of spots available. Different sites are available to different sorbates, depending on size and charge, resulting in different sorbate residence times in the layer. When a large surface area is present and the solution is dilute, relation with sorbate concentration is linear [Kulik, 2009]. Adsorption affects solubility because it changes interfacial free energy and surface area which is the driving force for dissolution [Parks, 1990]. Differences in initial surface energy can thus create points of concentrated dissolution, or etch pits. In such a point, all elements are released quickly due to the high amount of dislocations [Burch *et al.*, 1993; Blum and Lasaga, 1987]. However, the features are a point of debate, since no evidence is found in measured rates and strains [Casey *et al.*, 1988 and others].

Adsorption thus provides bond weakening by formation of silanol (OH) complexes, which is the first step of cation release. The second step is hydrolysis which breaks the bonds and releases the metals. The latter stage is rate controlling for the entire reaction. Both steps are induced by dissolved H^+, explaining the roughly linear relationship between reaction rate and hydrogen activity [Lasaga, 1990]. Most minerals have more than one type of bonds to break, all metals having a specific reactivity depending on their configuration. This reactivity is changed by proton adoption [Sherman, 2009]. Since all bonds have their own rate of breaking, a leached layer is often observed. This can be explained by preferred leaching (non-stoichiometric dissolution) of weakly bond elements [Schott *et al.*, 2012]. Incongruent dissolution is common under far-from-equilibrium conditions [Helgeson *et al.*, 1984] and is caused by a balance between fluid composition and ions in the mineral (and their solubility). Feldspars often show Al-depletion at the surface; 3 protons are needed to break it free [Oelkers *et al.*, 2009]. At the interface of a leached layer and the parent- or daughter-mineral, Hellmann *et al.* (2003) found a sharp chemical profile, suggesting that no diffusion from grain to edge occurred and that the leached layer purely formed by incongruent dissolution. The slowest dissolving cation keeps the lattice structure together. Because of variable compositions, perthitic feldspar shows internal variation

in dissolution rate, albite dissolving the fastest [Helgeson *et al.*, 1984; Lee and Parsons, 1995]. Oelkers (2001) uses the incongruent dissolution theory to make a multiple-step overview of mineral dissolution. For feldspars, first univalent cations are exchanged with H^+, after which protons start to attack Al and least of all Si. At neutral to high pH, no preferential dissolution occurs [Hamilton *et al.*, 2001; Hellmann *et al.*, 2003]. At low pH, however, higher charged ions are relatively harder to release, making dissolution incongruent. pH also has effects on which aqueous phases will form. Especially for aluminium (and slightly for silica), different binding states with $(OH)^-$ or H^+ provided by the fluid are possible [Arnórsson and Stefánsson, 1999]. Reaction rates thus depend on activity of both protons in solution and metals in the mineral, the latter being the most important.

Another way to interpret the quartz-rich leached layer is as a precipitate [Ruiz-Agudo *et al.*, 2012]. These authors discovered etch pits below the 'leached layer', suggesting that the dissolving surface was covered by a precipitate of quartz. This reduced the reactive surface and slowed the reaction down. Although the bulk fluid was undersaturated in SiO_2, the fluid-mineral interface was oversaturated in it, causing quartz precipitation. The importance of the chemistry of the fluid boundary layer was also noted by Putnis and Mezger (2004) in KBr-KCl mineral replacement.

In fluid-silicate systems, activity of water and ions in a fluid is reduced by CO_2-addition and increased at chlorine addition, higher pressures and temperatures. With increasing temperature, the amount of dissolved Na decreases and K increases. Upon heating, sodic phases will precipitate and K-rich phases will be consumed (Na/K in rock increases) [Philpotts and Ague, 2009]. This is albitisation. Temperature dependence of dissolution rates is visible in activation energy, which depends on temperature in two ways: contribution of enthalpy (ΔH) on formation of proper surface reaction sites and activation energy of the particular activation complex [Schott *et al.*, 2009].

Often, mainly the aluminium content is used to determine feldspar dissolution rates, especially under far-from-equilibrium conditions [Chou and Wollast, 1985; Oelkers *et al.*, 1994; Oelkers, 2001]; reaction rates increase when Al content decreases. Dissolution rates depend on chemical affinity and have an inverse relationship with dissolved Al-concentrations. This is different for anorthite [Oelkers and Schott, 1995] because the Si:Al ratio is 1, meaning that Si-O bridging bonds do not have to be broken [Schott *et al.*, 2009]. Lattice distortion (Al-O bonds become stretched while Si-O bonds

are shortened) allows fluids to penetrate deep in the crystal [Criscenti *et al.*, 2005], speeding up the process.

3.2.7 Feldspar dissolution rates

Surface kinetics, thus, show that dissolution rates depend on many factors. Previous studies have experimentally determined feldspar dissolution rates under different PT-conditions and pH. One of the first workers to show pH dependence at low temperature albite dissolution were Chou and Wollast (1985); they showed that at neutral pH (4–8) dissolution was much slower (fig. 5a). At slightly higher temperatures of 70 °C, all dissolution rates were a factor 10 faster. The paper of White *et al.* (2001) provides a feldspar dissolution database at low temperature and pressure (table 1), showing similar pH dependence for K-feldspar with dissolution rates ten times as slow as for albite. Oligoclase shows a flattening at high pH, dissolution rates remaining low (fig. 5b, Oxburgh *et al.*, 1994). Lu *et al.* (2013) have shown that at much higher temperatures of 200 °C and 300 bars, albite stays soluble for a longer time than K-feldspar (table 2). This explains the preferred dissolution of albitic lamellae (observed by Parsons and Lee, 2009 among others).

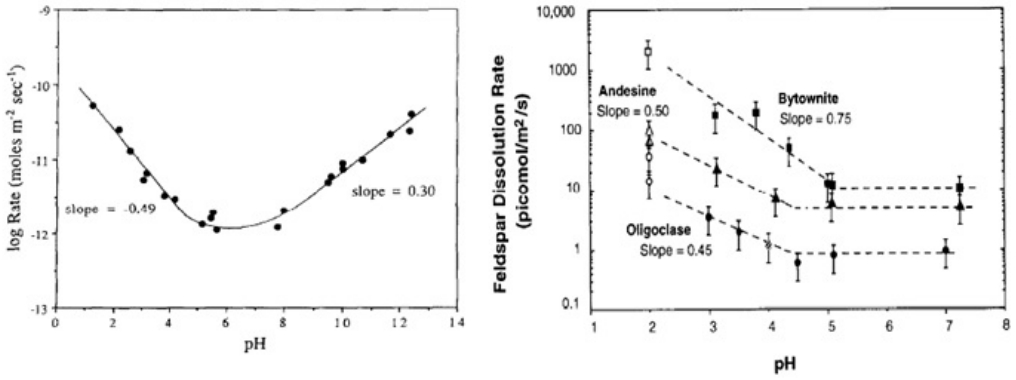

Figure 5: a) Dissolution rate of albite as a function of pH [Chou and Wollast, 1985]; b) Feldspar dissolution rates as a function of pH [Oxburgh et al., 1994].

The presence of Cl^- in solution (table 2) does not show a marked increase in dissolution rates that is mentioned before by Philpotts and Ague (2009) but it means that more ions can be carried in dissolution before precipitation starts.

Table 1: Feldspar dissolution rates at low pressure and temperature [White et al., 2001]

Mineral	**Temperature** (°C)	**Pressure (bars)**	**pH**	**Dissolution rate** ($moles/m^2/s$)	**Reference**
Albite	25	1	4	$5 * 10^{12}$	Knauss and
			5	$3 * 10^{12}$	Wolery, 1986
			6	$1 * 10^{12}$	
			8	$3 * 10^{12}$	
			9	$9 * 10^{11}$	
			10	$7 * 10^{11}$	
Albite	70	1	4.11	$1 * 10^{11}$	Knauss and
			7.80	$1 * 10^{11}$	Wolery, 1986
			9.59	$7 * 10^{10}$	
			10.77	$1 * 10^{10}$	
Albite	80	1	3	$3 * 10^{12}$	Burch *et al.*,
			8	$4 * 10^{11}$	1993
Oligoclase	25	1	2	$1 * 10^{11}$	Casey *et al.*,
			3	$3 * 10^{12}$	1991
			4	$1 * 10^{12}$	Oxburgh *et al.*,
			5	$1 * 10^{12}$	1994
			7	$1 * 10^{12}$	

Table 2: Feldspar dissolution rates at higher pressures and temperatures (from: Lu et al., 2013)

Mineral	**Temperature** (°C)	**Pressure (bars)**	**pH**	**Dissolution rate** ($logmol/m^2/s$)
Anorthite	150	4.8	4.56	-7.23
		5.3		-6.77
		6		-6.66
Albite	100	5.8	3.99	-9.43
	150	6.7	4.59	-8.55
	200	2.63	5.44	-8.83
		7.15	4.80	-8.43
		26.2	4.70	-8.56
Labradorite	200	7.1	4.88	-8.48
	100	1	3.19	-8.34
Alkali feldspar in KCl solution	200	300	4	-8.64
Alkali feldspar in NaCl solution	200	300	5	-8.98
Albite in NaCl	150	300	3.7	-9.62

3.2.8 Saturation index

When the reaction proceeds and transport processes do not remove all dissolved ions, the system goes towards equilibrium and most minerals go towards congruent or stoichiometric dissolution; this means that ratios between components are the same in the fluid as in the dissolving mineral. Because the line of stoichiometric saturation lies above the solutus in a Lippmann diagram, it is closer to supersaturation in a particular mineral phase, which will cause a precipitate if kinetics allow it. Saturation state is often used to define the solubility status of a component to define whether dissolution or precipitation will occur. The saturation index Ω is defined as the Ion Activity Product Q (or IAP) divided over the equilibrium constant K_{BA}; increased activity causes easier incorporation in the precipitating phase. At $\Omega < 1$, a solution is undersaturated which usually leads to dissolution. IAP can be linked to chemical affinity, $A = -RTln(Q/K) = -RTln(\Omega)$. This affinity A, positive at undersaturation, represents the energy difference between reactants and products. Another way to denote dissolution of mineral BA in terms of free energy change is given by

$$\Delta G_{BA} = \Delta G^0_{BA} + RTln\frac{[B^{n+}][A^{n-}]}{a_{BA}} \tag{11}$$

where $\Delta G_{BA} > 0$ means mineral growth. Both the kinetic (saturation) and thermodynamic (energy) approach are useful in some cases [Prieto, 2009]. The study of Burch *et al.* (1993) has analysed changes in dissolution related to undersaturation, showing rapid dissolution far from equilibrium, and stoichiometric element uptake at both acidic and basic fluids. The stoichiometric release implies that none of these elements really inhibits the dissolution reaction as it continues, but that the surface remains free to release ions.

3.2.9 Precipitation kinetics

When the concentration of components in a solution reaches the saturation limit, the fluid is oversaturated in one mineral and at nucleation (favourable kinetics), a precipitate will form. Nucleation is the first step in mineral precipitation, which starts with very small points, where the surface free energy is of major importance. For a nucleus to form, surface and volume effects compete. The theory used to describe nucleation here is the Classical (or capillary) Nucleation Theory of Adamson (1960; Markov, 1995). During

nucleation, $\Delta G = -nk_BTlnI + 4\pi\rho^2\sigma$, the first term representing the change in chemical potentials in the fluid and solid phase of n growth units. If this is negative, Gibbs free energy is at its maximum value (about 1/3 of the surface energy), so the infinite solid phase is stable. However, particles are never infinite, and the second term includes these surface effects. Nuclei are formed and resorbed randomly, their probability to grow depends on the amount of nuclei. When their number per volume exceeds I_c, nucleation increases rapidly. The next step is growth, which is limited by either surface kinetics or diffusion to supply particles. Due to a higher relative surface area, smaller particles are more soluble and can dissolve to re-precipitate on bigger crystals [Lifshitz and Slyozov, 1961]. This coarsening process is called Oswald ripening and can affect all small particles, from crystals to liquid droplets and pores. Growth of two similar minerals can also occur, which causes competition at the available sites at the nucleus; the more soluble of the two often stays in solution longer [Fritz and Noguera, 2009].

3.2.10 Coupled dissolution-precipitation

In some cases, the daughter mineral keeps the shape of the parent, which is called epitaxial overgrowth. It is most likely in replacement by a mineral with a similar crystal structure, because of similar lattice sites for the new phase to bind ions to. Interfacial energy at the dissolving surface is lowered [Putnis, 1992], making it easy for the dissolved ions to catch on and grow from there. This occurs in a thin fluid boundary layer [Putnis and Mezger, 2004] which can have a different composition than the rest of the fluid, and transport from here to the bulk fluid must be taken into account. Such an overgrowth shows that dissolution and precipitation are closely coupled in both space and time, meaning that nucleation must be rapid compared to dissolution.

In the early days, coupling between dissolution and precipitation was seen as a 'partial equilibrium state' [Helgeson, 1971]. In this, (1) feldspar dissolution is the rate limiting and irreversible process that drives the system, (2) precipitation is instantaneous, (3) the solution is in equilibrium or undersaturated in secondary phases all the time, and (4) according to the phase rule only three phases are present at each moment. However, more recent studies have shown that old minerals do not necessarily dissolve at fluid evolution under far-from-equilibrium conditions [Zhu *et al.*, 2004] and others have shown secondary minerals to be stable outside their stability

field [Lasaga *et al.*, 1994; Zhu and Lu, 2009]. The study of Alekseyev *et al.* (1993) closely describes different stages during albite dissolution accompanied by sanidine precipitation at 300 °C, 88 bars and a pH of 9.0. The coupled process starts at conditions far-from-equilibrium, when the solution is extremely low in ions from the rock and dissolution will occur rapidly. At this stage, free energy does not limit reaction rates but surface area is the controlling factor [Lasaga *et al.*, 1994]. Congruent dissolution will lead to a rapid increase in components in solution, which, with time, will continue until the saturation index of another mineral is reached. After nucleation, this mineral will precipitate which inhibits dissolution (also observed by Fu *et al.*, (2009) at different PT-conditions and pH) of the primary mineral by reducing its reactive surface area, and changes its Al:Si-ratio. As a result, dissolution becomes incongruent. Precipitation continues but lowers the saturation index of that secondary mineral, until it becomes controlled by dissolution to supply material [Alekseyev *et al.*, 1997]. Dissolution becomes congruent and increases again, now being directly linked to precipitation. This 'quasi-steady state' close to equilibrium is very sensitive to changes in free energy, making quick changes in precipitating phase likely at small ion activity shifts [Burch *et al.*, 1993]. Under these circumstances, minerals that are just out of equilibrium do not necessarily dissolve but may remain in metastable equilibrium with new growing phases [Lasaga *et al.*, 1994]. Zhu and Lu (2009) confirm by modelling that the secondary phase is not always in equilibrium with the fluid phase and that the phase may remain present in the rock after further fluid evolution. Clay precipitation causes solution composition to stay closer to feldspar, reducing the speed of dissolution [Zhu *et al.*, 2004; Ganor *et al.*, 2007]. Because of slow precipitation kinetics, a close inter-dependence between dissolution and precipitation exists [Lasaga, 1984], maintaining a steady state longer, as observed with clays. In the model of Zhu and Lu (2009), congruent feldspar dissolution acted as a limiting factor when the reaction was at steady state. Phases were found to precipitate after pressure and temperature conditions were no longer in the stability field of that particular mineral, which shows the strong coupling between dissolution and precipitation processes. The fluid was supersaturated in both phases the entire time. So the old partial equilibrium theory proposed by Helgeson is contradicted by not following saturation indices, deviating reaction paths leaving remnants, and secondary mineral paragenesis. The principle does hold, however, for faster equilibrating systems such as feldspar-water reactions at higher P and T conditions [Zhu and Lu, 2009].

3.2.11 Reaction paths

Reaction paths look at evolution of solution composition and mineral growth or reaction progress. Feldspar dissolution in contact with a pure solution without initial Si and Al is governed by the kinetic rate law, resulting in a mineral precipitation sequence upon dissolution [Fu *et al.*, 2009; Zhu and Lu, 2009; Zhu *et al.*, 2010]. This secondary mineral precipitation removes Si and Al form the solution, keeping up feldspar dissolution; a positive feedback loop is created with a weak compositional link. Lasaga (1981) and Steefel and Van Cappellen (1990) show deviations from the expected mineral growth evolution when precipitation is not instantaneous; this is not in partial equilibrium but at a 'quasi-steady state'. Models of Zhu and Lu (2009) between 90 °C and 300 °C for feldspars show also that partial equilibrium does not hold and that paragenesis of minerals can occur. Alekseyev *et al.* (1997) have shown that secondary mineral precipitation can slow down dissolution. So if not through composition, how are dissolution and precipitation coupled?

Helgeson *et al.* (1984) describe the principle of reactive surface area, which relates to available reactive surface sites [Furrer and Stumm, 1986]. Burch *et al.* (1993) have used this concept to explain the sigmoidal dependence of reaction rate on free energy change: two simultaneously occurring reaction mechanisms connect them, etch pits far-from-equilibrium and planar surface sites under near-equilibrium conditions. Because the etch pits idea is much debated, Oelkers (2001) and co-workers explained the sigmoidal graph by the surface process of cation removal to form an activated complex. Reaction rates are more likely influenced by free energy changes at low temperatures, where coupling of reactions is stronger, and opening of etch pits would require more negative free energy change at low temperatures [Zhu, 2009].

4 Analytical methods

Microstructural and qualitative chemical analysis of the samples was carried out on carbon coated thin sections using a JEOL JCM-6000 NeoScope Benchtop Scanning Electron Microscope with a thermionic electron gun. Backscattered electrons were imaged and energy dispersive X-ray analysis (EDS) was done using an accelerating voltage of 15kV. Quantitative chemical analysis was obtained using a JEOL JXA-8600 superprobe which did wavelength dispersive X-ray analysis (WDS). These two methods using X-rays are compared in the Appendix. Optical microscopy was done on a Leica DMRX light optical polarization microscope in combination with the program Image Analysis QWIN Pro.

Bulk rock quantitative analysis for major (>1 wt%) and minor (0.1–1 wt%) oxides was executed using a Thermo ARL 9400 sequential X-ray fluorescence (XRF) spectrometer, in which the detection limit lies at 100 ppm. The samples were ground to produce a crystal powder with grains of 1–2 μm in size, of which a glassy pearl was made for analysis. Trace elements (Rb, Sr, Y, Zr, Nb, Cs, Ba, La, Ce, Pr, Nd, Sm, Eu, Gd, Tb, Dy, Ho, Er, Tm, Yb, Lu, Hf, Ta, Pb, Th and U) were measured in an inductively coupled plasma mass spectrometer (ICP-MS). Of each sample, 125 mg was diluted in an acid of 2.5 mL 48% HF and 2.5 mL of 3:2 solution of 72% $HClO_4$: 65% HNO_3, heated to 90 °C and left over night. Then the samples were placed on a hotplate of 160 °C and dried to form a gel. To this, 25mL 4.5% HNO_3 was added and the sample was heated to 90 °C, after which analysis could be done.

Rock densities were determined by measuring the samples both dry and when submerged in water. The relative densities of dry and wet rock are coupled through the buoyancy force of the water pushing the sample up. Buoyancy relates to rock volume as it represents the weight of the displaced water. Thus, to calculate the relative density from two weight measurements, the dry weight was divided over the difference between dry and wet weight (which is the buoyancy force).

In situ X-ray tomography was done using a Phoenix X-ray nanotom micro CT-scan. The sample was rotated and every position was imaged using X-rays, which show density differences. These images were put together in the Volume Graphics software to create a 3D-image.

5 Results

5.1 Field descriptions

Larvikite rocks show discolouration in the field due to hydrothermal alteration. This is shown as a yellow, orange, red or even white replacement of the blue larvikite crystals. Figure 6 shows the rock appearance on different scales, from the reddening on a large scale (fig. 6a) to the sharp interface between altered and unaltered rock (fig. 6b) to even a grain scale discolouration (fig. 6c). Figure 6b also shows the interesting other features in the area such as fracturing and the previously mentioned formation of pseudotachylytes. In the appendix, photographs of six specimens that will be discussed in more detail are displayed. The grain scale discolouration of Figure 6c will be discussed in section *6.2*.

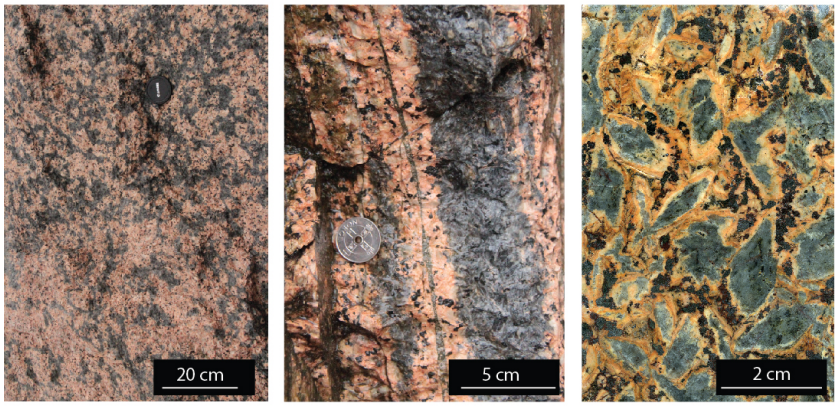

Figure 6: Field images of the larvikite/tønsbergite contact. a) Appearance of blue larvikite relics in side the reddish tønsbergite alteration; b) Closeup of the interface between the two rock types, showing a sharp contact and a thin pseudotachylyte right of the coin; c) Rock slab showing grain comsumption and the formation of a yellow/red and black precipitate.

5.2 Petrography

To describe the extent of hydrothermal fluid interacting with a rock, six samples have been studied, each displaying a different stage of alteration. They were collected from the area between Larvik and Tønsberg, in SE-Norway. Below a mineralogical and textural description of hand specimens and thin sections (if present) is given based on the order of degree of alteration. Photographs of all hand specimens are provided in the appendix.

- LT-3 is the most pristine larvikite. This rock has a porphyritic texture and consists for more than 90% of large, euhedral blue feldspar crystals with a grain size of 1–5 cm. In between, mm-sized grains of blue feldspar are present. The matrix also contains a few dark pyroxenes and Ti- and Fe-oxides. At the exposed surface of this rock, the sample appears weathered and there is a red discolouration between the feldspar crystals. Under the optical microscope, twins and perthites are observed in the feldspar crystals.

- LT-12-3 contains blue relics of the old feldspar ranging from 0.5–1 cm. In between, a fine grained white matrix can be observed which separates the feldspar grains. It makes up 50% of the sample and appears to occur in bands. In it, black minerals are present and no blue feldspars. The matrix is opaque under the optical microscope and displays some twins; on the edges next to feldspars, pumpellyite, Ti- and Fe-oxides are present.

- LT-1 shows 1 cm relics of the blue feldspars, surrounded by a light pink to orange discolouration. At the weathered surface of the rock, the feldspar alteration appears light green. The fresh surface shows that there are 2 areas: some relic crystals are light blue, and others light pink to almost white, with a greenish core, often slightly elongated. These areas appear as bands within the specimen. The very fine grained matrix (20%) around it is orange to red in colour and it runs in between the relics as a mm-thick band. A black, mm-scale shiny precipitate is also visible in the matrix between the feldspar relics (10%), sometimes accumulating in the same shape as the feldspar relics which make up 70% of the rock. Under an optical microscope, the orange parts appear cloudy while the relic is transparent. These two phases are intergrown with the maintenance of crystal structure (fig. 7).

- TØ-12-8 is similar in appearance to LT-1 but altered even more, displaying pink colours between small, light pink to white fragments of the old feldspar. The relics are up to 1 cm in diameter and in some, the core is also affected by the reddening. The matrix around the relics now is up to 0.5 mm thick and all relics have lost their blue colour. The same black precipitate is observed as in LT-1, where it is also located inside the feldspar relics and occurs as larger aggregates.

- TØ-12-9 is the most altered one, representing tønsbergite rock. It consists of a fine grained, porous red matrix with mm-scale minerals in which the 0.5–1 cm long elongated fragments of the old blue feldspar (20%) are separated by the reddish matrix. This relic feldspar is discoloured at the edges, going from pink at the contact with the matrix to green at the core. Thin fractures are visible with naked eye, being filled with a white/light blue precipitate. This calcite precipitate shows twins when viewed under the optical microscope. Cores of feldspar relics show cross-hatched twinning. The matrix contains some very small black minerals which do not form aggregates.

- LT-2A represents the syenitic intrusion found close to the larvikite rock. It is a fine grained igneous rock (grain size of 0.1–5 mm) consisting mainly of orange to reddish felsic minerals. At the contact with larvikite, this matrix is also present in between the 1–5 cm blue larvikite crystals and no discolouration is observed here; the syenitic structure appears to continue between the unzoned larvikite feldspars. The larvikite is somewhat fractured and shows a thin layer of orange discolouration at the edges. Under the optical microscope, the feldspars display twins. The same structure is observed as for LT-3 but now on a mm-scale.

5.3 Bulk rock compositions

Table 3 and Fig. 8 show results of the bulk rock analysis of all six samples described. The fact that the total of all compounds does not add up to 100% is due to Loss On Ignition (LOI), which is shown in the table. It accounts for the loss of volatile components such as water in micas or amphiboles upon sample preparation. When it is added to the total, all samples are within a 1.5% error for a 100% total.

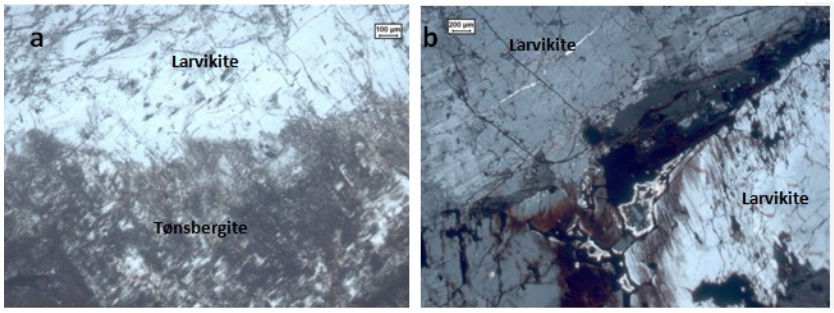

Figure 7: Feldspar replacement structures as viewed under the optical microscope. a) PPL image showing cloudiness where a fine grained porous feldspar grows next to bright larvikite; b) XL image of red discolouration growing along the twinning direction. Also, a rim is observed around the crystal between the two feldspars. The larvikite feldspar displays exsolution lamellae.

Major and minor oxide content is similar in all samples, showing no major element fluxes. The only deviating specimen is the syenite vein (sample LT-2A) with a higher SiO_2-percentage and lower Al_2O_3-content. Differences in these two oxides are caused by the different magmatic origin of syenite, which results in a higher amount of other minerals than feldspar and lower amount of alkali ions; in the other specimens, $CaO + Na_2O + K_2O$ is roughly constant around 14 wt%. Between $Na_2O + K_2O$ and CaO there is a negative correlation; also, CaO is positively coupled to Al_2O_3 (fig. 8a). Alkali oxides are the highest in sample LT-1; there appears to be no connection between these trends and degree of alteration.

An even better indicator for chemical change during alteration involves trace element analysis. Because of their low abundance, relative changes in trace elements appear large and fluid addition can cause notable changes in element ratios. Normalized Rare Earth Element patterns in the larvikites are shown in Fig. 9; chondrite normalization (fig. 9a) shows an increase of REE-content in the more altered samples. When compared to granitic rocks (fig. 9b), the curve is flat, which could be expected for an intermediate igneous rock. It closely resembles the granite pattern but has slightly higher values.

In both normalized graphs, all specimens show strikingly similar trends except for Eu, which is present in the same amount (approximately 4 parts per million) in all samples. To image this anomaly better, the expected value Eu* (lying on the trend line) is divided over the actual Eu-content

Table 3: Bulk rock composition (oxides in wt% , trace elements in ppm with a standard deviation of 9%)

Sample	**LT-3**	**LT-12-3**	**LT-1**	**TØ-12-8**	**TØ-12-9**	**LT-2A**
SiO_2	58.99	59.48	55.55	58.22	55.53	62.57
Al_2O_3	19.04	18.31	19.15	18.05	16.02	16.94
TiO_2	1.13	0.94	1.15	1.27	1.44	0.47
Fe_2O_3	5.68	3.98	5.57	5.25	6.59	4.04
MnO	0.13	0.13	0.1	0.15	0.2	0.1
CaO	4.77	3.27	6.31	3.75	4.43	3.34
MgO	1.3	0.96	1.27	1.11	1.67	1.07
Na_2O	5.1	6.27	5.75	6.11	5.44	5.4
K_2O	3.54	4.3	2.5	3.95	4.49	3.78
P_2O_5	0.53	0.31	0.53	0.49	0.45	0.48
Total	100.22	97.95	97.86	98.34	96.25	98.2
LOI	0.16	0.45	0.98	0.89	3.86	0.77
Density	2.69	2.64	2.68	2.70	2.65	2.65
Rb	113.4	90.9	46.3	114.2	122.5	158.5
Ba	1122.4	867.7	443.5	780.8	716.0	480.8
Th	15.2	12.4	9.0	9.3	23.9	27.0
U	4.3	3.4	2.5	2.5	7.1	8.1
Nb	164.4	149.1	103.4	153.3	207.6	124.7
Ta	10.0	9.0	6.8	9.1	13.0	8.9
La	117.0-	99.2	80.7	120.2	126.7	131.7
Ce	261.1	201.7	168.7	260.1	295.3	291.8
Pb	9.7	9.0	3.2	7.1	9.6	12.5
Pr	31.0	22.5	19.2	29.7	33.3	33.4
Nd	112.0	76.6	67.4	103.8	119.2	116.6
Sr	1260.0	591.5	948.4	668.5	326.0	720.7
Sm	19.3	12.5	11.1	16.8	20.8	20.0
Hf	6.2	6.0	4.9	5.5	28.0	5.2
Zr	201.8	181.2	181.4	176.8	1218.4	132.0
Eu	5.6	4.0	4.1	4.2	4.5	3.7
Gd	15.3	10.0	8.8	13.4	17.0	16.1
Tb	2.01	1.4	1.2	1.7	2.3	2.2
Dy	10.7	7.5	6.1	9.2	12.6	12.4
Ho	1.9	1.4	1.1	1.6	2.3	2.3
Y	46.7	34.2	27.0	40.7	56.3	59.2
Er	5.1	3.8	3.0	4.4	6.4	6.4
Tm	0.7	0.6	0.5	0.6	0.9	0.9
Yb	4.1	3.3	2.4	3.6	5.5	5.6
Lu	0.6	0.5	0.4	0.6	0.8	0.8

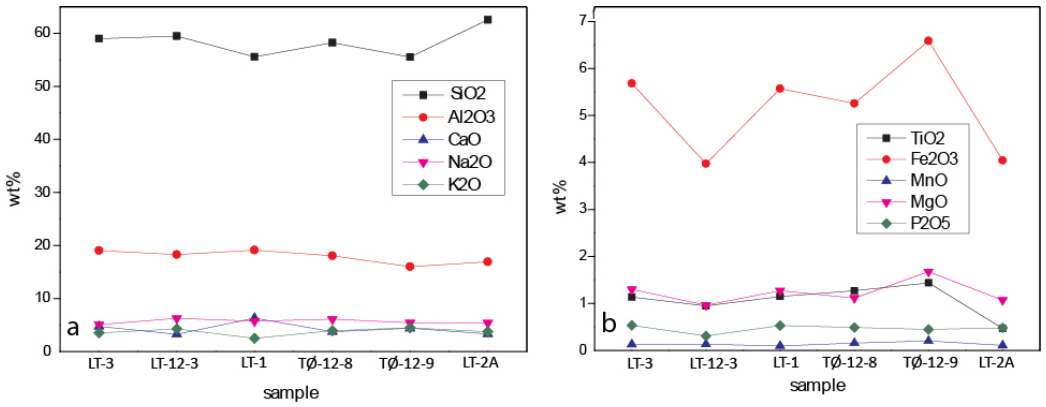

Figure 8: Major (a) and minor (b) element oxides displayed as weight percentages. Fe_2O_3 is displayed in the minor oxide graph since it is not a major constituent of feldspar.

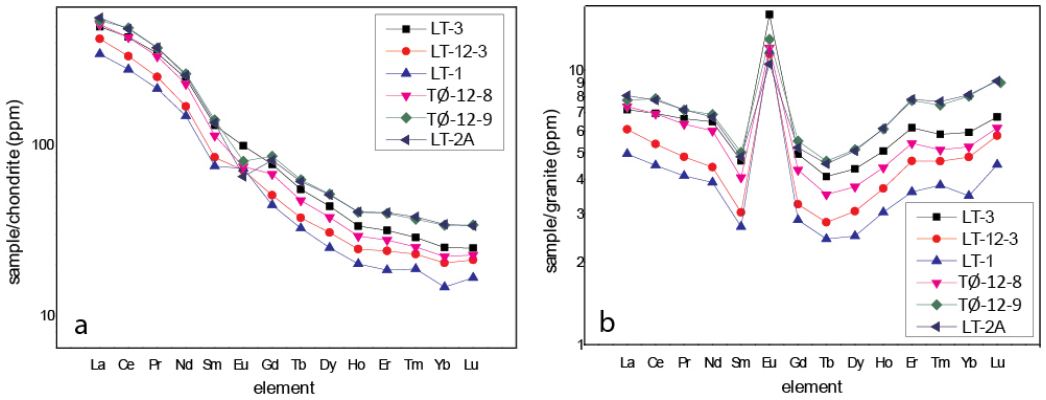

Figure 9: a) Chondrite normalized pattern, showing a clear Eu anomaly or the LT-1, TØ-12-8 and TØ-12-9 samples; b) Granite normalized data. The feldspar rocks of this study show a REE pattern that is comparable to that of the granite except for the Eu-anomaly. No change in REE pattern is observed with increasing degree of alteration.

(fig. 10a). The figure confirms that LT-12-3 and LT-1 have higher values than expected (positive anomalies) while other samples show values that are lower than expected. With the exception of specimen LT-1, a rough trend of Eu-decrease is observed with alteration.

To quantify the relative HREE enrichment observed in the chondrite normalized pattern, the Ce/Yb-ratio is plotted for each sample in Fig.10b. Ratios vary between 10 and 20, all showing a 10 times better incorporation of LREE (represented by Ce) than HREE (represented by Yb).

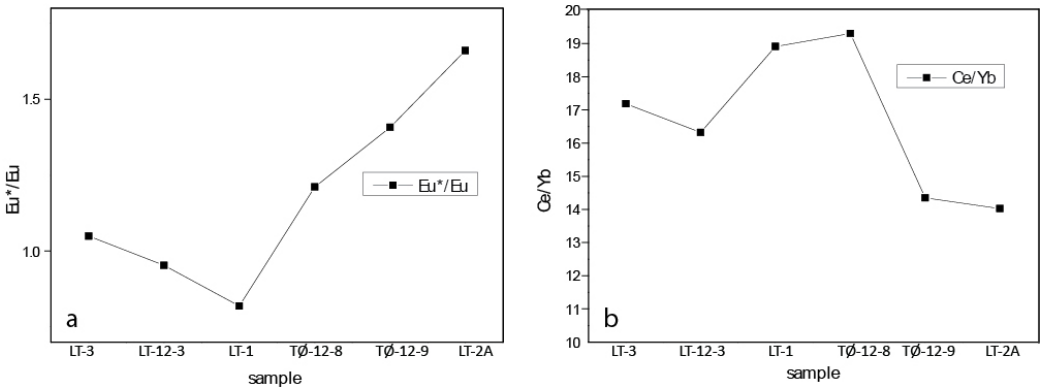

Figure 10: a) Chondrite normalized expected Eu-content Eu (halfway between Sm and Gd) divided over the actual Eu-content; b) Chondrite normalized Ce over Yb content as comparison of different fractionation for LREE (Ce) and HREE (Yb).*

Trace elements that are known to be good substitutes for alkali ions, mostly LILE such as Ba and Sr, are shown in Figure 11; they are compared with the mole per cent of Na, K and Ca present. Absolute values of these elements are 100–1000 ppm, much higher than other trace elements because of their good substitution of alkali ions in feldspar. The graphs suggest a link between Rb, Ba, Nb and K, Na as well as Sr and Ca, except for sample TØ-12-9, which deviates.

In order to quantify observed element exchange, a simple mass balanced reaction can be made to relate the pristine sample to the most altered one (table 4). Since they are considered to be linked through fluid flow, mole percentages of cations are used rather than oxide weight percentages; Si^{4+} can be found as H_4SiO_4 in solutions, releasing H^+ during feldspar replacement. Trace elements are left out of this, because their contents are too low

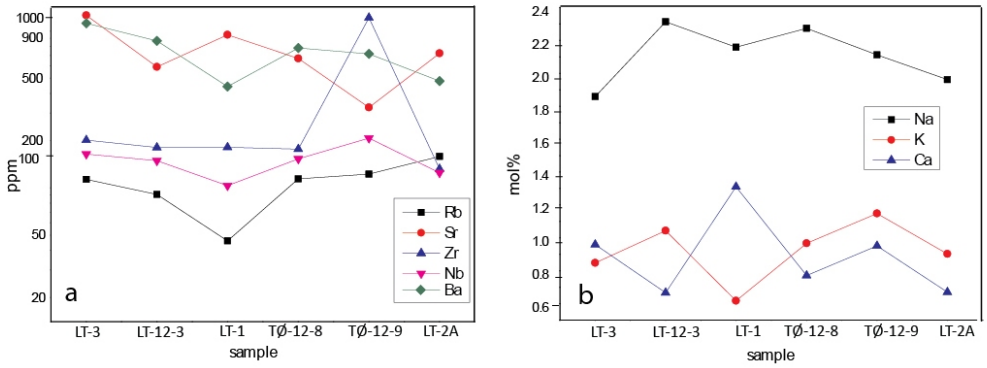

Figure 11: Possible substitution for alkali ions in the feldspar structure. a) Alkali substituting trace elements in ppm; b) Alkali ion content in feldspar in mol%.

to be mentioned in major element redistribution. Volume is considered to be constant throughout the reaction, and because of their similar densities, 1 mole of larvikite is said to form 1 mole of tønsbergite.

Table 4: Exchange of cations in moles between larvikite (LT-3) and tønsbergite (TØ-12-9) for mass balanced calculation

Element	**LT-3**	**TØ-12-9**	**Gain/Loss (moles)**
Al	0.7505	0.8291	0.0786
K	0.4494	0.189	-0.2604
Ba	0	0.0013	0.0013
Fe	0	0.0036	0.0036
Si	1.9832	2.048	0.0648
Na	0.231	0.5372	0.3062
Ca	0.0292	0.0012	-0.028

These amounts of gain and loss result in the following reaction (both mass and charge balanced):

$$Larv + 0.08Al^{3+} + 0.06H_4SiO_4 + 0.31Na^+ \leftrightarrow Tøns + 0.26K^+ + 0.03Ca^{2+} + 0.24H^+.$$

As expected from Figure 7, no large fluxes are observed. Minor amounts of Al^{3+} and Si^{4+} must have been available in the fluid, as well as larger amounts

of Na^+. At the same time, some K^+ and a bit of Ca^{2+} and H^+ were released during the reaction.

5.4 Feldspar mineralogy

Besides chemical changes in bulk rock composition, alteration processes are visible in rock textures. This paragraph describes observed textures and mineral chemistry, involving feldspar unmixing and formation of new phases after complete feldspar weathering. Special attention was paid to minor phases that could cause discolouration. These minerals (often with a high backscattering intensity) appear to be concentrated in pores and have sizes up to 10 μm. Other larger minerals were also sampled but no chemical zonation was observed.

5.4.1 LT-3

This most pristine sample optically exists of 90% feldspars and some minor dark phases. When imaged using backscattered electrons, the large crystals are continuous in texture but three types of feldspar are distinguished and intergrown: (1) a dark non-porous one, on a μm scale showing an alternation of darker and lighter flame structures known as perthites; (2) a darker porous one and (3) a light porous one surrounding both (fig. 12). Large crystals of continuous dark feldspar are bordered by smaller areas of the light, patchy feldspar, the contact between them being sharp. The transition between dark porous and non-porous feldspar is equally sharp but less easy to observe. It is located close to the boundary with light feldspar as well as along cracks. Pores of the dark feldspar are sometimes filled with minor phases (fig. 12b). The majority of the area, however, consists of the dark non-porous feldspar.

Compositions of all three feldspar types are measured and shown in Figure 13. As could be expected from the bulk rock data, variations are observed only in alkali content. Non-porous dark feldspar is ternary and considered to be unaltered larvikite of $Or_4Ab_{81}An_{15}$, approximately. It shows non-porous darker and lighter flames of feldspar, being richer in Na and Ca or K, respectively. The present iron can be both trivalent and divalent, substituting for either Al and Si or for Ca, Na an K in the feldspar structure, respectively. Despite the fact that this sample is not heavily altered, cracked crystals display the beginning of the alteration reaction, with darker or lighter porous plagioclase growing inside fractures. The dark one is pure albite but the

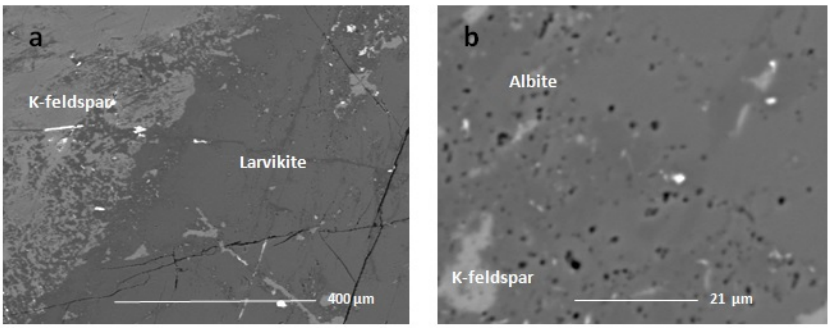

Figure 12: BSE-images of sample LT-3. a) The clear colour difference between continuous dark feldspar, darker porous feldspar (along cracks) and light feldspar. b) More detailed contact between the 3, focusing on porosity and minor phases included.

light one is intermediate between albite and K-feldspar. Some minor phases (see appendix) inside pores of both feldspar types are identified as hematite, pumpellyite and quartz. Larger hematite and pyroxene are also present.

In figure 14, the different groups are plotted separately in a ternary diagram. The non-porous feldspar is ternary in composition, being closest to the albite corner. The porous one with low backscattering intensity is close to pure albite while the porous high intensity feldspar plots close to the orthoclase composition.

5.4.2 LT-12-3

Sample LT-12-3 shows the same three types of feldspar as sample LT-3, although the specimen contains different phases inside the pores (fig. 15). Some cracks are visible, but alteration does not seem to be spatially related to them (fig. 15b). The formation of light feldspar ($Or_{96}Ab_4$) is not observed as a straight front as in LT-3 but appears more patchy, present together with the dark porous one ($Or_1Ab_{95}An_4$), forming the tønsbergite alteration. Only small patches of the non-porous dark material are left, surrounded by the patchy feldspars of both higher and lower backscattering intensity.

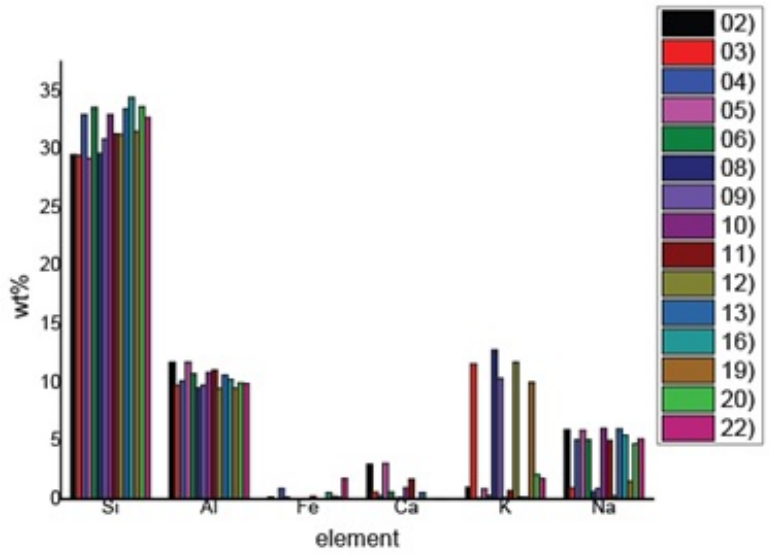

Figure 13: Element abundance (wt%) of all measured feldspars in sample LT-3. Alkali content is the main varying factor that divides the three groups of feldspar: 2, 5 and 11 represent non-porous larvikite; 19 a K-rich lamella and 20 and 22 a Na- and Ca-rich lamella; 3, 8, 9 and 12 the porous K-feldspar; and 4, 6, 10, 13 and 16 the porous albite.

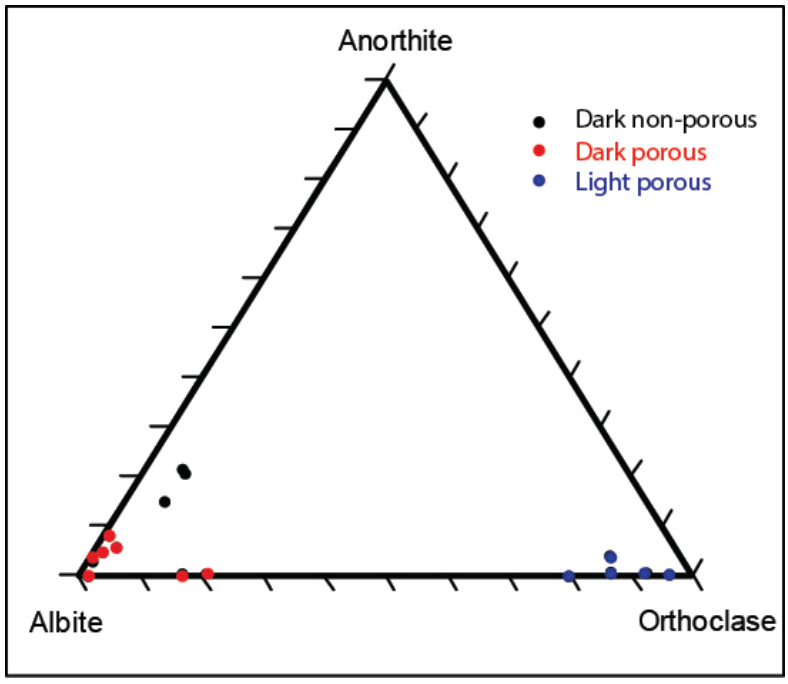

Figure 14: Three groups are observed using backscattered electron imaging on sample LT-3: around 80% Ab but ternary is the dark non-porous phase. The pure albite is the dark porous phase and pure orthoclase is the light (sometimes porous) phase.

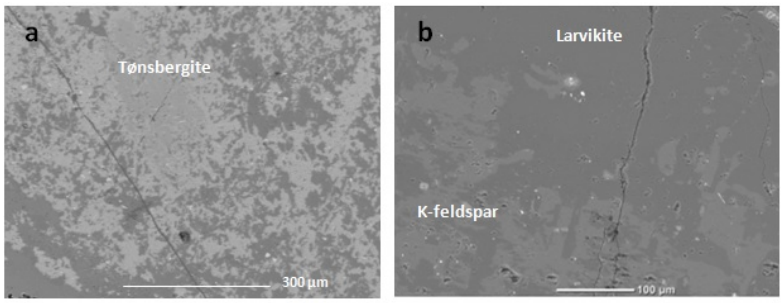

Figure 15: BSE-images of sample LT-12-3. a) Light altered appearance of the rock showing the patchy variety in mineralogy. b) The sharp front where the lighter feldspar is formed within the specimen, also showing porosity.

Compositional comparison in figure 16 shows a distribution similar to sample LT-3. Only few spots of the pristine ternary larvikite were present. Pure endmembers of Ab and Or are measured, representing the dark porous and the light feldspar in Fig. 15, respectively. Intermediate feldspar compositions are also observed. Pores are filled with micas and other hydrated phases. Possibly some small crystals of anorthite are present as well, included in both porous Ab and porous Or and vary slightly in composition; in some, minor amounts of Fe are present.

Compared to figure 14 for sample LT-3, feldspars in this specimen are closer to all end compositions, except for the dark ternary larvikite that is still the same. Only a few intermediate feldspars show up, the one being a mixture of Na and K (represented by the dot on the bottom line in Fig. 16) being the most striking. It was observed as a darker part in the light porous feldspar (fig. 15a).

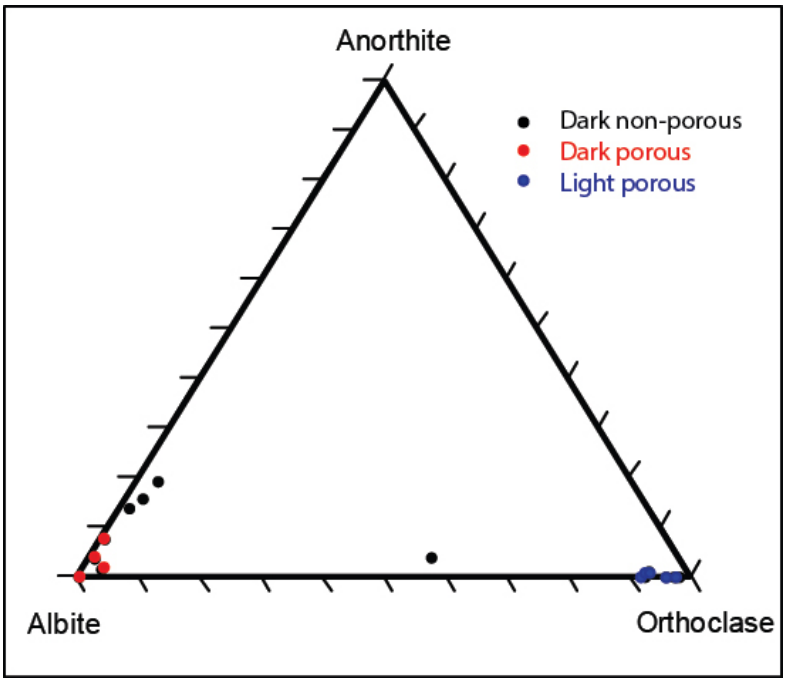

Figure 16: Ternary diagram showing the feldspar compositions in sample LT-12-3. Low backscattering intensity porous feldspar is represented by the cluster near albite; the light one is shown in the orthoclase corner.

5.4.3 TØ-12-9

In the altered sample of TØ-12-9 much smaller grains (μm) are present. Some large larvikite feldspar relics are observed, being severely altered and showing discolouration. Imaging of the centre of such grains shows porous patchy material, both light and dark porous feldspar phases are present. No clear core-rim structure is observed (fig. 17), only a sharp alteration rim at the edge of this crystal, from the dark porous variant to light feldspars and minor phases (10–100 nm) on the outside. Locally, pores are absent in these parts but the composition is never ternary (representing unaltered feldspar). Fractures in this sample can be observed with naked eye; alteration does not always follow these features.

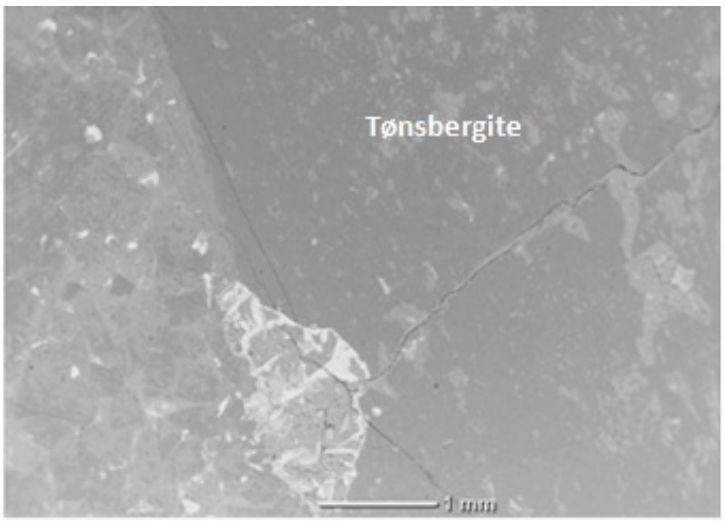

Figure 17: BSE-image of the edge of a larvikite relic in TØ-12-9 shows a fine grained red tønsbergite rock with more continuous, dark porous feldspar in the relic, combined with the lighter orthoclase alteration.

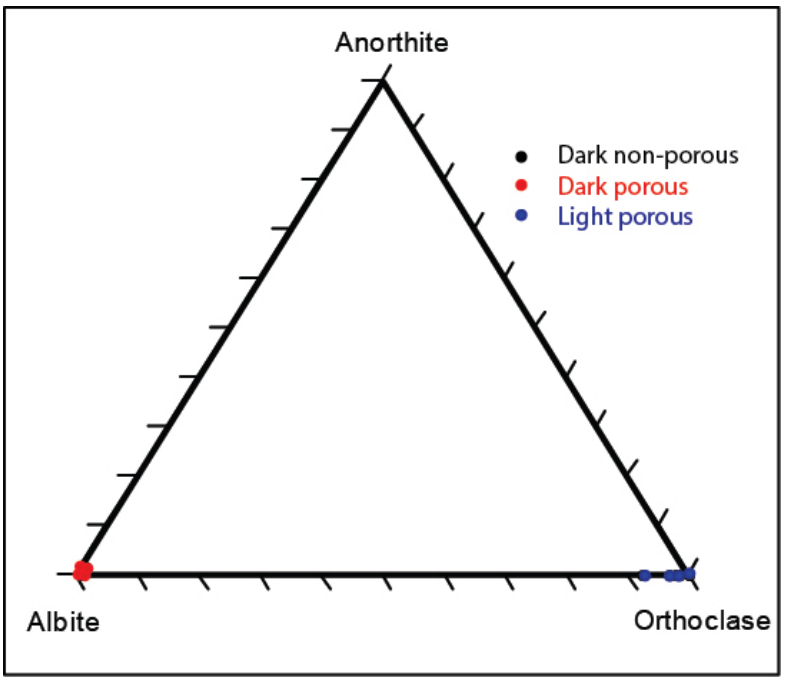

Figure 18: Ternary diagram of TØ-12-9 showing the dark porous feldspar (albite corner) and the light porous one (orthoclase corner) without any intermediate compositions. This implies that the re-equilibration has been completed and that the entire mineral has been unmixed.

Chemical spot analysis confirms that the old ternary larvikite is gone. The relic crystal is built up of two groups of feldspar compositions (fig. 18), either pure albite or K-feldspar. It is clear from this diagram that the feldspar compositions have shifted even further towards the endmembers. No intermediate compositions are observed. The patchy appearance is due to the many minor phases, partially filling the pores. They include several types of mica, quartz, calcite, apatite, hematite and titanite. Some of these also appear as larger euhedral crystals.

5.4.4 LT-2A

LT-2A shows the syenite vein. This sample displays a very different structure (fig. 19a), with more and fine grained minerals of euhedral shapes. There is no preferred orientation. The larvikites in contact with syenite do not display a clear alteration rim, and not many fractures are present. Compositionally, there appears to be no large difference between the larvikites and the matrix between euhedral minerals in the syenite (fig. 19b). The feldspars are ternary and do not display porosity.

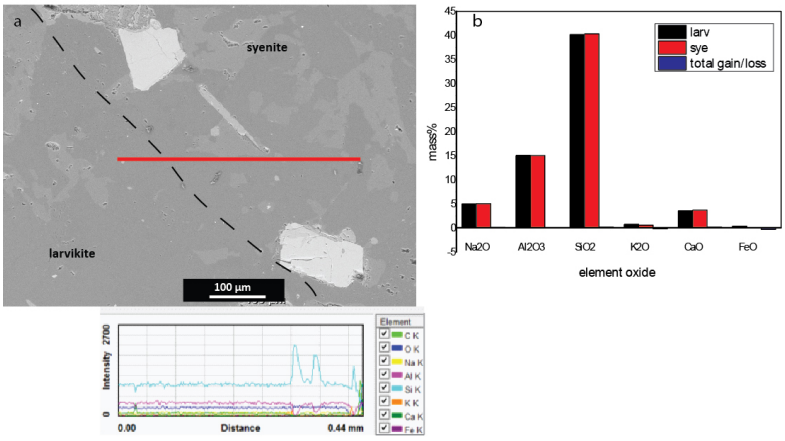

Figure 19: a) EDS line scan of syenite vein (top right) next to larvikite rock (bottom left). The brighter mineral it crosscuts is quartz, and the matrix in both rock types is the same in feldspar composition, seen on the graph to the right. b) EDS measured composition of feldspar in syenite and larvikite matrix, showing hardly any differences.

5.4.5 Sample comparison and summary of results

All specimens show a range of feldspar compositions (see Appendix, Fig. 20 and table 5 for data), all pseudomorphs, the main groups being non-porous ternary feldspar (original larvikite around $Or_4Ab_{81}An_{15}$) with a low backscattering intensity, darker porous albite and light K-feldspar, which in some cases can be seen to follow fractures. Some light patches are not porous. Original larvikite is only observed in LT-3 and LT-12-3, and some parts in LT-2A. Locally it contains parts of Na- and Ca-rich material ($Or_1Ab_{90}An_9$) and flames of lighter, non-porous K-feldspar, representing exsolution lamellae. Dark porous patches are present in all samples, mainly albitic in composition. In the less altered specimens however, traces of Ca and even K are not uncommon. Lighter feldspars always contain K, and sometimes minor amounts of Na. In sample LT-12-3, fairly intermediate compositions between the dark and light porous material are observed; LT-3 also has two less developed intermediate feldspar measurements, still being closer in composition to the unaltered non-porous dark feldspar. Only sample TØ-12-9 contains light non-porous patches that are pure K-feldspar. In all other specimens, the non-porous parts represent a mixed feldspar composition. The light porous patches however, present in all samples, are always $> 95\%$ Or. They grow irregularly next to the dark porous feldspar. In summary, with increasing alteration the measured feldspars become closer to the possible endmembers; the dark non-porous original larvikite (with some occasional non-porous exsolution lamellae) disappears and is replaced by darker and lighter porous patches of albite and orthoclase, respectively. An overview based on feldspar types is shown in Figure 20 and table 5. Corresponding spot analysis data from the microprobe are present in the appendix along with images corresponding to their location in the specimen.

Table 5: Average composition based on feldspar type. Data are plotted in Fig. 20

	Or	**An**	**Ab**
average dark	4.213	15.044	80.743
average dark porous	1.200	3.681	95.124
average light porous	95.885	0.173	3.942

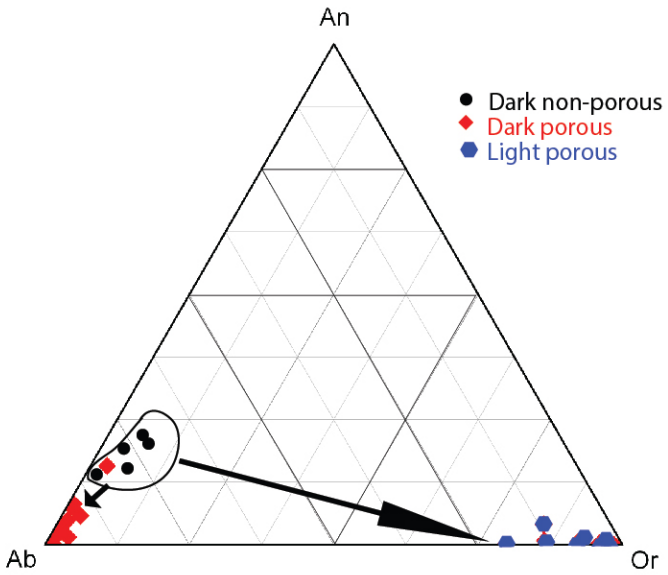

Figure 20: Composition of the different feldspar phases obtained from all samples. The dark circled one is ternary and represents larvikite, while the porous phases are close to albite and orthoclase endmembers. Arrows show the trend of unmixing from the ternary composition.

5.5 X-ray tomography and internal rock structure

The porosity observed using electron microscopy can be imaged in 3 dimensions, as well as boundaries between different grains and other features of the sample structure. This is done using X-rays, which penetrate the sample and capture density differences. Low density features are displayed darker than high density areas. A 3D-reconstruction of sample LT-1 (fig. 21 a-b) and a slice viewed from the top (fig. 21 c-d) are shown below with a resolution of 10 μm. Because the densities of altered and unaltered feldspar rocks are very close (table 3), no distinction between feldspar crystals was observed. Instead, slightly lower density areas were spotted as lines within the top view, sometimes following fractures (fig. 21 c-d). The exact grey-value of these areas was filtered out and highlighted in yellow. In 3 dimensions these

features appear to line up, which will be interpretated in section *6.2.1* of the discussion. Additionally, 10–100 μm pores were found next to some of the pyroxene crystals. However, these were not very common.

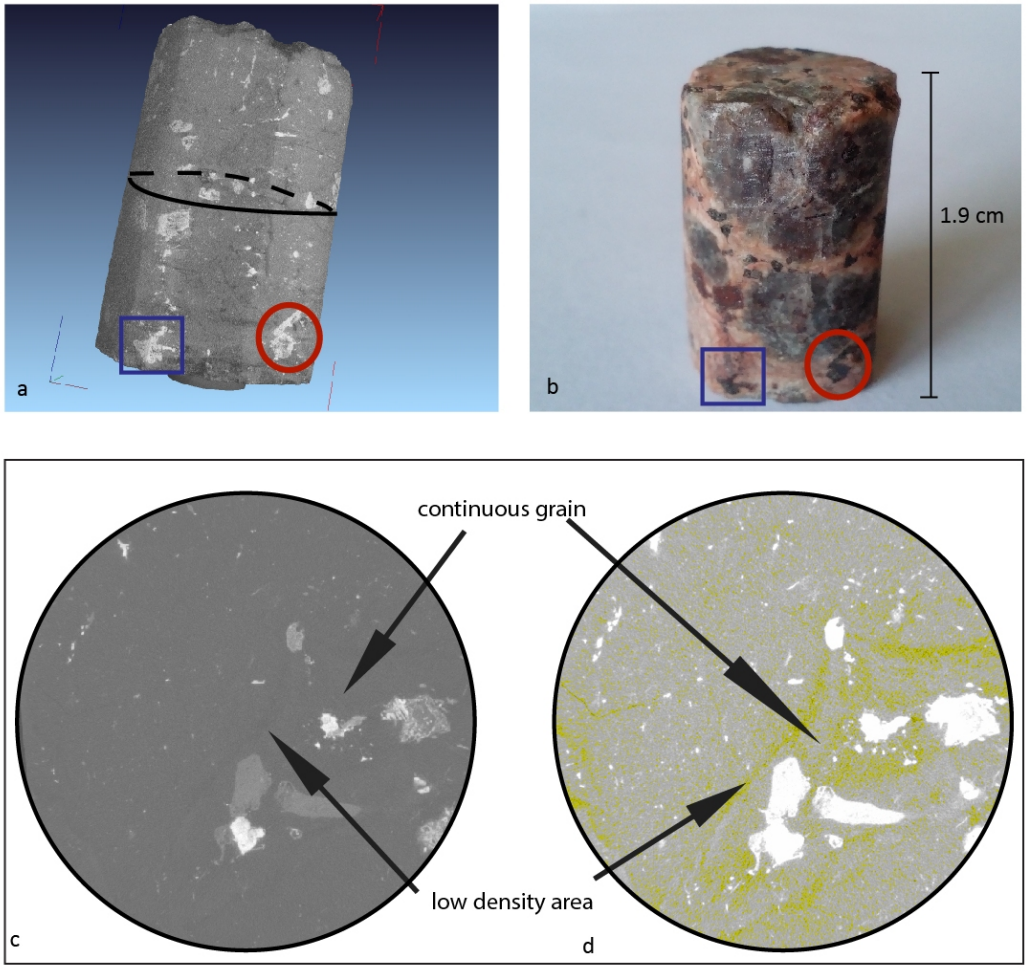

Figure 21: a) 3D-reconstruction and b) photograph of sample LT-1. The red circle and blue square indicate the same minerals in both images. Top views at the height of the black circle in a) are provided, with c) the unfiltered image and d) a filtered one. Slightly lower density areas are highlighted in yellow.

6 Discussion

6.1 Mineralogy

6.1.1 Primary origin of the larvikite rocks: REE patterns

Previous studies on the larvikites have been described in the geological setting, where trace elements have been used to determine their magmatic origin. Very similar values were found in this study, but textures such as intergrowths with pyroxene (indicating a two-stage cooling history, Neumann *et al.*, 1992) and mineral zoning are not observed. The hypersolvus monzonitic rock started crystallising under anhydrous conditions [Andersen *et al.*, 2010], resulting in a single feldspar phase that unmixes at cooling [Philpotts and Ague, 2009] and formed perthites (fig. 7b). Crystallisation temperatures are estimated around 850–860 °C, and high values for Zr, Sr and Rb with respect to Ni and Cr indicate that larvikites formed from a melt derived from deep lithospheric mantle [Neumann, 1980]. Uniform Th/U ratios found by Sundvoll (1978a) rule out contamination but show enrichment of this mantle source. High LILE (possibly also from low degree of partial melting) in all the rocks from the Oslo rift area point in the same direction [Neumann *et al.*, 1992]. Despite a deep source, the larvikite rock is intermediate to acidic and has thus experienced some fractionation.

The absent or even negative Eu anomaly in larvikites (fig. 9a) could be explained by magma evolution [Neumann, 1980]. When Eu^{3+} is reduced to Eu^{2+} due to low fO_2, it is easier incorporated in feldspars which results in negative anomalies after previous plagioclase fractionation. This would be accompanied by increasing REE content and decreasing Sr and Ba, which is not observed in larvikite rocks. Eu should thus occur as its oxidized form to cause the current pattern. Another oxidation state indicator is the Ce anomaly, where Ce^{4+} instead of Ce^{3+} would imply oxidation. This is absent in larvikites, showing that the Eu anomaly should not be interpreted as a redox-state indicator but has another explanation.

Andersen and Sørensen (2003) mention that LREE-enrichment is observed both in larvikites (fig. 9b) and the later intruded rock types around it. This phenomenon can be explained by magmatic evolution or by fluid addition after crystallisation [Rasmussen *et al.*, 1988]. Due to the low REE content in hydrothermal fluids, only very high fluid: rock ratios can leave a clear signature of the fluid on the rock [Bau, 1991]. Normally, the LREE/HREE

signature is more likely to be left over from magma crystallisation, since it is hard to transport REEs in water. Eu anomalies must then be explained by partition coefficients in the magma for specific minerals. Feldspars are known to easier incorporate LREE because of their resemblance to Ca (especially Eu^{2+}) and Na ions [Philpotts and Ague, 2009].

Strongly differing trace element patterns in rocks from the same area imply REE mobility, most likely by a post-magmatic fluid. In such hydrothermal fluids, sorption onto minerals is highest for stronger charged and smaller sized ions, which leave the fluid and adsorb to crystals. Under acidic conditions, sorption processes control the REE pattern and lead to a pattern with $La/Lu > 1$; Eu is reduced to Eu^{2+} which is the bigger, generally less easily incorporated variant, resulting in a positive anomaly in the remaining liquid [Bau, 1991]. Fluid overprinting would thus lead to a striking positive anomaly, which is not observed for the larvikite rocks. In a crystallising magma, ratios between ions that are similar in charge and size should remain constant because their abundance can be explained by CHArge-and-RAdius-Controlled (CHARAC) behaviour: their incompatibility depends on these two factors only. Bau (1996) uses Y/Ho and Zr/Hf ratios; non-constant values indicate overprinting by aqueous solutions or silicate melts, or other types of fractionation. Larvikite specimens show rather constant Y/Ho and Zr/Hf ratios (fig. 22), falling in the CHARAC-field of Bau (1996) for intermediate rocks. This makes it unlikely for the trace element pattern to be formed by fluid infiltration and overprinting. Instead, it provides information on the degree of magmatic evolution, which is approximately the same for all rock specimens and was already described and interpreted by Neumann (1980). When all samples are compared to a granite (fig. 8b), they show similar trends with slightly increasing values with alteration. This increase could be caused by normal magmatic evolution but this is not likely since all samples are larvikites. Only for the later intruded, more evolved LT-2A syenite this assumption holds.

All samples behave as should be expected for silicate melts: they show magmatic REE patterns, not influenced by fluid infiltration. This means that the above statements about magmatic origin based on REE are justified, and that the infiltrating fluid has not caused overprinting in trace elements. Oxidizing conditions and pH of the pattern can therefore not be interpreted as fluid indicators but are coupled to magmatic evolution, as interpreted in previous studies and described above. Albitisation, a fluid-alteration process often observed associated with feldspars, would show significant loss of K

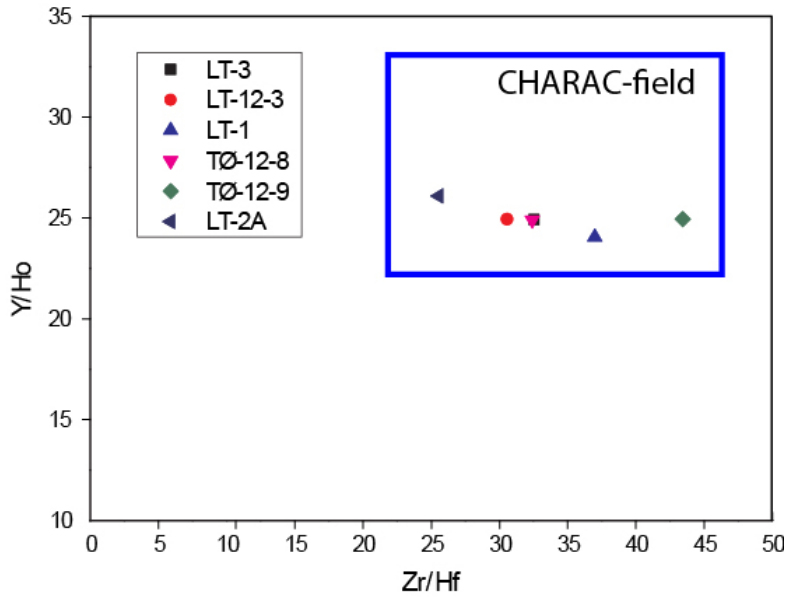

Figure 22: CHARAC-field defined by Bau (1996) of larvikite rocks, showing constant values in trace elements. This makes it unlikely to be caused by fluid overprinting (see text for explanation).

(and Ba) while Na, and elements substituting it (Ca, Sr and Hf) should show an increase. Also, the total REE would decrease [Engvik *et al.*, 2009]. The opposite is observed here, ruling out albitisation as overprinting process.

6.1.2 Elemental exchange

Trace element patterns and bulk rock comparison (fig. 8 and table 3) of all samples have shown that rock alteration was not likely accompanied by large element fluxes. To study this in more detail, isochons (fig. 23) were constructed to compare the element oxide content (in wt%) from table 1 in pristine (sample LT-3) and altered rock. Due to epitaxial overgrowth, the volume change is assumed to be negligible; other possible assumptions would involve constant mass or element immobility, for which is found no evidence. Because the same trend is observed in all samples, alteration continues with roughly constant Na_2O, K_2O and Fe_2O_3 (6, 4 and 7 wt%, respectively) while CaO and Al_2O_3 are slightly depleted. Sample LT-1 deviates from these in an inverse alkali exchange pattern due to its higher CaO content.

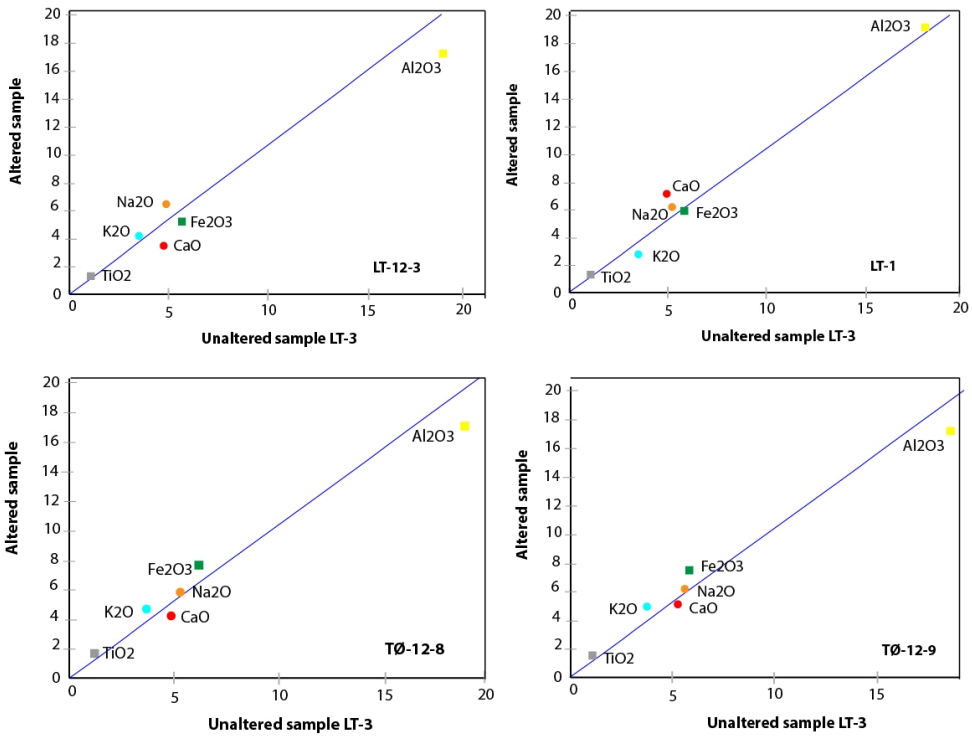

Figure 23: Isochon diagrams with constant volume assumption, the blue line represents the isochon. The bottom right corner of each graph shows the altered sample, and LT-3 is taken to be the unaltered sample in every case. Oxides are given in wt%, trace elements in ppm. Such bulk rock analysis shows a roughly constant rock composition throughout alteration.

Another way to show possible element exchange is by comparing element oxide ratios (fig. 24). For feldspar, the main replacement is expected to be in alkali ions, which are compared below; if Na_2O/K_2O has changed, element exchange has occurred by loss or gain of one or both elements. All specimens, however, confirm the previous assumption that no such exchange has taken place, the ratio in the unaltered sample (LT-3) being close to that in each of the altered ones. For comparison, each alkali oxide is compared to SiO_2 content; SiO_2/Na_2O and SiO_2/K_2O ratios are smaller in the altered samples than in the pristine LT-3, implying a relative depletion in SiO_2 or enrichment

in Na_2O and K_2O. For SiO_2/CaO the opposite is true, having experienced enrichment in SiO_2 or depletion in CaO during alteration. Finally, the ratio between SiO_2 and Al_2O_3 is constant for all samples. Because these elements form the tetrahedral mineral backbone and their ratio does not change, a variation of alkali ions is more likely. Both Na and K are enriched in equal amounts, the SiO_2/Na_2O ratio going from 11 to 10 and the SiO_2/K_2O ratio going from 17 to approximately 14. Simultaneously, Ca is lost, increasing the SiO_2/CaO ratio. Sample LT-1 shows the opposite trend, enhancing the SiO_2/K_2O ratio and decreasing the SiO_2/CaO ratio.

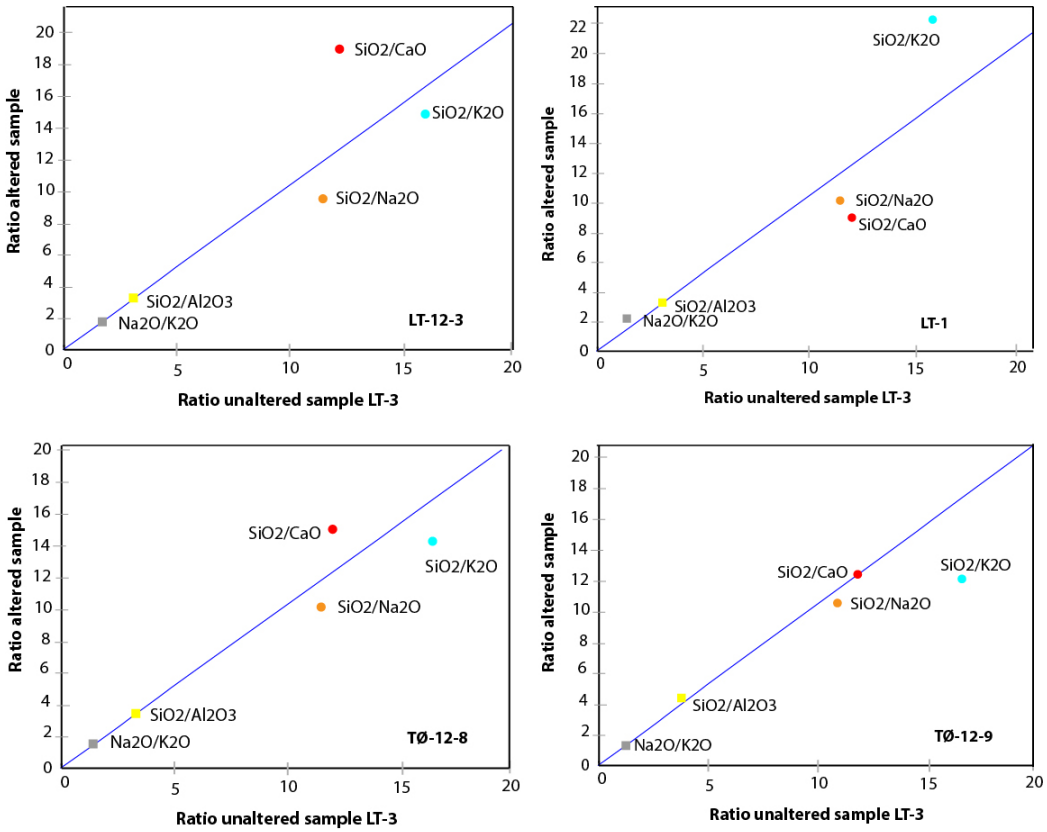

Figure 24: Component ratio diagram, showing ratios between different elements compared in unaltered and altered rock. The lower right corner shows the sample to which each graph applies; again, LT-3 is taken to be the unaltered sample. Ratios between SiO_2 and Al_2O_3 as well as Na_2O and K_2O remain constant in all samples while others change (see text).

Alkali enrichment is an indicator for temperatures of infiltrating fluids. With increasing temperature, the amount of dissolved Na it can carry decreases and K increases. At heating, sodic phases will precipitate and K-rich phases will be consumed (the Na/K-ratio in rock increases) [Philpotts and Ague, 2009]. Because K and Na are enriched in equal amounts, the fluid must have been of intermediate temperature. Further constraints to fluid temperatures are given by the lack of trace element overprinting signatures. Seewald and Seyfried (1990) discovered that at temperatures below 300 °C, most trace elements and metals do not dissolve and cannot be transported by hydrothermal fluids. Na, Si, Cl, K and Ca on the other hand are still mobile. This combination is observed in larvikites and fluids below 300 °C are expected. As absolute values of dissolved REE go down with temperature [Michard, 1989], higher fluid: rock ratios are needed to cause overprinting. Therefore, overprinting can be absent if the amount of fluid is very low. REE mobility is also less at high pH and low Cl-content [Michard, 1989].

6.1.3 Mutual replacement processes

Despite the lack of large element fluxes, rock appearances and mineralogical textures clearly show that alteration has happened. This means that mutual replacement processes must have taken place, re-equilibrating the rock without mass transfer.

The slight change in alkali ion content shown in Fig. 23 and 24 accompanies unmixing textures at the reaction front. Keeping the total alkali content constant (table 3), porous albite and K-feldspar rims form, being compositionally close to the endmembers which indicates formation at low ($< 500°C$) temperatures [Smith and MacKenzie, 1958]. However, at larvikite dissolution, also Ca would be released. Since only very few minor anorthite patches are observed in the newly formed feldspars, Ca seems to concentrate in minor phases such as apatite, calcite and titanite. These phases are located in pores, which are formed during the alteration process (reactive transport). So element redistribution in the ternary feldspar results in rims of feldspars high in K and Na as well as precipitates of Ca-rich minor phases in pores. These new phases may be responsible for the red appearance of the altered rock: many small hematite and mica crystals are observed.

The original blue colour of the old larvikite is not explained by the presence of minor phases but by iridescence of the feldspar by cryptoperthites [Ribbe, 1975]. This perthitic structure is another phase of feldspar ordering,

often associated with cooling after crystallisation; it is only observed in the more pristine samples of LT-3 and LT-12-3 and is thus said to predate the fluid introduction and redistribution described above. This automatically explains the disappearance of the blue colour when the feldspar unmixes and forms rims of separate end member compositions. Changes in alkali content can thus be related to two different processes.

Unmixing by exsolution Exsolution is a process driven by strain energy within a crystal, based on cooling. At lower temperatures, vibration energy decreases and the lattice starts distorting around small cations (Na and Ca) in the feldspar structure [O'Neil and Taylor, 1967]. In order to reduce the strain energy, a perturbation grows and forms a front at which cation ordering starts. The new phases, either with large K or Ba ions or with Na and Ca ions, have their own crystal structure that grows outward, following crystallographic axes, expelling non-fitting atoms [Yund and McCallister, 1970]. These diffuse through the material until they find an energetically stable location in a lamella. All blue larvikite cores display such areas as wavy patches close to the orthoclase end member in a matrix of Na- and Ca-rich feldspar. Because atoms must move through the solid crystal, diffusion is very slow and element paths are short. At cooling, the process ceases; Smith and MacKenzie (1958) experimentally found that only temperatures above 500 °C accommodate such volume diffusion. Lee and Parsons (1995, 1997) have observed similar textures in rocks from the Shap granite, which they said had formed by several stages of alteration. Based on the composition of the two phases that were formed simultaneously, perthites were calculated (using the geothermometry of Fuhrman and Lindsley, 1988) to have formed at temperatures around 570–590 °C. However, larvikite rocks show too low Ca-content to result in the almost pure orthoclase lamellae of the model [Fuhrman and Lindsley, 1988], not following the calculated trends of Fig. 25. Therefore, their pattern cannot be linked to a specific PT-condition. The lack of correlation may be due to the absence of full equilibrium or to offset by a later process. These geothermometers can therefore not be used.

Re-equilibration in the presence of a fluid The later process that totally redistributes elements in the larvikites resulted in porous textures with almost pure feldspar phases. One possibility to cause this is heating, speeding up the sluggish diffusion process. However, no new magmatic textures are

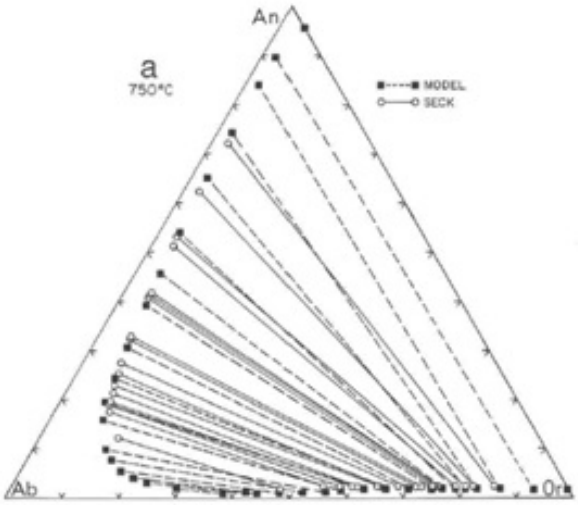

Figure 25: Isotherms from model of Fuhrmann and Lindsley at 750 °C *and 1 kb.*

observed and the reaction front is very steep, which makes diffusion unlikely, as well as porosity which would impede diffusion. Also, the element pathway has become much longer. A better way to explain the texture is by water infiltration, the fluid acting as a (rapid) means of transport for ions [Orville, 1963]. Dissolution of the old mineral is followed by precipitation of material elsewhere, transporting elements only as far as the water has infiltrated, which is along a steep reaction front [Putnis *et al.*, 2005]. The mechanism is driven by disequilibrium of the fluid with the rock, based on ion activity and ion concentration. A slight change in one of these factors may be able to explain the sudden transition from porous albite to porous K-feldspar, both precipitating from the same solution.

Recall from the introduction that the equilibrium constant K for a reaction $2A + B \leftrightarrow C$ is $K = \dfrac{X_C}{[X_A^2 X_B]}$ or log K= log X_C –2log X_A –log X_B, in which X is the concentration of an ion in solution. Activity a of a component in solution is related to its concentration as $X = a/\gamma$, where γ is the activity coefficient. Increasing activity results in easier incorporation of the ion in minerals. This causes a shift in the mineral stability field; mineral formation accompanied by it is considered to be in equilibrium with the solution. The Na-rich core with K-rich rim shows a relatively higher Na activity in the core.

Because equilibrium conditions depend on composition of the solution (activity coefficients, concentration, pH, alkalinity), of the rock and of external PT-conditions for the whole system, small changes in any of these factors may have caused the shift in the stable mineral phase. At equilibrium, the activity of a certain component is the same in both present phases. Because K-feldspar and albite are found thoroughly intergrown, equilibrium conditions oscillated between precipitation of these two phases, showing that the solution was close to the boundary between mineral stability fields. This contradicts the Na-increase and K-decrease shown in the mass balance reaction. Towards the end, however, only K-feldspar was stable, possibly replacing the previous albite-K-feldspar intergrowth and explaining the light rim around altered feldspars.

Since dissolution for aluminosilicates is often incongruent [Helgeson *et al.*, 1969b] and absolute values for activity are hard to determine, activity diagrams plot cation ratios with H^+ against each other to show mineral stability at different temperatures. Instead of calculating an activity diagram for this case, a previously constructed diagram (fig. 26) is used for the system $KCl - H_2O - H_4SiO_4$ [Plümper and Putnis, 2009], showing that some Cl^- was present, but not enough to facilitate REE-mobility. Stability fields of both minerals are next to each other for all shown temperatures. No sericite is observed in larvikite rocks so Na and K activities were relatively high. For the assumed simultaneous precipitation of porous albite and orthoclase, the system must have quickly reached supersaturation in both phases, being at the boundary between these two mineral stabilities and staying there; no dissolution of either of these minerals occurred. This situation applies for a large range of fluid compositions and temperatures. Fortunately, the lack of REE pattern overprinting constrains fluid temperatures to the lines below 300 °C, all showing that more Na^+ than K^+ is present in the solution. At albite precipitation, the activity of Na^+ will decrease in the system since its concentration in the solution decreases. At this point, K^+ will be relatively more active, shifting the conditions to the K-feldspar stability field and precipitating this mineral. Consequently, K^+ activity will go down, moving the solution back to the albite field. This oscillation can explain the observed intergrowth of albite and K-feldspar. Rock texture influences dissolution: the presence of exsolution lamellae can speed it up, albite dissolving faster [Holdren and Speyer, 1985, 1987; Arnórsson and Stefánsson, 1999; Parsons and Lee, 2009]. Porosity however does not seem to be concentrated in albite patches.

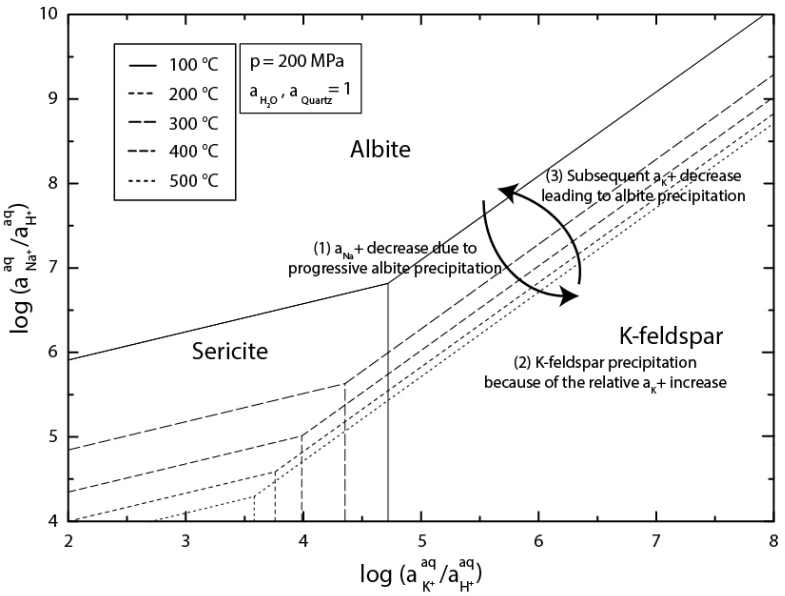

Figure 26: Activity-activity diagram showing stability fields of albite and orthoclase at several temperatures and 200MPa. Modified from: Plümper and Putnis, 2009.

For the activity approach, the system must be closed, without much water present; this is confirmed by the lack of REE pattern overprinting. Throughout the reaction, elements are considered to be conserved and =1 (so a quite diluted system).

Comparing exsolution and dissolution based on chemical features Both processes mentioned above involve the unmixing of a ternary feldspar, diffusing or precipitating to form a more stable phase under the new conditions. To make a distinction between the two, and to give information on the state of alteration, alkali ratios are plotted of a pristine, slightly and severely altered sample. These show two trends of alteration, one involving porosity generation and the formation of pure endmembers and the other involving perthites of more intermediate compositions. Comparing stoichiometric values of Na+Ca with K (fig. 27 a-c) will show the amount of exsolution; Na+Ca represent the smaller ion lamellae (if Ca is not equal to zero) being distorted at cooling while K represents the lighter lamellae. A comparison

of Na+K with Ca is made (fig. 27 d-f) to show degree of dissolution, since after complete dissolution, no Ca will be left in the feldspars. They are transformed to porous albite and K-feldspar endmembers, shown as dark porous and light in backscattered electron images in the Results section and Appendix. In this way, both chemical and textural evidence is used to make a distinction between alteration processes in the high temperature feldspar (related to magmatic processes) and the low temperature (hydrothermal) feldspar types.

Figure 27 a-c displays the first step of chemical ordering in the crystals, resulting in similar chemistry in relatively unaltered samples of LT-3 and LT-12-3. These show ternary compositions for all points, while TØ-12-9 shows only pure endmembers. Because Ca=0 for that specimen, it was not exsolution that resulted in this chemistry, but water entering the rock which led to the dissolution mechanism, displayed in Fig. 27 d-f. That diagram again shows that sample LT-3 and LT-12-3 are quite similar when it comes to feldspar compositions. Both contain a dark ternary feldspar phase, a dark porous one lower (around 0.2 cations per unit) in Ca and a light phase that consists almost entirely of Na+K. The total amount of cations appears to be smaller in the dark porous phase, around 2.2 where it is 3.0 in the other phases, which can be explained by the fact that this is a mixed feldspar, containing also impurities such as Fe, Ba or Sr which are not included the diagram. The observed bulk rock positive correlation between Na, K, Ba, Rb and Nb as well as between Ca and Sr is not further investigated because trace elements concentrate in minor phases at feldspar alteration. Opposite to LT-3 and LT-12-3, sample TØ-12-9 shows very low values of Ca in all phases. Even compared to the dark porous and light phases of the other samples, the Ca-content is lower. In TØ-12-9, Ca has left the feldspar crystals entirely, concentrating in additional secondary phases like apatite, calcite and titanite; this is also where trace elements are found in high concentrations. The light feldspar phase in TØ-12-9 shows a larger range of alkali compositions than the other samples.

Because the ratio of Na+K vs Ca gives insight in the degree of feldspar dissolution, it can be stated that from LT-3 to LT-12-3 the dissolution has not been pervasive enough to cause significant loss of Ca. This is confirmed by the appearance of these samples (see Appendix), both showing blue relic crystals. For the TØ-12-9 sample, however, Ca is thoroughly removed, even from the core of the biggest crystals. This elemental redistribution is shown in Fig. 28, as well as with textural change in Fig. 29.

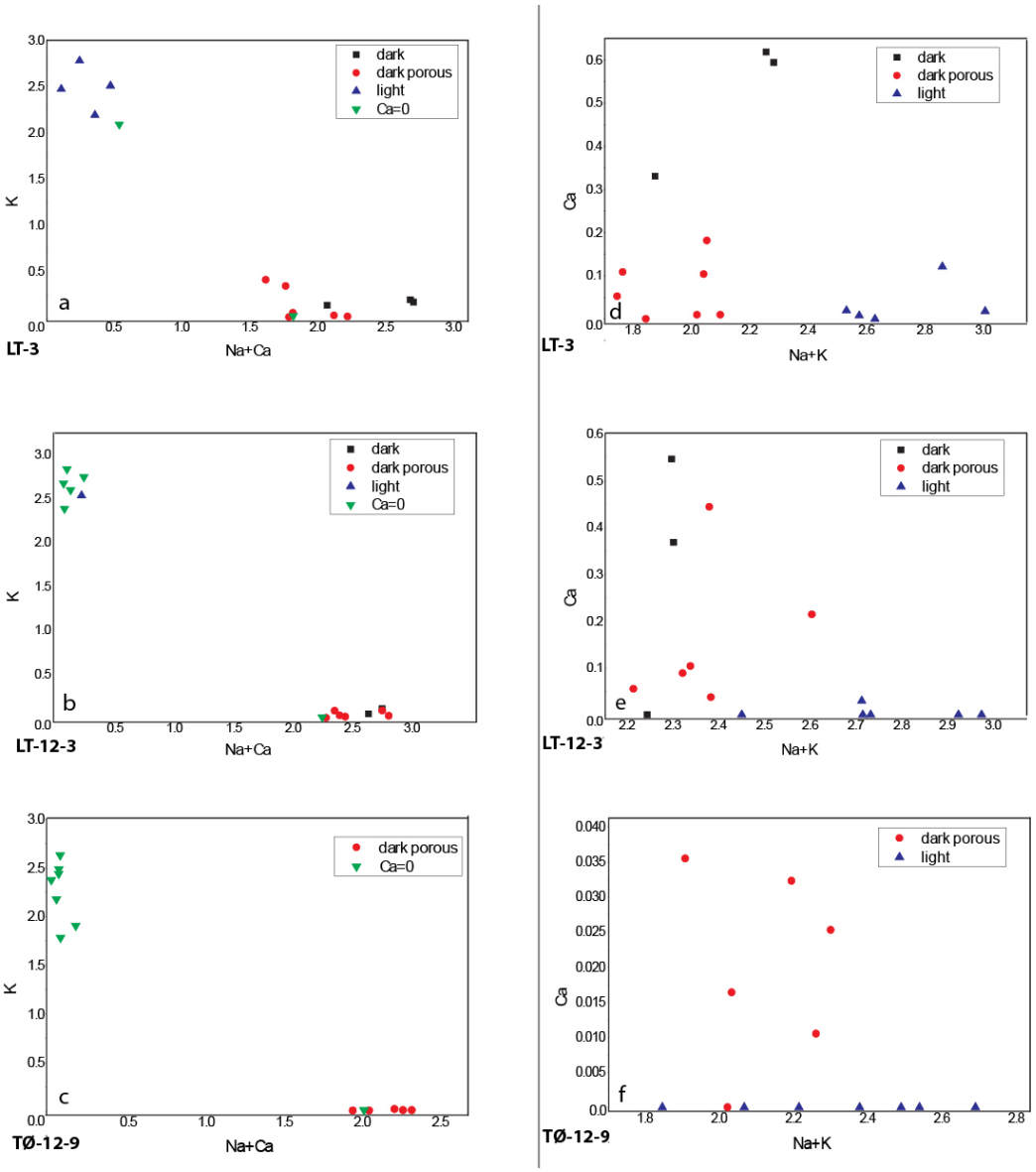

Figure 27: Alkali ion content in samples LT-3, LT-12-3 and TØ-12-9, representing increasing alteration. Alkali content is given in stoichiometry, the number on the x- and y-axes representing the atoms per 1 formula unit or 8 oxygen atoms. Na+Ca vs K graphs show perthite formation (a-c) while diagrams with Na+K vs Ca show re-equilibration (d-f). With increasing degree of alteration, feldspars become more pure in composition and TØ-12-9 shows equilibration in the fact that Ca=0. Perthites disappear when equilibration occurs.

An increasing degree of alteration results in the same trends of unmixing and re-equilibration, only in a progressing degree. This implies that alteration was constant throughout the rock, and that the PT-conditions did not change significantly during the reaction.

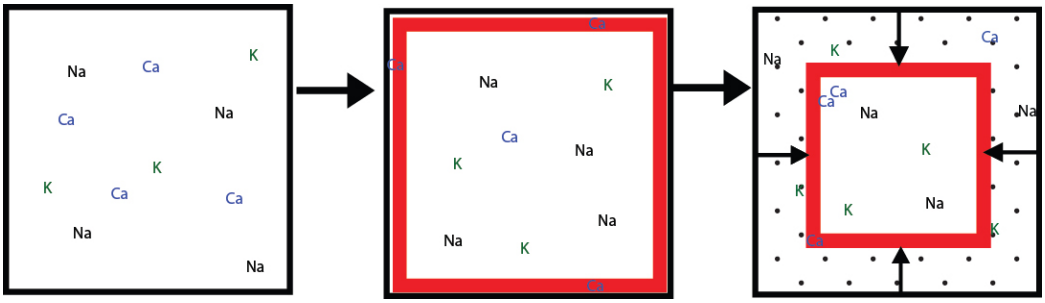

Figure 28: Chemical redistribution during the reaction. The original larvikite has a homogeneous distribution of Na, K and Ca. During grain boundary migration and later grain consumption and epitaxial overgrowth, Ca is removed from the core and Na and K are redistributed in rims outside the core.

Other mineral phases Associated with the feldspar equilibration, other minerals have precipitated in the created pores. These hold elements that are not incorporated in feldspars, such as Mg, Ti, Fe and REE. Also, Ca is found inside in such phases and has not left the rock entirely, which shows that the assumption of conservation of elements is correct. Phases such as hematite (Fe_2O_3), calcite, apatite, titanite, pumpellyite and micas formed, which constrain fluid conditions further. The presence of trivalent iron in hematite implies that conditions were slightly oxidizing. Micas show that water was incorporated in some crystals. Pumpellyite presence constrains pressures, being around 1–3 kb (which falls in the range of the activity diagram) and temperatures between 100 and 250 °C. The pores controlled growth of these minor phases. Because they are found equally distributed over the altered rock, alteration was indeed constant over the whole rock. No pattern is observed in the precipitation of these minor phases to imply otherwise.

6.1.4 Chemistry of the infiltrating liquid

From the above, it can be concluded that the fluid in contact with the rock has not altered its chemistry severely. Because of this, no quantitative data can be obtained for the chemistry of the fluid. However, the appearance of the rock has been changed, free energy reduction facilitated through equilibration by water addition as a retrograde mineral reaction. This means that the water was able to act as a means of transport for ions already present in the rock, making it possible to qualitatively describe PT-conditions of the system. Also, because feldspar precipitation occurs, enough K^+ and Na^+ must have been available in the fluid to not only dissolve, but also form new feldspars. No precise fluid composition can be given and the question of fluid origin remains open for future research.

The presence of pumpellyite and lack of Rare Earth Element overprinting during the reaction shows that the temperature of the infiltrating fluid was just below 300 °C. Bau (1996) stated that the formation of complexes is not considered important when rocks fall within the CHARAC-field (fig. 20) so complexing agents such as F, CO_3^{2-} or $(OH)^-$ are expected to be absent. Cl^-, however, is present (see chemical system of Fig. 26) but is said to be not important for the REE pattern and complexation. Since H^+ is formed during the reaction, pH decreases; it does not become so low as to influence trace element mobility or ionic activity of Na^+ and K^+. Instead, the reaction has been of the same manner throughout the whole rock, even with increasing degree of alteration the same endmembers were formed.

From the pure re-equilibration without formation of out-of-equilibrium minerals or their relics, the fluid composition is considered to be close to the rock composition. If not, minerals like gibbsite or kaolinite would have formed [Lasaga *et al.*, 1994]. Instead, other phases were found in the pores, formed after feldspar precipitated. These minor phases are located in pores, attributing to the colour change of the rock (such as hematite, pumpellyite and titanite). Pumpellyite-facies conditions constrain the system to 1–3 kb and temperatures around 250 °C. Combined with the absence of gibbsite and kaolinite, it means that the activity-activity diagram of Fig. 26 is applicable and the reaction must have taken place with a fluid slightly higher in Na^+ than K^+.

The close resemblance between rock and infiltrating fluid could either be explained by previous re-equilibration of the solution with the rock, of which no evidence is observed anywhere near the larvikite rocks, or by a similar

origin. The latter would imply that the fluid was most likely magmatic, left from larvikite crystallisation. In this case, the REE-pattern would differ from the rock because fractionation of trace elements in water is very different from that in minerals. This would result in overprinting if the amount of fluid was large enough. The quick change in saturation in both albite and K-feldspar, however, confirms that only a small batch of fluid was present to cause the observed alteration.

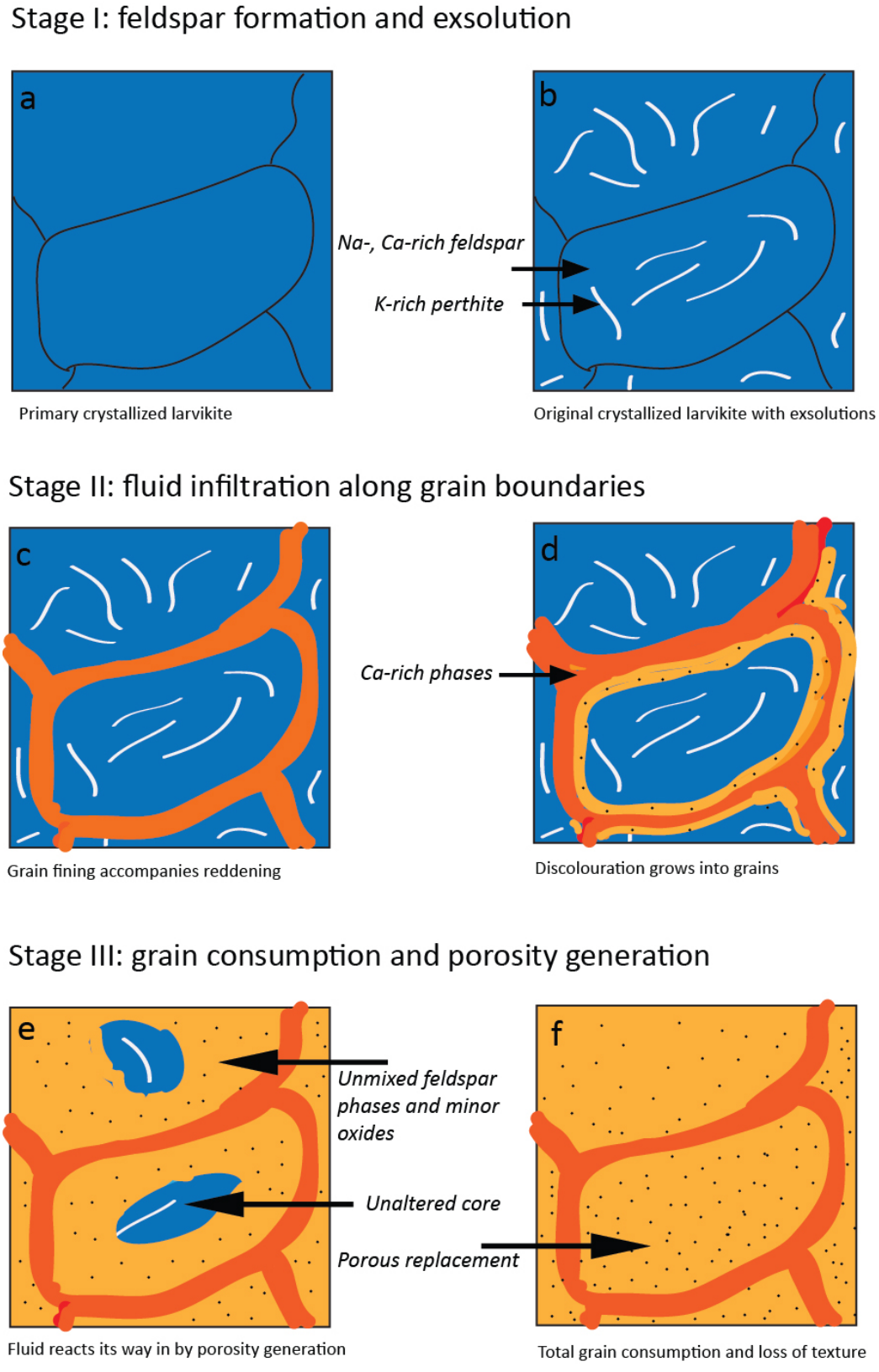

Figure 29: Overview of replacement reaction steps in the larvikites, including some remarks on element distribution and textural changes.

6.2 Mechanisms of fluid flow

Now that the chemistry of the infiltrating fluid is discussed, it is important to analyse the physical aspects of fluid flow through the rock. Main questions are related to the processes that caused fluid movement and the taken fluid pathway, as well as reasons for a continuous contact with fresh rock. Textures of the altered samples are of vital importance, showing formation of yellow to red cloudy feldspar around blue relic cores and intergranular rims of altered red material (fig. 6c, 29). Blue feldspar grain centres have not been unmixed chemically so they bear no evidence for contact with the fluid. However, in the more altered specimens, cores have been discoloured and must have been reached by the fluid. This implies that with increasing alteration, not only grain boundaries were in contact with the fluid but also grain cores. Alteration has thus been a multiple-step process. This first step of intergranular layer formation is observed in all samples and becomes more pronounced with increasing degree of alteration; the second step involves migration of fluids into grains with a sharp reaction front, consuming them and forming cloudy feldspar. It is often observed as a network of discolouration within the rock. The least altered samples (LT-3 and LT-12-3, see Appendix for photographed specimens), however, only show alteration in between the grains. Differences in speed and colour between inter- and intra-granular alterations imply that two different mechanisms were at work. The first one was the primary stage of fluid infiltration and has moved quickly over long distances through the rock. The latter has started up later, not being present in all altered samples. Its progress is different in every specimen, being almost complete in TØ-12-9. These two alteration features with the mechanisms behind them will be discussed separately.

6.2.1 Intergranular discolouration

In the larvikite rocks, reddening in between grains shows a gradual reaction front, implying a diffusion mechanism. Because it follows the grain boundaries (and occasionally cracks), it is thought to be caused by grain boundary diffusion. At these sites, loose atomic bonds result in a higher occurrence of dislocations which eases diffusion [Zhang, 2010]. Small grains have a relatively higher amount of such bonds and an enhanced chemical potential to cause reactions; this often results in dissolution and other surface reactions. For the coarse grained larvikites, however, this cannot be the case and a

diffusion process is more likely. The localized discolouration can either be explained by faster diffusive mass movement due to the open structure, or by fluid infiltration that was limited to the grain boundaries. Since reddening often indicates a change in oxidation state (oxidizing the present iron), the fluid hypothesis is favoured, transporting oxygen and other elements. It has sped up the diffusion process by reducing the energy needed for cation bond breaking. Also, it provided space for the atoms to diffuse to; grain boundary diffusion occurred locally without whole-rock-alteration. From the previously discussed chemical alteration analysis, it was concluded that the infiltrating water was most likely around 250 °C, too low for significant volume diffusion to occur within minerals. Because of their more open structure, boundaries are richer in elements which cannot normally be incorporated in mineral structures (like H^+). Combined with water, these formed the black precipitate observed in LT-12-3 and LT-1.

Farver and Yund (1995) experimentally determined grain boundary diffusion rates in feldspar aggregates, showing the importance of water along grain boundaries. Water unsaturated conditions allow ionic complexes to form on the boundary, resulting in a thin layer [Rubie, 1986] which enhances grain boundary diffusion rates, possibly by hydrolysis of Si-O bonds making weaker ones. For cation diffusion, this state is not very different (factor of 5–10) from water-absent conditions; for oxygen, however, it may have large effects because this quickly forms molecular water which can be transported [Farver and Yund, 1995]. These different values suggest a diffusion-controlled process; transport by fluid flow would lead to similar rates for all ions.

If more fluid is present, the dihedral angle θ between fluid-solid interfaces gives an indication whether fluid was connected (θ <60 °C) or not (θ >60 °C) [fig. 4, Watson *et al.*, 1990]. The truly wetting scenario, where transport rates are dominated by dissolution and ionic diffusion in the flow [Thompson, 1983] is very rare in silicate rocks due to mineral textures of these materials [Farver and Yund, 1995]. Instead, a thin connected fluid film is present at dihedral angles (θ <60 °C), limited by diffusion of material towards the grain boundary [Thompson, 1983] which is very sluggish at low temperatures. To give insight in the larvikite internal structure, X-ray images were made from different angles. These were combined to form a 3D-image, in which yellow areas represent features with a slightly lower density in a field of continuous material. Because their density is lower and the yellow dots line up, these parts are interpreted as porous areas, the resolution being too large to show the pores themselves. When the yellow areas of Fig. 21 are shown in a three-

dimensional image (fig. 30), they appear to form connected lines and even planes. These are interpreted to be grain boundaries. Unfortunately, structures are not very well outlined and no wetting angle can be determined. Instead, their connectivity is used as an indicator for the amount of fluid present. Most yellow dots appear in clusters on a plane, which shows that water formed a thin film along the whole grain boundary; three large unaltered grains of larvikite are visible without any internal porosity, surrounded by a matrix of finer material with some pores. Alteration paths can be followed throughout the rock. Since full wetting is unlikely [Watson *et al.*, 1990; Farver and Yund, 1995], the theory of connected channels which are limited by grain boundary diffusion of ions to the channels is most likely here.

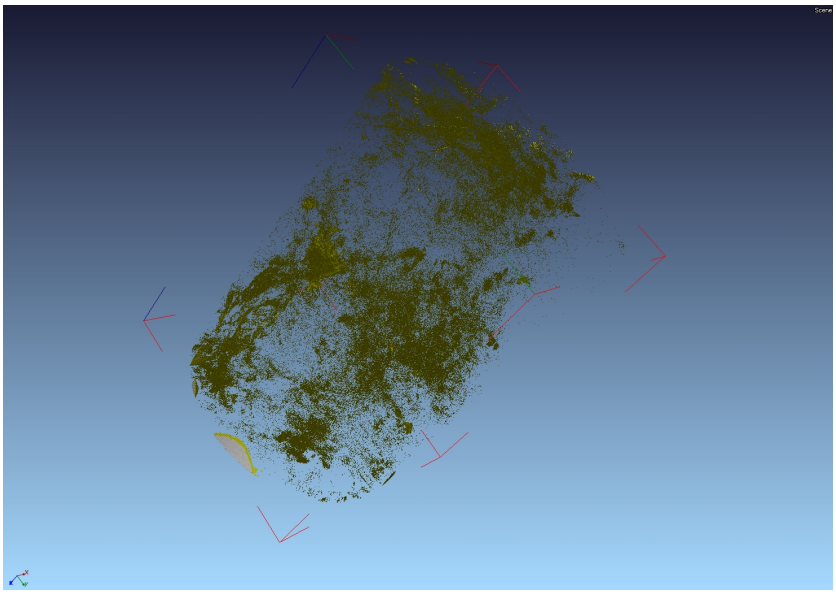

Figure 30: 3D structure of porous grain boundaries. The top right shows swarms of yellow dots which are connected, forming a grain boundary, as well as halfway on the left side. 3 large larvikite crystals can be recognized, on the top right, middle and right bottom.

Larvikite feldspars show no severe cracking of minerals, proving that fluid pressures were not high enough to cause hydrofracturing. There was enough fluid to reach an extensive band within the rock and seep through the grain boundaries. So a large enough quantity of localized water flow under low pressure entered the rock, which contained boundaries along which connected

fluid channels could form for ionic transport. This is consistent with the previously mentioned expected chemistry of the water.

In the larvikite rocks, water thus caused diffusion of material along the grain boundaries, resulting in a reddened layer depleted in feldspar components and enriched in more incompatible elements. Water could easily enter the rock in this way, diffusing through the more open structure of grain boundaries and occasional cracks. The Larvik Plutonic Complex shows bands which display such discolouration, confirming that infiltration was rapid and could affect larger areas but was constrained to regions with smaller grains to infiltrate in between. Only in the centre of these bands, grains have become consumed by the other mechanism. Apparently, more water or a longer residence time was needed for this process and that was not possible in the whole region.

6.2.2 Grain consumption

Microtextures inside altered grains show a sharp reaction front between the unaltered mineral and the orange discolouration, which is pseudomorphically overgrown. These features imply an interface-coupled dissolution-precipitation mechanism [Xia *et al.*, 2009; Putnis and Putnis, 2007; Putnis and John, 2010], based on surface kinetics. Another confirmation for this process is the generation of porosity, either being caused by volume decrease (which is too small in feldspar replacement, Hövelmann *et al.*, 2010) or by a difference in solubility between parent and daughter [Putnis, 2009] at full consumption of the parent. The reaction proceeds due to porosity generation, keeping the rock in contact with the fluid as the front migrates inwards [Engvik *et al.*, 2008; Hövelmann *et al.*, 2010; Putnis and Austrheim, 2010]. In this way, a reactive fluid can create its own pathway through mineral grains, changing physical properties of the medium during the reaction. This concept is called reactive transport. Porosity can be transient; some pores are closed later on, filled with tiny bright minerals. Closure of pores may be a result of Oswald ripening, the relatively high surface energy making it favourable to destroy small pores at the expense of larger ones.

Another hypothesis coupling dissolution and precipitation is described by Maliva and Siever (1988). It focuses on the stress that a growing mineral exerts on its surroundings, causing pressure dissolution of the minerals around. This process slows down with time because of supersaturation in the dissolved phase. Dissolution is thus spatially limited to the contact with

growing minerals. For the feldspar crystals in larvikite, this is highly unlikely because alteration occurs all around the grain, eating its way in. The kinetically-controlled mechanism is also more applicable since in feldspar replacement reactions, overgrowth is epitaxial as product and parent share a crystal structure.

Isotope studies of feldspars in contact with an alkali chloride solution have shown that oxygen exchanges during the reaction. This implies that it is not just a simple cation diffusion process but full dissolution-precipitation [Orville, 1962; O'Neil and Taylor, 1967], resulting in a porous product filled with dislocations [Hövelmann *et al.*, 2010]. Often these reactions are accompanied by losses of trace elements [Engvik *et al.*, 2008], but not in the larvikites. Here, fluids provide a means of re-equilibration to reach a more favourable energetic state. In feldspars, energy change is often related to strain energy from perthites. Strained parts are more soluble [Parsons and Lee, 2009], especially albite dissolving easier. The ease of the process depends on interfacial fluid composition and texture of the parent to act as a substrate for nucleation. The first factor is shown in similar replacement textures in a KBr-KCl system, which are found to be controlled by the composition of a thin fluid boundary layer [Putnis and Mezger, 2004; Putnis *et al.*, 2005]. Pseudomorphic overgrowths in this system are caused by the close coupling between parent and daughter crystal structure.

Larvikite textures thus imply that when fluid remains in contact with the minerals, dissolution starts. Dissolved ions may now be transported, but epitaxial growth implies rapid reprecipitation [Putnis and Austrheim, 2010], making transport over long distances unlikely. The lack of dissolution-precipitation mechanism in the beginning of water infiltration in larvikites may be related to the amount of fluid. If the solution was not wetting, small isolated pockets of fluid were present. These would not be able to dissolve large parts of the grains without quickly reaching the saturation index for another mineral, starting precipitation. Only when more fluid infiltrated, larger amounts of each crystal could be altered and only at connectivity of pores, the reaction could continue by constant fluid replenishment. Oxygen isotopes could be used to determine the size of the flux [Parsons and Lee, 2009].

Dissolution Feldspar replacement is driven by a reduction in free energy of the system, which occurs rapid because of water infiltration. Gibbs free

energy is dependent on an entropy term that drives diffusion, and an enthalpy term, which describes pressure as well as chemical potential and concentration of the species in solution (recall Eq. 3 from the introduction). The thermodynamic state of aqueous species is of vital importance for this interface-coupled dissolution-precipitation, the system responding quickly to small changes. Stability of a phase in a solution is described as chemical potential, dependent on ion activity in a fluid, which is (recall from Equation 4) $\mu_i = \mu_i^0 + RTln(a_i) = \mu_i^0 + RTln(\gamma_i c_i)$, with μ_i^0 as standard chemical potential, a_i is activity, γ_i is the activity coefficient and c_i is concentration [Oelkers *et al.*, 2009].

For water-rock interaction, focus on the kinetics behind dissolution and precipitation is more important than equilibrium calculations. Activity-activity diagrams are based on a quickly established equilibrium, in which only one phase precipitates. Technically this is not the case in the larvikites, which form albite and K-feldspar simultaneously. However, mineral stability can be shown in an activity-activity diagram (fig. 26) where conditions at the boundary of two stability fields can explain co-precipitation. Because of a kinetically-controlled process, phases are metastable at near-equilibrium conditions and minerals can precipitate outside their stability field and coexist with another phase [Lasaga *et al.*, 1994; Zhu *et al.*, 2004].

Many authors have described the reaction of a non-magmatic or nonmetamorphic (without initial Si, Al or K) fluid in contact with feldspars [Helgeson, 1971; Burch *et al.*, 1993; Lasaga *et al.*, 1994; Alekseyev *et al.*, 1997; Fu *et al.*, 2009; Zhu *et al.*, 2010; Lu *et al.*, 2013] and tried to determine fluid compositions. At feldspar dissolution, this system shows a range of precipitates when the fluid starts to equilibrate with the rock, from gibbsite and kaolinite to feldspars near equilibrium. Although in the larvikites only feldspar-feldspar replacement is observed, these studies can still be used to discuss feldspar dissolution mechanisms, which are the same no matter what precipitate is formed. Because only feldspar was formed and no relics of former secondary minerals are present, the fluid must have been close to equilibrium with the dissolving rock during precipitation. Other evidence that supports this is the constant Si:Al ratio during alteration (table 3 and fig. 24), not altering the major component ratios (which would be the case when gibbsite or kaolinite are precipitated). Also, the rapid shift in precipitated mineral phase is due to quickly reached stoichiometric supersaturation because there is a narrow range of fluid compositions in which equilibrium is reached with intermediate compositions [Putnis, 1992].

When temperatures of a solution increase, it can hold less dissolved Na and more K [Philpotts and Ague, 2009]. Because both phases precipitate in the larvikites, temperatures must not have favoured one over the other and must have been intermediate. However, further away from the front some samples show only K-feldspar is present, indicating a possible later equilibration to favour K-precipitation and a drop in Na^+-activity relative to K^+ (so a cooling trend).

Precipitation When the equilibrium approach (not kinetics) is used, increasing ionic concentrations in a solution can continue until a saturation limit is reached. At this point, the fluid is oversaturated in one mineral and upon nucleation, a precipitate will form. Fu *et al.* (2009) have shown that secondary growing minerals do not inhibit dissolution in a system where clean water reacts with a granite. During feldspar dissolution, the amount of free H^+ in solution is said to decrease; the opposite trend is observed for larvikite when going from unaltered to altered rock. This difference is explained by consumption of SiO_2 (aq) rather than H_4SiO_4, which would alter the pH; the former is used by Fu *et al.* (2009) while the latter is used for larvikite. An amorphous layer is also formed [Zhu *et al.*, 2004, 2006] which can either be due to leaching (hypothesis of Nesbitt *et al.*, 1991 and Schott *et al.*, 2012) or due to silica precipitation [Hellmann *et al.*, 2003; Ruiz-Agudo *et al.*, 2012].

A negative saturation index (SI) for albite shows the ongoing dissolution process of hydrolysis, while a positive one for K-feldspar shows (over)saturation with time. This results in a preferential dissolution of Na-lamellae [Parsons and Lee, 2009], which consumes H^+. K-feldspar dissolution also uses H^+ to form muscovite (illite) under more neutral pH and kaolinite and boehmite under more acidic conditions. Feldspar-feldspar replacement occurs at neutral pH. Fig. 31 shows the significant shift in mineral stability when Na_2O is replaced by K_2O in a system that is the same in every other aspect. Changes in ionic composition cause large shifts in the stability field. Ion availability is also related to dissolved minerals further away. For isotopes and REEs, small distributional differences can be observed and element immobility may not be a valid assumption, which would severely change the reactions we work with [Putnis, 2009].

Coupled processes In the feldspars, epitaxial overgrowth is observed, showing the close inter-dependence of dissolution and precipitation men-

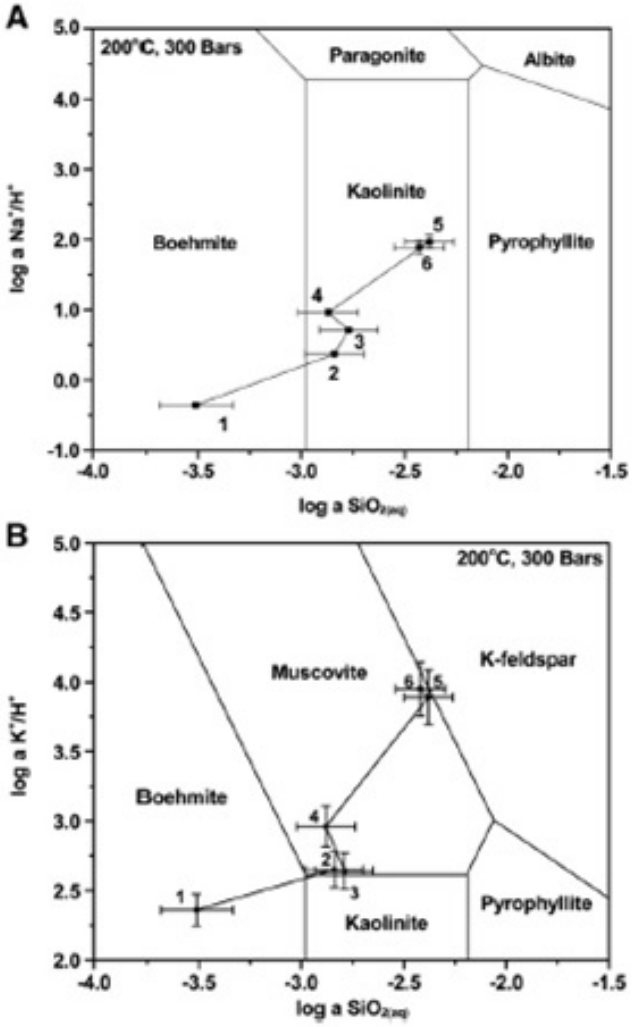

Figure 31: Two mineral phase diagrams, one for Na_2O (a) and one for K_2O (b) showing the difference that ionic composition can make for mineral stability fields. From: Fu et al., 2009.

tioned by many authors [Putnis and Mezger, 2004; Putnis *et al.*, 2005; Xia *et al.*, 2009]. Nucleation thus occurred quickly after dissolution, showing that the solution must have been close to equilibrium for both minerals. At this point, small changes in ion activity can cause a rapid change in precipitating phase [Burch *et al.*, 1993]. Also, metastability and simultaneous precipita-

tion of phases can occur [Lasaga *et al.*, 1994; Zhu and Lu, 2009]. This would explain the close intergrowths of porous albite and K-feldspar in the larvikite rocks; the solution was close to supersaturation for both mineral phases, precipitating feldspars that are either Na- or K-rich. At this 'quasi-steady state' [Alekseyev *et al.*, 1993] it is not uncommon for phases to grow simultaneously and stay in existence despite being just outside their stable field. However, pressure-temperature conditions must have remained close to the boundary between these two, shown in the activity-activity diagram of Fig. 26 in order to maintain this structure through time. No secondary electron images, displaying surface relief, were made to investigate secondary mineral growth at the feldspar surface.

6.3 Large scale implications

If fluid inflow occurs under high pressure or leads to volume increase, reaction-induced fracturing may occur [Jamtveit *et al.*, 2009]. With this rock fracturing, massive fluid flow is facilitated [Putnis and Austrheim, 2010]. Despite the severe hydrothermal alteration in the larvikites, no such textures are observed. Instead, pervasive alteration was caused by a long period of continued fluid-rock interaction. Fluid flow is dependent on pathways within the rock, either pre-existing or created by the alteration mechanisms. In the larvikite rocks, fluid first infiltrated along grain boundaries and continued through interface-coupled dissolution-precipitation (fig. 29), the pathway being created by porosity increase. Despite porosity generation, the volume has remained constant since no cracking occurred, showing that porosity was facilitated by relative solubilities between parent and daughter rock. The grain boundary diffusion mechanism also proceeded by water, which acted as a means of lowering activation energy to make redistribution of elements possible. This fluid followed pre-existing paths and has not induced cracking because of its low amount.

Discolouration and alteration are often related to the proximity of (syenite) veins, although analysis of sample LT-2A has shown no alteration next to the syenite. This implies that the fluid has come from syenite intrusions but has not caused fracturing; only an extensional tectonic environment could have facilitated infiltration and intrusions without severe cracking. Fluid flow is induced by extension, a gradient in hydraulic head allowing migration to the surface. Indications for additional gradients in pH, temperature, oxidation state or other chemical driving forces are not observed since alteration

textures appear uniform throughout the rock.

The lack of bulk rock chemical change implies that no large mass transfer has occurred. It is therefore not likely that this infiltration event has led to the Kodal apatite-ilmenite-magnetite deposits.

6.4 Future studies

In order to decipher large-scale fluid movement through the continental crust, further research is needed to understand the speed of replacement fronts and the 'lifetime' of interconnected porosity networks. The current research has only dealt with the chemical and physical aspects of the reaction, and has not made any assumptions for the speed and duration of the reaction. However, these factors may turn out to be of vital importance for re-equilibration; for example, how fast could dissolution-precipitation go, and how much time was there for the process? Was the same small amount of water slowly seeping through the rock and altering everything or it was a larger amount coming in from all sides? These questions are a topic for further study and will involve isotope analysis.

For geospeedometry, the stable lithium isotopes are a useful tool. ^6Li and ^7Li become fractionated during diffusion due to their different diffusion coefficients, ^6Li diffusing much more rapid. Measuring the δ^7Li at several distances from the reaction front can thus shed light on the speed of this first step of grain boundary diffusion [John *et al.*, 2012] and on reaction progress. The duration and rate of the reaction can be estimated from this. Once reaction rates are known, better temperature and chemical constraints can also be placed on the system and an estimate of fluid composition and pH can be given.

Another application of stable isotopes often used for fluid origin is the analysis of oxygen and hydrogen. Because of the large mass difference between the stable isotopes of each element, these isotopes act differently during geochemical processes and become easily fractionated during processes such as crystallisation or evaporation. Therefore, the combination of hydrogen and oxygen isotope values in a fluid can be used to determine that fluids' source. For the atmosphere, values for both elements are known and a Meteoric Water Line (fig. 32) is made to plot the ratios of $\delta^{18}O$ and δD at the poles and the equator. Hydrothermal fluids often originate from meteoric water, but have reacted with the surrounding minerals. Since rock is much higher in oxygen than in hydrogen, the fluid compositions evolve in a straight

line to the right of the MWL. Deuteric fluids are even further away from the meteoric water in composition. Using the relation between $\delta^{18}O$ and δD, it is easy to distinguish meteoric from deuteric water, a question that remains open after the completion of this study.

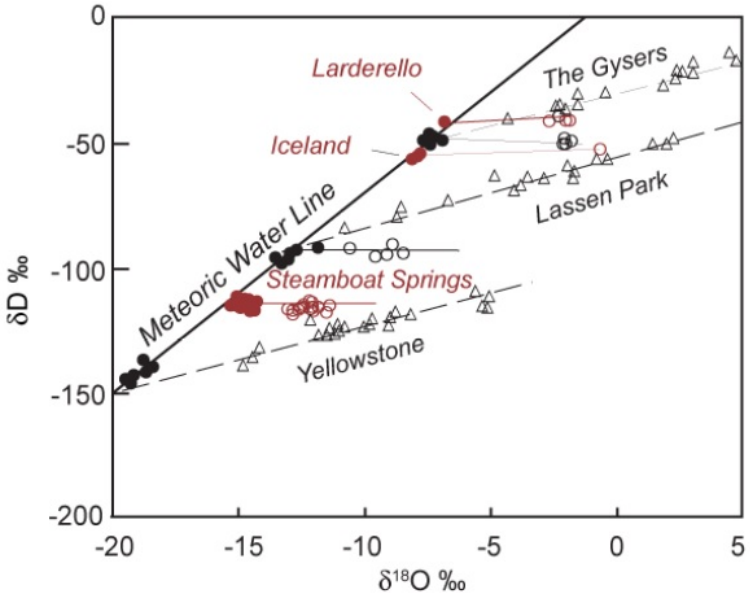

Figure 32: Meteoric Water Line (black solid) showing lines of $\delta^{18}O$ and δD evolution for several hydrothermal systems. Closed circles represent meteoric water compositions; open circles and triangles represent geothermal waters. From: Craig, 1963.

7 Conclusions

In the feldspathic mineralogy in the Larvik Plutonic Complex in SE Norway, evidence for alteration has been captured in both textures and mineral chemistry. After crystallisation from an intermediate magma under anhydrous conditions around 850 °C, cooling induced ordering of the ternary feldspar structure. This resulted in thin lamellae or perthites, which cause the blue iridescence in larvikite crystals. A second stage of feldspar alteration is considered to be hydrothermal and visible in orange to red discolouration. Fine grained red material was observed between grains, representing grain boundary diffusion that was facilitated by minor water infiltration. Incompatible elements concentrated on these boundaries and formed a black mineral in the presence of water. More severe alteration is seen as a second hydrothermal stage, where crystals have a rim that ranges from not to completely altered and porous feldspar. The presence of pores pleads against the mechanism of diffusion, which will be impeded by them, and a sharp contact between unaltered and altered mineral is another indication for fluid-induced re-equilibration (in which case the fluid access was reaction-limiting). These factors combined with pseudomorphous replacement of the old feldspar suggest that the mechanism behind this is **interface-coupled dissolution-precipitation**. Pores constitute to the continuation of this reaction, because they increase the reaction surface and create a network for fluid replenishment. Perthites speed up dissolution, albite being more soluble. However, pores were not found to be concentrated in one particular mineralogy.

No large element fluxes are observed to accompany this textural change. Especially the ratio between SiO_2 and Al_2O_3 is very constant. Variation in alkali content is shown in the mass balanced equation but there is no textural evidence for severe loss in K. Instead, Na^+ and K^+ appear to be enriched in feldspars in equal amounts (while Ca is lost), forming porous patches of albite and K-feldspar that co-precipitated, indicating that the fluid must have been of intermediate temperatures. However, around altered minerals a rim of pure K-feldspar is often present, which implies a later stage cooling to favour K-precipitation. The newly formed tønsbergite is chemically the same as the old larvikite rock. Reddening can only be explained by formation of hematite fragments in pores, which grew during the fluid-rock interaction. The ternary feldspar is unmixed in pure albite and K-feldspar. Calcium from the larvikite has become incorporated in minor phases such as apatite,

calcite, titanite and pumpellyite.

Because bulk rock chemistry remains the same and no fracturing is observed, constant volume and conservation of mass are assumed. The system is considered to be dilute, making it easy for ions to be transported by the fluid. The lack of bulk rock chemical alteration, however, implies that no large mass transfer has occurred. It is therefore not likely that this infiltration event has led to the nearby Kodal ore deposits.

Trace element contents within the rock have also stayed constant throughout the reaction. REE immobility rules out the process of albitisation, where great loss in these elements is expected to accompany a Na-increase. Because temperatures above 300 °C are needed for trace metals to become mobilised and major elements can migrate at slightly lower temperatures, the fluid must have been at 250–300 °C. Immobility of REEs could also be due to a low fluid: rock ratio or **the absence of complexing agents** such as $(OH)^-$ or F, which shows that the water was not very high in pH. A low pH on the other hand would cause severe feldspar dissolution and precipitation of other phases. **pH is therefore considered to be neutral**. Since this alteration purely involved a feldspar-feldspar replacement, the fluid must have been close to feldspathic in composition, and quickly equilibrating to form a new feldspar phase out of the dissolved ions, which would inhibit mass transfer. Quick precipitation is also likely if **only small amounts of fluids are present**. The feldspar activity-activity diagram has shown that the system contained $KCl - H_2O - H_4SiO_4$, minor phases estimate the fluid to be around **250 °C, 1–3 kb and slightly oxidizing**, and at the boundary between K-feldspar and albite stability which shows a slightly higher Na content. Indications for gradients in pH, temperature, oxidation state or other chemical driving forces are not observed since alteration textures appear uniform throughout the rock.

Since the fluid composition was close to feldspathic, the fluid origin can either be enriched in feldspar components by previous mineral dissolution (without replacement) or be deuteric. No proof for large amounts of feldspar dissolution has been found. Therefore, the reaction may be caused by deuteric fluids, just like perthite formation. The current reaction may be an extreme form of magmatic unmixing.

The absence of a chemical change shows that this reaction was purely a re-equilibration to reduce free energy in the system. The old larvikite had become energetically unstable at the present conditions but re-equilibration could not occur due to the energy barrier to start the reaction. At wa-

ter infiltration, this threshold was lowered and the more stable phase with unmixed feldspars could form. The first step was infiltration along grain boundaries, facilitating grain boundary diffusion. When more water infiltrated, the dissolution-precipitation reaction continued to order the feldspar, resulting in a full unmixing. Excess elements formed minor phases inside pores, generated during fluid infiltration. Water acted as a fast means of transport to minimize the free energy in the system by textural changes. The mutual replacement reaction was in fact a retrograde mineral change. Therefore, the alteration is visible as bands through the rock which clearly show where the fluid has been. Small amounts of fluid can thus affect large areas because fluid was able to react through grains and access fresh rock. Future work is needed to determine on the lifetime of porosity and speed of the replacement front.

8 Acknowledgements

I would like to thank Oliver Plümper for providing the samples, supervising this thesis and supporting me during the research. Also, thanks goes to Tilly Bouten for her assistance with the electron microprobe analyses and Peter van Krieken for help with the Leica optical microscope and density measurements. Auke Barnhoorn and Wim Verwaal of the Technical University in Delft are thanked for their help with the X-ray tomography. Additionally, I am grateful to my roommates in room N214 for their nice company.

9 References

Aagaard, P. and Helgeson, H.C. (1982). Thermodynamic and kinetic constraints on reaction rates among minerals and aqueous solutions-I. Theoretical Considerations. Amer. J. Sci. 282, 237-285

Adamson, A.W. (1960). Physical Chemistry of Surfaces. Interscience Publishers

Alekseyev, V. A., Medvedeva, L. S., Prisyagina, N. I., Meshalkin, S. S. and Balabin, A. I. (1997). Change in the dissolution rates of alkali feldspars as a result of secondary mineral precipitation and approach to equilibrium. Geochim. Cosmochim. Acta 61, 1125-1142

Andersen, T., Erambert, M., Larsen, A.O. and Selbekk, R.S. (2010). Petrology of Nepheline Syenite Pegmatites in the Oslo Rift, Norway: Zirconium Silicate Mineral Assemblages as Indicators of Alkalinity and Volatile Fugacity in Mildly Agpaitic Magma. J. Petr. 51(11), 2303-2325

Andersen, T. and Sørensen, H. (2003). Microsyenite from Lake Mykle, Oslo Rift: Subvolcanic rocks transitional between larvikite and nordmarkite. NGU-bull. 441, pp. 25-31

Arnórsson, S. and Stefánsson, A. (1999). Assessment of feldspar solubility constants in water in the range 0 °C to 350 °C at vapor saturation pressures. Am. J. Sci. 299, 173-209

Bau, M. (1991). Rare-earth element mobility during hydrothermal and metamorphic fluid-rock interaction and the significance of the oxidation state of europium. Chem. Geol. 93, 219-230

Bau, M. (1996). Controls on the fractionation of isovalent trace elements in magmatic and aqueous systems: evidence from Y/Ho, Zr/Hf, and lanthanide tetrad effect. Contrib. Min. Petr. 123, 323-333

Bergstøl, S. (1972). The jacupirangite at Kodal, Vestvold, Norway. A potential magnetite, ilmenite and apatite ore. Min. Dep. 7, 233-246
Berner, R.A. and Holdren, G.R. Jr (1977). Mechanism of feldspar weathering. Some observational evidence. Geol. 5, 369-372
Blum, A.E. and Lasaga, A.C. (1987). Monte Carlo simulations of surface reaction rate laws. In: Stumm, W. (ed.) Aquatic Surface Chemistry: Chemical Processes at the Particle-Water Interface, pp. 255-292
Blum, A. and Lasaga, A. (1988). Role of surface speciation in the low-temperature dissolution of minerals. Nature 331(6155), 431-433
Blum, A. E. and Lasaga, A. C. (1991). The role of surface speciation in the dissolution of albite. Geoch. Cosmoch. Acta 55, 2193-2201
Blum, A.E., Yund, R.A. and Lasaga, A.C. (1990). The effect of dislocation density of dissolution rate of quartz. Geoch. Cosmoch. Acta 54, 283-297
Böttcher, M.E. (1997a). Experimental dissolution of $CaCO_3$-$MnCO_3$ solid solutions in CO_2-H_2O solutions at 20 °C -I. Synthetic low-temperature carbonates. Sol. St. Ionics 101-103, 1263-1266
Bowden, P. (1985). The geochemistry and mineralization of alkaline ring complexes in Africa (a review). J. Afr. Earth Sc 3, 17-40
Brady, J.B. and Cherniak, D.J. (2010). Diffusion in Minerals: an Overview of Published Experimental Diffusion Data. In: Zhang, Y. and Cherniak, D.J. (ed.) Diffusion in Minerals and Melts. Rev. in Min. and Geoch, vol. 72, pp. 899-920
Brantley, S.L., Kubichi, J.D. and White, A.F. (2008). Kinetics of Water-Rock Interactions. 1rst ed. Springer, New York
Brantley, S. L. and Stillings, L. (1996). Feldspar dissolution at 25 °C and low pH. Am. J. Sci. 296, 101-127
Brown, W.L. and Parsons, I. (1984). The nature of potassium feldspar, exsolution microtextures and development of dislocations as a function of composition in perthitic alkali feldspars. Contrib. Mineral. Petr. 86, 335-341
Brown, W.L. and Parsons, I. (1988). Zoned ternary feldspars in the Klokken intrusion: exsolution microtextures and mechanisms. Contrib. Mineral. Petr. 98, 444-454
Brøgger, W.C. (1890). Die Mineraliën der Syenitpegmatitgänge der südnorwegischen Augit- und Nephelinsyenite. Z. Kristall. 16
Burch, T.E, Nagy, K.L. and Lasaga, A.C. (1993). Free energy dependence of albite dissolution kinetics at 80 °C and pH 8.8. Chem. Geol. 105,

137-162
Carmichael, I.S.E. (1967). The mineralogy and petrology of the volcanic rocks from the Leucite Hills, Wyoming. Contr. Min. Petr. 15, 24-66
Casey, W., Carr, M.J. and Graham, R.A. (1988). Crystal defects and the dissolution kinetics of rutile. Geoch. Cosmoch. Acta 52, 1545-1556
Casey, W.H., Westrich, H.R., Arnold, G.W. and Banfield, J.F. (1989a). The surface chemistry of dissolving labradorite feldspar. Geoch. Cosmoch. Acta 53, 821-832
Casey, W.H., Westrich, H.R., Massis, T., Banfield, J.F. and Arnold, G.W. (1989b). The surface of labradorite feldspar after acid hydrolysis. Chem. Geol. 78, 205-218
Casey, W. H., Westrich, H.R. and Holdren, G.R. (1991). Dissolution rates of plagioclase at pH=2 and 3. Am. Min. 76(1-2), 211-217
Cherniak, D.J. (2010). Cation Diffusion in Feldspars. In: Zhang, Y. and Cherniak, D.J. (ed.) Diffusion in Minerals and Melts. Rev. in Min. and Geoch, vol. 72, pp. 691-734
Chou, L. and Wollast, R. (1984). Study of the weathering of albite at room temperature and pressure with a fluidized bed reactor. Geoch. Cosmoch. Acta 48(11), 2205-2217
Chou, L. and Wollast, R. (1985). Steady state kinetics and dissolution mechanisms of albite. Am. J. Sci. 285, 963-993
Craig, H. (1963). The isotopic composition of water and carbon in geothermal areas. Nucl. Geol. on Geoth. Areas. In: Tongiorgi, E. (ed.), pp. 17-53, Pisa: CNR Lab. Geol. Nucl.
Criscenti, L.J., Brantley, S.L., Mueller, K.T., Tsomaia, N. and Kubicki, J.D. (2005). Theoretical and ^{27}Al CPMAS NMR investigation of aluminium coordination changes during aluminosilicate dissolution. Geoch. Cosmoch. Acta 69(9), 2205-2220
Dahlgren, S. (2010). The larvik plutonic complex: The larvikite and nepheline syenite plutons and their pegmatites. The Langesundsfjord. History, Geology, Pegmatites, Minerals, pp. 26-37.
Deer, W.A., Howie, R.A. and Zussman, J. (2001). Rock forming minerals 4A, Framework Silicates: Feldspars. 2nd ed. The Alden Press, Oxford UK
Dohmen, R. and Milke, R. (2010). Diffusion in Polycrystalline Materials Grain Boundaries, Mathematical Models, and Experimental Data. In: Zhang, Y. and Cherniak, D.J. (ed.) Diffusion in Minerals and Melts. Rev. in Min. and Geoch, vol. 72, pp. 921-970

Engvik, A.K., Golla-Schindler, U., Berndt-Gerdes, J., Austrheim, H. and Putnis, A. (2009). Intragranular replacement of chlorapatite by hydroxy-fluor-apatite during metasomatism. Lithos 112(3-4), 236-246

Engvik, A.K., Putnis, A., Fitz Gerald, J.D and Austrheim, H. (2008). Albitisation of granitic rocks: The mechanism of replacement of oligoclase by albite. Can. Min. 46, 1401-1415

Eyring, H. (1935). The activated complex in chemical reactions. J. Chem. Phys. 3, 107-115

Farver, J.R. (2010). Oxygen and Hydrogen Diffusion in Minerals. In: Zhang, Y. and Cherniak, D.J. (ed.) Diffusion in Minerals and Melts. Rev. in Min. and Geoch, vol. 72, pp. 447-508

Farver, J.R. and Yund, R.A. (1995). Grain boundary diffusion of oxygen, potassium and calcium in natural and hot-pressed feldspar aggregates. Contr. Min. Petr. 118, 340-355

Fritz, B. And Noguera, C. (2009). Mineral Precipitation Kinetics. In: Oelkers E.H., Schott J. (eds.) Thermodynamics and Kinetics of Water-Rock Interactions. Rev. in Min. and Geoch., vol. 70, pp. 371-410

Fu, Q., Lu, P., Konishi, H., Dilmore, R., Xu, H., Seyfried, W. E. Jr. and Zhu, C. (2009). Coupled alkali-feldspar dissolution and secondary mineral precipitation in batch systems: 1. New experiment data at 200 °C and 300 bars. Chem. Geol. 91, 955-964

Fuhrman, M.L. and Lindsley, D.H. (1988). Ternary-feldspar modeling and thermometry. Am. Min. 73, 210-215

Furrer, G. and Stumm, W. (1986). The coordination chemistry of weathering-I. Dissolution kinetics of d-Al_2O_3 and BeO. Geoch. Cosmoch. Acta 48, 2405-2432

Ganor, J., Lu, P., Zheng, Z. and Zhu, C. (2007). Bridging the gap between laboratory measurements and field estimations of weathering using simple calculations. Environ. Geol. 53, 599-610

Hamilton, J.P., Brantley, S.L., Pantano, C.G., Criscenti, L.J., and Kubicki, J.D. (2001). Dissolution of nepheline, jadeite and albite glasses: Toward better models for aluminosilicate dissolution. Geoch. Cosmoch. Acta 65(21), 3683-3702

Harlov, D.E. and Austrheim, H. (2013). Metasomatism and the Chemical Transformation of Rock: The Role of Fluids in Terrestrial and Extraterrestrial Processes. 1rst ed. Springer-Verlag, Berlin

Helgeson, H.C. (1971). Kinetics of mass transfer among silicates and aqueous solutions. Geoch. Cosmoch. Acta 35, 421-469

Helgeson, H.C., Delaney, J.M, Nesbitt, H.W. and Bird, D.K. (1978). Summary and critique of the thermodynamic behavior of aqueous electrolytes at high pressures and temperatures-IV. Calculation of activity coefficients, osmotic coefficients and apparent molal and relative partial molal properties to 600 °C and 5 kb. Am. J. Sci. 281, 1249-1516

Hellmann, R., Eggleston, C.M., Hochella, M.F. and Crerar, D.A. Jr. (1990). The formation of leached layers on albite surfaces during dissolution under hydrothermal conditions. Geoch. Cosmoch. Acta 54, 1267-1281

Helgeson, H.C., Garrels, R.M. and Mackenzie, F.T. (1969b). Evaluation of irreversible reactions in geochemical processing involving minerals and aqueous solutions-II. Applications. Geoch. Cosmoch. Acta 33, 455-481

Helgeson, H. C., Murphy, W. M. and Aagaard, P. (1984). Thermodynamic and kinetic constraints on reaction rates among minerals and aqueous solutions-II. Rate constants, effective surface area, and the hydrolysis of feldspar. Geoch. Cosmoch. Acta 48, 2405?2432

Hellmann, R. (1994). The albite-water system: Part I. The kinetics of dissolution as a function of pH at 100, 200 and 300 °C. Geoch. Cosmoch. Acta 58, 595-611

Hellmann, R., Penisson, J.-M., Hervig, R.L., Thomassin, J.-H., Abrioux, M.-F. (2003). An EFTEM/HRTEM high resolution study of the near surface of labradorite feldspar altered at acid pH: evidence for interfacial dissolution-reprecipitation. Phys. Chem Min. 30, 192-197

Holdren, G.R. Jr. and Berner, R.A. (1979). Mechanism of feldspar weathering-I. Experimental studies. Geoch. Cosmoch. Acta 43(8), 1161-1171

Holdren, G.R. and Speyer, P. (1985). pH dependent changes in the rates and stoichiometry of dissolution of an alkali feldspar at room temperature. Am. J. Sci. 285, 994-1026

Holdren, G.R. and Speyer, P. (1987). Reaction rate-surface area relationships during the early stages of weathering-II. Data on eight additional feldspars. Geoch. Cosmoch. Acta 51, 2311-2318

Hövelmann, J., Putnis, A., Geisler, T., Schmidt, B.C., Golla-Schindler, U. (2010). The replacement of plagioclase feldspars by albite: observation from hydrothermal experiments. Contrib. Min. Petr. 159, 43-59

Iiyama, J.T. (1979). Trace Element Distribution in Rock-Forming Silicates. The Alkali and Alkaline Earths

Jamtveit, B., Putnis, C.V., Malte-Sørenssen, A. (2009). Reaction induced

fracturing during replacement processes. Contr. Min. Petr. 157, 127-133

John T., Gussone N., Podladchikov Y.Y., Bebout G.E., Dohmen R., Halama R., Klemd R., Magna T., Seitz H.-M. (2012). Volcanic arcs fed by rapid pulsed fluid flow through subducting slabs. Nature Geosc. Let. 5, 489-492

Kinnaird, J.A. (1985). Hydrothermal alteration and mineralization of the alkaline anorogenic ring complexes of Nigeria. J. Afr. Earth Sc. 3, 229-252

Knauss, K.G. and Wolery, T.J. (1986). Dependence of albite dissolution kinetics on pH and time at 25 °C and 70 °C. Geoch. Cosmoch. Acta 50, 2481-2497

Kulik, D.A. (2009). Thermodynamic Concepts in Modeling Sorption at the Mineral-Water Interface. In: Oelkers E.H., Schott J. (eds.) Thermodynamics and Kinetics of Water-Rock Interactions. Rev. in Min. and Geoch., vol. 70, pp. 125-180

Labotka, T.C., Cole, D.R., Fayek, M., Riciputi, L.R. and Staderman, F.J. (2004). Coupled cation and oxygen exchange between alkali feldspar and aqueous chloride solution. Am. Min. 89, 1822-1825

Langmuir, D. (1997). Aqueous environmental geochemistry. Prentice Hall, New Jersey

Lasaga, A.C. (1981). Transition State Theory. Rev. Mineral 8, 135-169

Lasaga, A.C. (1984). Chemical kinetics of water-rock interactions. J. Geophys. Res. 89, 4009-4025

Lasaga, A.C. (1990). Atomic Treatment of Mineral-Water Surface Reactions. In: Hochella, M.F. and White, A.F. (eds.) Mineral-Water Interface Geochemistry: Rev. Mineral 23, 17-85

Lasaga, A.C., Soler, J.M., Ganor, J., Burch, T.E. and Nagy, K.L. (1994). Chemical weathering rate laws and global geochemical cycles. Geoch. Cosmoch. Acta 58(10), 2361-2386

Lee, M.R. and Parsons, I. (1995). Microtextural controls of weathering of perthitic alkali feldspars. Geoch. Cosmoch. Acta 59, 4465-4488

Lee, M.R. and Parsons, I. (1997). Dislocation formation and albitization in alkali feldspars from the Shap granite. Am. Min. 82, 557-570

Lifshitz, I.M and Slyozov, U.V. (1961). The kinetics of precipitation from supersaturated solid solutions. J. Phys. Chem. Solids 19, 33-50

Lindberg, P.A. (1985). Fe-Ti-P mineralizations in the larvikite-lardalite complex, Oslo Rift. Norsk. geol. und. Bul. 402, 93-98

Lippmann, F. (1980). Phase diagrams depicting the aqueous solubility of binary mineral systems. N. Jahrb. Min. Abh. 130, 243-263

Lu, P., Fu, Q., Seyfried, W.E. Jr., Hedges, S.W., Soong, Y., Jones, K. and Zhu, C. (2013). Coupled alkali feldspar dissolution and secondary mineral precipitation in batch systems-2: New experiments with supercritical CO_2 and implications for carbon sequestration. Appl. Geoch. 30, 75-90

Maliva, R.G. and Siever, R. (1988). Diagenetic replacement controlled by force of crystallization. Geol. 16, 688-691

Markov, I.V. (1995). Crystal growth for Beginners: fundamentals of nucleation, crystal growth and epitaxy. World Scientific, Singapore, New Jersey, London, Hong Kong.

Michard, A. (1989). Rare earth element systematics in hydrothermal fluids. Geoch. Cosmoch. Acta 53, 745-750

Muir, I.D. (1962). The paragenesis and optical properties of some ternary feldspars. Norsk Geol. Tisddkr. 42, 477-492

Muir, I.J., Bancroft, G.M. and Nesbitt, H.W. (1989). Characteristics of altered labradorite surfaces by SIMS and XPS. Geoch. Cosmoch. Acta 53(6), 1235-1241

Muir, I.J., Bancroft, G.M., Shotyk, W. and Nesbitt, H.W. (1990). A SIMS and XPS study of dissolving plagioclase. Geoch. Cosmoch. Acta 54, 2247-2256

Muir, I.J. and Nesbitt, H.W. (1991). Effect of aqueous cations on the dissolution of labradorite feldspar. Geoch. Cosmoch. Acta 55, 3181-3189

Muir, I.D. and Smith, J.V. (1956). Crystallization of feldspars in larvikites. Z. Kristall. 107, 182-195

Nesbitt, H.W., Macrae, N.D. and Shotyk, W. (1991). Congruent and incongruent dissolution of labradorite in dilute, acidic, salt solutions. J. Geol. 99(3), 429-442

Neumann, E.R. (1980). Petrogenesis of the Oslo Region Larvikites and Associated Rocks. J. Petr. 21(3), 499-531

Neumann, E.R., Olsen, K.H., Baldridge, W.S. and Sundvoll, B. (1992). The Oslo-rift: A review. Tectonophysics 208, 1-18

Neumann, H. (1944). Silver deposits at Kongsberg: the mineral assemblage of a native silver-cobalt-nickel ore type. Norges geologiske Undersøkelse, vol. 162. Aschehoug i komm., Oslo.

Niedermeier, D.R.D., Putnis, A., Geisler, T., Golla-Schindler, U., Putnis, C.V. (2009). The mechanism of cation and oxygen exchange in alkali feldspars under hydrothermal conditions. Contrib. Min. Petr. 157, 65-76

Norton, D.L. and Dutrow, B.L. (2001). Complex behaviour of magma-hydrothermal processes: Role of supercritical fluid. Geoch. Cosmoch. Acta 65(21), 4009-4017

Nunes, J.L. (1979). Amazonites de Mocambique. Communic. Serv. Geol. Portugal LXIV, 71-79

Oelkers, E.H. (2001). General kinetic description of multioxide silicate mineral and glass dissolution. Geoch. Cosmoch. Acta 65, 3703-3719

Oelkers, E.H., Bénézeth, P. and Pokrovski, G.S. (2009). Thermodynamic Databases for Water-Rock Interaction. In: Oelkers E.H., Schott J. (eds.) Thermodynamics and Kinetics of Water-Rock Interactions. Rev. in Min. and Geoch., vol. 70, pp. 1-46

Oelkers, E.H., Golubev, S.V., Chaïrat, C., Pokrovsky, O.S. an Schott, J. (2009). The surface chemistry of multi-oxide silicates. Geoch. Cosmoch. Acta 73(16), 4617-4634

Oelkers, E.H., Schott, J. and Devidal, J.L. (1994). The effect of aluminum, pH , and chemical affinity on the rates of aluminosilicate dissolution reactions. Geoch. Cosmoch. Acta 58, 2011-2024

Oelkers, E.H. and Schott, J. (1995). Experimental study of anorthite dissolution and the relative mechanism of feldspar hydrolysis. Geoch. Cosmoch. Acta 59, 5039-5053

Oftedahl, C. (1948). Studies on the igneous rock complex of the Oslo Region XI. The feldspars. Skr. Norske Vidensk.-Akad. Oslo, I. Mat.-naturvidensk. Kl. 3.

Oliver, N. (1996). Review and classification of structural controls on fluid flow during regional metamorphism. J. Metam. Geol. 14(4),477?492

Oliver, N.H.S., Cleverley, J.S., Mark, G., Pollard, P.J., Fu, B., Marshall, L.J., Rubenach, M.J., Williams, P.J. and Baker, T. (2004). Modeling the Role of Sodic Alteration in the Genesis of Iron Oxide-Copper-Gold Deposits, Eastern Mount Isa Block, Australia. Econ. Geol. 99, 1145-1176

O'Neil, J.R. and Taylor, H.P. (1967). The oxygen isotope and cation exchange chemistry of feldspars-I. Am. Min. 52, 1414-1437

Orville, P.M. (1962). Alkali metasomatism and feldspars. Norsk Geol. Tidsskr. 51, 283-316

Orville, P.M. (1963). Alkali ion exchange between vapour and feldspar phases. Am. J. Sci. 261, 201-237

Orville, P.M. (1972). Plagioclase cation exchange equilibria with aqueous chloride solution: Results at 700 °C and 2000 bars in the presence of quartz. Am. J. Sc. 272, 234-272

Oxburgh, R., Drever, J.I, Sun, Y.T. (1994). Mechanism of plagioclase dissolution in acid solutions at 25 °C. Geochem. Cosmochem. Acta 58, 661?669

Paces, T. (1972). Chemical characteristics and equilibration in natural water-felsic rock-CO_2 system. Geoch. Cosmoch. Acta 36(2), 217-240

Parks, G.A. (1990). Surface energy and adsorption at mineral/water interfaces: An introduction. Rev. Mineral 23, 133-176

Parsons, I. (1965). The Feldspathic Syenites of the Loch Ailsh Intrusion, Assynt, Scotland

Parsons, I. and Lee, M.R. (2009). Mutual replacement reactions in alkali feldspars-I: microtextures and mechanisms. Contrib. Min. Petr. 157, 641-661

Petersen, J. S. (1978). Structure of the lamikite-lardalite complex, Oslo-Region, Norway, and its evolution. Geol. Rundschau 67, 330-342

Peterson, N.V. (1972). Oregon sunstones. The Ore Bin, State of Oregon, Dept. Geol. Min. Industr. 34, 197-215

Petroviç, R., Berner, R.A. and Goldhaber, M.B. (1976). Rate control in dissolution of alkali feldspar. I. Study of residual feldspar grains by X-ray photoelectron spectroscopy. Geoch. Cosmoch. Acta 40, 537-548

Philpotts, A.R. and Ague, J.J. (2009). Principles of Igneous and Metamorphic Petrology. 2nd ed. Cambridge University Press

Pichavant, M. and Manning, D. (1984). Petrogenesis of tourmaline granites and topaz granites; the contribution of experimental data. Phys. Earth Planet Inter. 35, 31-50

Pina, C.M and Putnis, A. (2002). The kinetics of nucleation of solid solutions from aqueous solutions: a new model for calculating non-equilibrium distribution coefficients. Geoch. Cosmoch. Acta 66, 185-192

Plümper, O. and Putnis, A. (2009). The Complex Hydrothermal history of Granitic Rocks: Multiple Feldspar Replacement Reactions under Subsolidus Conditions. J. Petr. 50(5), 967-987

Prieto, M. (2009). Thermodynamics of Solid Solution-Aqueous Solution Systems. In: Oelkers E.H., Schott J. (eds.) Thermodynamics and Kinetics of Water-Rock Interactions. Rev. in Min. and Geoch., vol. 70,

pp. 47-86
Putnis, A. (1992). Introduction to Mineral Science. 5th ed. Cambridge University Press
Putnis, A. (2009). Mineral Replacement Reactions. In: Oelkers E.H., Schott J. (eds.) Thermodynamics and Kinetics of Water-Rock Interactions. Rev. in Min. and Geoch., vol. 70, pp. 87-124
Putnis, A. and Austrheim, H. (2010). Fluid-induced processes: metasomatism and metamorphism. Geofluids 10(1-2), 254-269
Putnis, A., Hinrichs, R., Putnis, C.V., Golla-Schindler, U., Collins, L.G. (2007). Hematite in porous red-clouded feldspars: evidence of large-scale crustal fluid-rock interaction. Lithos 95,10-18
Putnis, A. and John, T. (2010). Replacement Processes in the Earth?s Crust. Elements 6, 159-164
Putnis, A. and Putnis, C.V. (2007). The mechamism of re-equilibration of solids in the presence of a fluid phase. Journ. of Solid State Chem. 180, 1783-1786
Putnis, C.V. and Mezger, K. (2004). A mechanism of mineral replacement: isotope tracing in the model system KCl-KBr- H_2O. Geoch. Cosmoch. Acta 68, 2839-2848
Putnis, C.V., Tsukamoto, K., Nishimura, Y. (2005). Direct observations of pseudomorphism: compositional and textural evolution at a fluid-solid interface. Am. Min. 90, 1909-1912
Raade, G. (1973). Distribution of radioactive elements in the plutonic rocks of the Oslo Region. Unpubl. cand. real. thesis, Univ. of Oslo, Norway
Rasmussen, E., Neumann, E.R., Andersen, T., Sundvoll, B., Fjerdingstad, D. and Stabel, A. (1988). Petrogenetic processes associated with intermediate and silicic magmatism in the Oslo-rift, south-east Norway. Min. Mag. 52, 293-307
Ribbe, P.H. (1975). Exsolution textures and interference colors in feldspars. In: Ribbe P.H. (ed.) Feldspar Mineralogy, Mineralogical Society of America, short course notes, 2. R-73-R-96
Rubie, D.C. (1986). The catalysis of mineral reactions by water and restrictions on the presence of aqueous fluid during metamorphism. Min. Mag. 50, 399-415
Ruiz-Agudo, E., Putnis, C.V., Rodriguez-Navarro, C. and Putnis, A. (2012). Mechanism of leached layer formation during chemical weathering of silicate minerals. Geol. 40, 947-950

Saigal, G.C., Morad, S., Bjørlykke, K., Egeberg, P.K. and Aagaard, P. (1988). Diagenetic albitization of detrital K-feldspar in Jurassic, Lower Cretaceous and Tertiary clastic reservoir rocks from offshore Norway-I: Textures and origin. J. Sed. Petr. 58, 1003-1013

Schott, J., Pokrovsky, O.S., Spalla, O., Devreux, F., Gloter, A. and Mielczarski, J.A. (2012). Formation, growth and transformation of leached layers during silicate minerals dissolution: The example of wollastonite. Geoch. Cosmoch. Acta 98, 259-281

Schott, J., Pokrovsky, O.S. and Oelkers, E.H. (2009). The Link Between Mineral Dissolution-Precipitation Kinetics and Solution Chemistry. In: Oelkers E.H., Schott J. (eds.) Thermodynamics and Kinetics of Water-Rock Interactions. Rev. in Min. and Geoch., vol. 70, pp. 207-258

Seewald, J.S. and Seyfried, W.E. Jr. (1990). The effect of temperature on metal mobility in subseafloor hydrothermal systems: constraints from basalt alteration experiments. Earth Plan. Let. 101, 388-403

Sherman, D.M. (2009). Surface Complexation Modeling: Mineral Fluid Equilibria at the Molecular Scale. In: Oelkers E.H., Schott J. (eds.) Thermodynamics and Kinetics of Water-Rock Interactions. Rev. in Min. and Geoch., vol. 70, pp. 181-206

Smith, J. V. (1974). Feldspar minerals. 11. Springer-Verlag

Smith, J.V. and MacKenzie, W.S. (1958). The alkali feldspars-IV. The cooling history of high-temperature sodium-rich feldspars. Am Min. 43, 872-889

Smith, J.V. and Muir, I.D. (1958). The reaction sequence in larvikite feldspars. Z. Kristall. 110, 1-20 Steefel, C.I. (2007). Geochemical Kinetics and Transport. In: Brantley, S.L., Kubichi, J.D. and White, A.F. (eds.) Kinetics of Water-Rock Interactions. 1rst ed. Springer, New York

Steefel, C.I. and Maher, K. (2009). Fluid-Rock Interaction: A Reactive Transport Approach. In: Oelkers E.H., Schott J. (eds.) Thermodynamics and Kinetics of Water-Rock Interactions. Rev. in Min. and Geoch., vol. 70, pp. 485-532

Steefel, C.I. and Van Cappellen, P. (1990). A new approach to modeling water-rock interaction: The role of precursors, nucleation , and Ostwald ripening. Geoch. Cosmoch. Acta 54, 2657-2677

Stumm, W., Furrer, G. and Kunz, B. (1983). The role of surface coordination in precipitation and dissolution of mineral phase. Croat. Chem. Acta 58, 593-611

Sundvoll, B. (1978a). Rb/Sr-relationship in the Oslo igneous rocks. In:

Neumann, E.R. and Ramberg, I.B. (eds.) Petrology and Geochemistry of Continental Rifts. D. Reidel Publ. Co.. 181-4.
Thompson, A.B. (1983). Fluid-absent metamorphism. J. Geol. Soc. London 140, 533-547
Verberne, R. (2013). Feldspar replacement in the vicinity of pseudotachylytes. Unpubl. Bachelor thesis, Utrecht University, the Netherlands
Watson, E.B., Brenan, J.M. and Baker, D.R. (1990). Distribution of fluids in the continental mantle. In: Menzies M.A. (ed.) Continental mantle. Clarendon Press, Oxford, pp. 111-125
White, A.F., Bullen, T.D., Schulz, M.S., Blum, A.E., Huntington, T.G. and Peters, N.E. (2001). Differential rates of feldspar weathering in granitic regoliths. Geoch. Cosmoch. Acta 65(6), 847-869
Widenfalk, L. (1972). Myrmekite-like intergrowths in larvikite feldspars. Lithos 5, 255-267
Willaime, C., Brown, W.L. and Gandais, M. (1973). An electron microscopic and X-ray study of complex exsolution textures in a cryptoperthitic alkali feldspar. J. Material Sc. 8, 461-466
Willaime, C. and Gandais, M. (1972). Study of Exsolution in Alkali Feldspars: Calculation of Elastic Stresses Inducing Periodic Twins. Phys. stat. sol. (a) 9, 529-539
Wyart, J. and Sabatier, G. (1958). The mobility of silicon and aluminium in feldspar crystals. Bull Soc Franc Mineral Cristall. 82, 223-226 (French)
Xia, F., Brugger, J., Chen, G., Ngothai, Y., O'Neill, B., Putnis, A. and Pring, A. (2009). Mechanism and kinetics of pseudomorphic mineral replacement reactions: A case study of the replacement of pentlandite by violarite. Geoch. Cosmoch. Acta 73, 1945-1969
Yund, R.A. (1984). Alkali feldspar exsolution: kinetics and dependence of alkali interdiffusion. In: Brown, W.L. (ed.) Feldspars and Feldspathoids: Structures, Properties and Occurrences, Springer, pp. 281-315.
Yund, R.A. and McCallister, R.H. (1970). Kinetics and mechanisms of exsolution. Chem. Geol. 6, 5-30
Zhang, Y. (2010). Diffusion in Minerals and Melts: Theoretical Background. In: Zhang, Y. and Cherniak, D.J. (ed.) Diffusion in Minerals and Melts. Rev. in Min. and Geoch, vol. 72, pp. 5-60
Zhang, Y., Ni, H. and Chen, Y. (2010). Diffusion Data in Silicate Melts. In: Zhang, Y. and Cherniak, D.J. (ed.) Diffusion in Minerals and Melts. Rev. in Min. and Geoch, vol. 72, pp. 311-408

Zhu, C. (2009). Geochemical Modeling of Reaction Paths and Geochemical Reaction Networks. In: Oelkers E.H., Schott J. (eds.) Thermodynamics and Kinetics of Water-Rock Interactions. Rev. in Min. and Geoch., vol. 70, pp. 533-569

Zhu, C., Blum, A. E. and Veblen, D. R. (2004). Feldspar dissolution rates and clay precipitation in the Navajo aquifer at Black Mesa, Arizona, USA. In: Wanty, R.B. and Seal, R.R.I. (eds.) Water-Rock Interaction. A.A. Balkema, Saratoga Springs, New York, pp. 895-899.

Zhu, C. and Lu, P. (2009). Coupled alkali feldspar dissolution and secondary mineral precipitation in batch systems: 3. Saturation indices of product minerals and reaction paths. Geoch. Cosmoch. Acta 73, 3171-3200

Zhu, C., Lu P., Zheng, Z. and Ganor, J. (2010). Coupled alkali feldspar dissolution and secondary mineral precipitation in batch systems: 4. Numerical modeling of kinetic reaction paths. Geoch. Cosmoch. Acta 74, 3963-3983

Zhu, C., Veblen, D. R., Blum, A. E. and Chipera, S. J. (2006). Naturally weathered feldspar surfaces in the Navajo Sandstone aquifer, Black Mesa, Arizona: electron microscopic characterization. Geoch. Cosmoch. Acta 70, 4600-4616

$Figure 3 : http://serc.carleton.edu/NAGTWorkshops/mineralogy/mineral_physics.html$